General Disclaimer

One or more of the Following Statements may affect this Document

- This document has been reproduced from the best copy furnished by the organizational source. It is being released in the interest of making available as much information as possible.

- This document may contain data, which exceeds the sheet parameters. It was furnished in this condition by the organizational source and is the best copy available.

- This document may contain tone-on-tone or color graphs, charts and/or pictures, which have been reproduced in black and white.

- This document is paginated as submitted by the original source.

- Portions of this document are not fully legible due to the historical nature of some of the material. However, it is the best reproduction available from the original submission.

66-51146

WAD: R572-Q4

Contract NAS 9-5424

September 15, 1966 - December 14, 1966

THE DEVELOPMENT OF A SEGMENTED, AXIALLY CONDUCTING, PYROLYTIC GRAPHITE REACTION CONTROL ENGINE

Fourth Quarterly Report

prepared by

Wright Aeronautical Division
Curtiss-Wright Corporation
Wood-Ridge, New Jersey 07075

for

NASA-MANNED SPACECRAFT CENTER

HOUSTON, TEXAS

WAD: R572-Q4

Copy 13

Contract NAS 9-5424

September 15, 1966 - December 14, 1966

THE DEVELOPMENT OF A SEGMENTED, AXIALLY CONDUCTING, PYROLYTIC GRAPHITE REACTION CONTROL ENGINE

Fourth Quarterly Report

prepared by

Wright Aeronautical Division
Curtiss-Wright Corporation
Wood-Ridge, New Jersey 07075

for

NASA-MANNED SPACECRAFT CENTER

HOUSTON, TEXAS

WRIGHT AERONAUTICAL DIVISION • CURTISS-WRIGHT CORPORATION • WOOD-RIDGE, N. J., U. S. A.

ABSTRACT

This is the fourth quarterly report covering the work performed under NASA contract NAS 9-5424 during the period from September 15 through December 14, 1966. The objective of this program is to demonstrate a flight type configuration of an Axially Conducting Engine (ACE) in which pyrolytic graphite (PG) wedges, restrained by an elastic structure, form the combustion chamber and nozzle of the engine.

During this quarter fabrication and cold flow testing of the integral spray injector for the flight engine configuration were completed. Initial hot firing evaluation of the injector indicated a low frequency instability problem. Design revisions intended to correct the problem are in process.

TABLE OF CONTENTS

ILLUSTRATIONS

ILLUSTRATIONS (Cont'd.)

ILLUSTRATIONS (Cont'd.)

LIST OF TABLES

I. INTRODUCTION

A. Program Scope and Objective

The program for the preliminary development of a segmented, axially conducting, 100 pound thrust pyrolytic graphite (PG) rocket engine includes thermal and structural analyses, design verification tests on rig engines, two flight configuration engine tests for final design demonstration, and an examination of engine compatibility with advanced propellants. The delivery of a flight configuration engine to NASA Manned Spacecraft Center will complete the program.

The objective of this program is to demonstrate the feasibility of the Axially Conducting Engine (ACE) concept for reaction control engine applications. Ultimately, the engine will be usable for buried and/or exposed installations on a spacecraft and will be capable of use with the fluorine family of advanced propellants.

The design conditions for the flight type ACE engine are as follows:

Vacuum Thrust:	100 lb with 40:1 nozzle area ratio
Chamber Pressure:	100 psia
Propellant Inlet Pressure:	235 $\pm$ 5 psia*
Fuel:	Monomethylhydrazine
Oxidizer:	Nitrogen Tetroxide
Oxidizer/Fuel Ratio:	1.4:1*
Specific Impulse:	290 seconds when operating with 40:1 area ratio nozzle for pulses of 1.0 second duration or longer.

* Revised per Contract Modification No. 1 dated 9/28/66.

Minimum Impulse Bit:	0.5 lb-sec
Life:	1000 seconds total time including a 500 second continuous run.
Weight:	Not specified but all efforts shall be made to attain a minimum value.

The Curtiss-Wright designation for the engine being developed under this contract is WLR-23.

B. Summary of Program Status

The third quarterly report described the progress of the program through completion of the rig engine testing, Phase II.

The primary effort during the fourth quarter concerned fabrication and evaluation of the integral spray injector. Cold flow tests prior to engine firing indicated close agreement of the propellant flow-pressure drop relationship between the integral spray injector and the injector used during the ACE rig engine tests.

The initial hot firing evaluation test series on the new injector revealed a low frequency (under 200 cps), high amplitude instability in the chamber pressure and propellant feed pressures. Investigation thus far indicates that the problem is associated with the internal manifolding of the injector. A design has been completed to allow modifications to the fuel manifold for test evaluation.

In addition to the injector development activity. the design of the flight configuration engine (Phase III, Task 2) has been completed. Raw material orders were placed in October for the Rene 41 housing forgings and plate material for the axial springs. Delivery of this material is scheduled for the third week in December. Fabrication of the wedge and watchband assembly is in process and is scheduled for completion by December 15.

The overall program status is outlined in the Figure 1.1 schedule. Evaluation testing (Phase III, Task 4) is somewhat behind schedule due primarily to the problem encountered with the integral spray injector. A revision will be issued when this development activity is completed.

II. FLIGHT CONFIGURATION ENGINE DESIGN

A. Summary

The flight engine configuration shown in Figure 2.1 consists of the rig engine wedge and watchband chamber assembly, a lightweight external housing, a close-coupled bi-propellant control valve and a 16-port swirl cup injector with integral fuel spray cooling.

The wedge and watchband chamber assembly is unchanged except for minor revision to the watchband prongs to facilitate installation in the flight housing. The thrust chamber is supported in the flight housing by pilot rings located at the injector end and the aft retaining plate.

The external housing is a stepped cylindrical structure with flanges at each end. The step provides a loading shoulder for the belleville springs. These springs have been relocated to the injector location from the nozzle exit position on the rig engine. This was done to provide an exit cone attachment arrangement and to eliminate the expansion joint in the nozzle gas stream. Axial expansion is taken between the lip of the spray ring on the injector and the front sealing washer of the thrust chamber assembly. The spring shoe for transmitting the axial load is fitted with an "O" ring which is free to slide in the small diameter of the outer housing. This arrangement seals the spring cavity in the housing from propellant and combustion gases.

The belleville springs are sized to provide an adequate sealing load at the front and rear sealing washers for all operating conditions of relative thermal growth (axial) between the housing and thrust chamber. One pair of parallel stacked belleville springs is presently used based on the thermal analysis. Space is allowed for installation of two additional sets of springs in series should greater growth compensation be required. A spacer is provided to fill the gap.

The aft retaining plate attaches to the rear flange of the housing and supports the aft end of the thrust chamber. It is also used to mount the engine to the test stand. This plate is considered to be test equipment and will be replaced by an exit cone when running the flight engine with a full expansion nozzle.

The injector is a high response 16-port swirl cup design similar to the rig injector except for the addition of integral fuel spray cooling manifolding and orifices. Propellant is supplied to the engine through a close-coupled Moog bi-propellant valve mounted on the back of the injector.

B. Integral Spray Injector

The integral spray injector is a direct copy of the internal passage design used on the injector for the rig engine test program. The new injector incorporates a fuel spray ring manifold with 16 orifices. The spray manifold is fed by a passage from the fuel manifold. This configuration replaces the pintles, pintle housing and separate feed system used on the rig engine. In addition the fuel manifold inlet hole was relocated (angular) closer to the oxidizer inlet to match the propellant holes on the Moog bi-propellant control valve. The injector configuration is shown in Figure 2.2.

There is an extra stock allowance which provides room for combustion chamber and spray manifold pressure taps, and a variable restriction plug for regulating the spray flow. When performance testing is complete, the injector will be reworked to the flight configuration shown in Figure 2.3.

An adapter pad attached to the back of the injector serves to mount the valve and to provide purge fittings and pressure taps.

Pertinent flow data are summarized in the Table 2.1.

C. Flight Configuration Arrangement

1. Design Requirements

The combined effects of loading, sealing requirements, and temperature were considered in the overall design of the flight engine.

a. Belleville Spring Loads

The analytical load-deflection and stress characteristics of a set of parallel stacked belleville springs for the flight engine is shown in Figure 2.4. The springs supplement the aerodynamic and pressure loads in determining the end washer sealing requirements.

The deflection requirement for the belleville springs at assembly is 0.055" to give a load of 590 pounds. Verification of this deflection will be made by spring rate tests on the springs after fabrication.

b. Aerodynamic and Pressure Loads

The aerodynamic and pressure loads on the flight engine were checked for six operating conditions

1. sealed engine
2. pressurized spring and chamber cavity
3. pressurized chamber cavity
4. pressurized spring cavity
5. installation
6. soak

Conditions 1, 2, 5 and 6 were used for all design analyses. Condition 2 prevails over conditions 3 and 4 by having the cavities cross-vented. This limits the maximum end washer load and maintains nearly constant bearing stresses. Condition 4 would overload the washers.

A summary of the sea level and vacuum engine loads is given for conditions 1 - 6 in Figures 2.5 through 2.10. These values, which include the belleville spring and metal O-ring clamping loads, are for a 500 second firing. The loads for other firing times are found by changing the spring and clamping loads per Figures 2.4 and 2.11 respectively, and recalculating the flight housing and aft retainer or exit cone loads for horizontal equilibrium.

Figures 2.12 and 2.13 are free body diagrams showing the end seal loads used in sizing the sealing washer bearing areas. The belleville spring loads are omitted and must be included to obtain total load. The end seal bearing stresses are checked at several firing times involving different spring loads and conditions of radial growth of the thrust chamber.

c. Thermal Growth

The belleville spring deflection requirements, due to the relative thermal growth between the thrust chamber and flight housing, are given in Figure 2.14. Maximum and minimum temperatures at the inside diameter of the spring are also shown. The values of temperature and relative thermal growth have been plotted on the spring rate curve (Figure 2.4) to give the spring load for the predicted temperature time history of the flight engine.

d. Thermal Analysis

A thermal model was prepared for the flight engine heat transfer analysis. The new model includes the relocated belleville springs, a flightweight housing and an aft retaining plate. The thrust chamber assembly is identical to the rig engine version. This thermal analysis includes the calculated heat transfer film coefficients which were correlated with the third rig engine test.

The results of the flight engine heat transfer analysis are shown in Figures 2.15 through 2.21 for test times of 50, 100, 200, 300, 400 and 500 seconds and for 200 seconds of soak.

Because of the consistantly lower measured watchband temperatures during the rig engine tests, the flight housing and aft retainer temperatures have been adjusted downward. These revised temperatures take into account a smaller flight housing heat sink and reflect a realistic estimate of the temperatures for design. A complete summary of the flight housing and aft retainer temperatures is given in Figure 2.22.

e. Materials

Materials for the new hardware components have been selected on the basis of temperature and structural requirements.

High temperature alloy Rene' 41 (WAD 7817) is used for the housing, aft retainer and belleville springs. Rene' 41 combines the advantages of good strength properties with high temperature capability and affords a margin of safety for steady state and duty cycle testing.

Inconel 600 is used for the spring shoe and pilot ring because of its lower coefficient of expansion (compared with stainless steel) to keep clearances for thermal growth to a minimum.

2. Structural Analysis

a. End Sealing Washers

Figures 2.23 through 2.28 summarize the flight engine end seal loads and bearing stresses for sea level and vacuum test conditions. Operating Conditions 1 to 4 are given at start-up, 200 and 500 second firing times. Operating conditions 5 and 6 are given at installation and 700 seconds (soak), and are included in the tabulation for conditions 1 to 4. The lettered sealing section A, B, C and D refer to the end seal load free body diagrams, Figures 2.12 and 2.13.

The sealing washer bearing height was based on the loads summarized in Figure 2.23, condition 1 which is the sealed engine operating at sea level.

Conditions 2 to 6 in Figures 2.24 through 2.28 are checked for compressive stress using the seal height and bearing area established in Figure 2.23.

The typical design compressive bearing stress in the pyrolytic end seal washers is 1000 psi, which is comparable with the value used in the rig engine configuration. During installation and soak, lower sealing stresses are developed because there are no aerodynic and pressure loads. The higher sealing stresses occur when the engine is firing.

Condition 4 is summarized in Figures 2.25 and 2.28. However, neither the loads nor the stresses will develop because the cavities are cross-vented. Without cross-venting it can be seen that the bearing stresses which could develop are higher than present design experience allows.

The end washers were also checked for out-of-plane moments due to the offset in loads on opposite sealing faces, and for the effects of transverse shear. The calculations are based on the loads summarized in Figure 2.23. The results of this study are shown in Figure 2.29.

The approximate yield strength for pyrolytic graphite in the "a" direction is 7,500 psi up to 2000^{o}F. The maximum calculated values do not exceed 2160 psi, giving a minimum factor of safety of 3.5. The shear stresses are compared with the values obtained from the rig engine configuration.

A check of condition 4 sea level which was voided by cross-venting, shows the overloading would result in bending stresses that are up to 99 and 70 percent higher, and transverse shear stresses that are 68 and 57 percent higher, in the front and rear washers respectively. Thus the minimum factor of safety in bending would reduce to 2.2 and the shear stresses would exceed the maximum design value in the rig engine.

b. Flight Housing

A stress analysis was conducted on the flight housing to determine the dimensions of various sections to insure structural integrity. The analysis was

performed for firing times of 200 and 500 seconds and a restart condition at 700 seconds, and for the most stringent of several loading conditions (both the spring cavity and chamber cavity pressurized).

The mechanical and pressure loads which are applied to the housing for this condition and the temperature distribution are outlined in previous sections. The thermal, mechanical, and pressure loads produce internally redundant shears and moments at the junctions of the cylindrical shells, rings, and annular plates which comprise the flight housing. The housing was cut at the sections indicated by locations 1 through 4 in Figure 2.30. The deflections and rotations of the boundary points, of these subsections of the housing, due to the unknown redundant shears and moments and the known mechanical, pressure, and thermal loading were determined. These deflections and rotations were equated for adjacent housing subsections, rendering a set of simultaneous equations which were employed to solve for the unknown redundant shears and moments.

The redundant shears and moments were determined for several cases with differing dimensions for the shell and plate thickness in the neighborhood of location 2, Figure 2.30. The configuration which yielded acceptable shears and moments is shown in Figure 2.30 and is stress analyzed herein. The redundant shears and moments for this case are listed in Tables 2.2 and 2.3, respectively. These loads are based on the conservative assumption that the boundary point at location 1 is fully restrained from rotating and deflecting due to mechanical loads and partially restrained due to thermal loads.

The maximum stresses in the housing computed for this loading condition are tabulated in Table 2.4. These maximum meridional and circumferential stresses are associated with a junction point and they occur at some well define distances from the junction; these distances are dependent on the direction and magnitude of the shear and moment applied at the end of the shell. In addition the shells were analyzed for local buckling at the points where hoop compression occurs. All stresses were found to be well within safe limits.

In computing the hoop compression in the flange at location 1, the conservative boundary condition which applied thermal restraint at this flange resulted in high stresses. A slip joint was then built into this end which allows the housing flange to radially deflect with respect to the injector flange after it has overcome any friction forces which are induced by the bolts which clamp the flanges together. A coefficient of friction of 0.45 results in a distributed shear of 383 lb/in and the flange hoop compression for this shear load is shown in Table 2.4.

III. TESTING

A. Summary

Details of the integral spray injector were cold flow tested prior to welding and final machining. The data showed a close agreement in flow-pressure drop characteristics with those established during rig engine testing.

Fabrication of the integral spray injector was completed early in November 1966. The injector was then cold flow tested with MMH fuel at the Malta Test Station to obtain a final calibration prior to hot firing. Instrumentation was provided to measure pressure at the inlet to the fuel manifold (downstream of the Moog valve) and in the spray manifold. The cold flow tests indicated a higher pressure drop from the fuel to spray manifold than was anticipated. With the variable restriction completely open, and the fuel manifold pressure set to provide proper fuel flow through the swirl cup, the spray flow obtained was 0.0385 lb/sec.

The spray flow was thus 20% lower than the value (.048 lb/sec) established during the rig engine testing. However, it was decided to initiate hot firing evaluation of the injector. The hot firing tests indicated that the injector at design point was producing a low frequency instability. Further exploratory testing was accomplished in the following areas:

1. The stability and performance characteristics were examined with no spray cooling by closing off the variable restriction between the fuel and spray manifold.

2. The Moog valve was replaced with test stand valves.

3. Testing was accomplished at other than design point to determine the effect on the instability.

4. Calibrated orifices in the propellant feed systems, just upstream of the engine, were removed.

These modifications had little or no effect on the nature of the instability; further review of the design and the test data indicated that the problem is associated with the injector internal manifolding. Modifications are in process to allow evaluation of a reduced flow area fuel manifold and changes to the relative position of the fuel to the oxidizer manifold.

B. Cold Flow Test of Integral Spray Injector

The ES156989 (see Figure 2.2) integral spray injector to be used on the WLR-23 flight configuration engine incorporates orifices and propellant manifold geometry designed to be identical to the ES156903N1 injector used in test firings of the WLR-23 rig engine. The major design change on the flight type injector was the integration of the spray cooling orifices and spray manifold within the injector body. A variable position restriction plug inserted in the spray cooling supply passage permitted adjustment of the spray cooling flow.

Each individual swirl cup orifice was calibrated using Normal Heptane as the flowing medium. The pressure was measured at inlet to the flow rig; the orifice outlet flow exhausted to atmosphere. Details of the individual orifice calibrations are given in Table 3.1 and the results plotted in Figure 3.1. In all cases, the test data has been reduced to propellant flow at 70°F.

The data shows that for a given orifice inlet pressure, the maximum deviation to the arithmetic mean flow was from +3.4% to -3.8% for the MMH orifices and from +2.7% to -2.0% for the N_2O_4 orifices. The flow uniformity between like orifices in this injector is superior to that obtained in the ES156903N1 rig injector which ranged from +6% to -4% for the N_2O_4 orifices and from +9% to -6% for the MMH orifices.

A comparison of the swirl cup orifice pressure drops with those of the rig injector is given below and indicates close agreement between the two injectors:

	ES156989	ES156903N1
N_2O_4 Orifice Δ P-psi	44	43
MMH Orifice Δ P-psi	64	71

After assembly of the swirl cup insert to the injector body, an overall injector calibration was made. Details of this calibration are given in Table 3.2 and plotted in Figure 3.2. Figure 3.2 also provides a summation of the flow calibration of the individual orifices; thus the injector internal manifold losses can be determined. At design flow the N_2O_4 manifold pressure drop is 6 psi, and the MMH pressure drop is 4 psi.

The spray cooling orifice ring was calibrated prior to welding into the injector body. Details of this flow calibration are given in Table 3.3 and plotted in Figure 3.3. The design flow of 0.048 lb/sec flow was obtained at an orifice pressure drop of 68 psi.

After welding the spray ring to the injector, cold flow testing was done on the Malta test stand using MMH propellant. With the spray cooling flow shut off completely, the measured swirl cup flow agreed within 1% with those values obtained in Figure 3.2. Flow test data with the spray cooling restriction plug fully open (allowing maximum flow to the spray cooling manifold) is also plotted in Figure 3.3. This indicates that the pressure drop sustained in the spray cooling supply line is approximately 40 psi at the design flow of 0.048 lb/sec. This value was greater than anticipated. Thus an injector inlet pressure setting, for correct swirl cup flow, provides a spray cooling flow of only 0.0385 lb/sec with the adjustable restriction fully open.

Using the cold flow data, the engine operating design point parameters would be as outlined below, assuming a swirl cup pressure of 105 psia and a combustion chamber pressure of 100 psia.

	N_2O_4	MMH
Engine inlet pressure - psia	175	200
Injector inlet pressure - psia	149	169
Spray manifold pressure - psia	--	140
Swirl cup flow - lb/sec	0.208	0.096
Spray cooling flow - lb/sec	--	0.0385

Under these conditions the spray cooling flow is 20% lower than desired. This is a result of the higher pressure drop between the fuel manifold and the spray manifold. To obtain design spray cooling flow, the spray orifice flow area would have to be increased or the area of the feed line from the manifold would have to be increased.

Rather than attempt these reworks at this time, it was decided to conduct a preliminary hot firing evaluation of the injector. This activity is discussed in the following section.

C. Hot Firing Evaluation of Integral Spray Injector

The integral spray injector was evaluated using the copper combustion chamber (ES156715). The installation and instrumentation arrangement was similar to that used on previous injector testing and is shown in Figures 3.4 and 3.5. Differences are listed below:

1. The separate spray cooling tank and feed system were no longer required, thus were eliminated.

2. A Moog bi-propellant valve was used as the engine start device rather than Eckel solenoid valves.

3. Instrumentation was added to measure propellant feed pressures downstream of the Moog valve, and fuel pressure in the spray manifold.

A total of 25 test points were run and pertinent test data is tabulated in Table 3.4 with combustion chamber pressure, and fuel and oxidizer feed pressure traces provided in Figures 3.6 through 3.30.

Run 23-97 was the initial design point test made. The transient combustion chamber pressure trace (Figure 3.6) indicates an incipient low frequency instability impressed on a low amplitude 600 cycle pressure oscillation. Random peaks to 80 psi were recorded in the combustion chamber pressure trace. The combustion chamber pressure fluctuations were reflected in both the oxidizer and fuel feed systems.

Additional runs were made to explore around design point to determine the extent of the area of instability. Runs through 23-106 were made in this exploration and, as can be seen from the traces (Figures 3.7 through 3.15) and the data in Table 3.4, all were unstable.

For example, run 23-101 was made at an overall O/F ratio of 1.17 with a swirl cup O/F ratio of 1.79. This point resulted in a chugging type low frequency instability. In run 23-105 the overall O/F ratio was increased to 1.60 with a swirl cup O/F ratio of 2.38. This setting produced an incipient chugging type instability with random pressure peaks to 56 psi.

It was then decided to evaluate the effect of eliminating the link between the fuel manifold and the spray manifold. This was easily accomplished by completely closing the variable restriction between the two manifolds. Test points 23-107 through 23-115 were made in this fashion. Traces are presented in Figures 3.16 through 3.24. O/F ratio settings from 1.65 to 2.42 were tested. Chugging was evident in all traces with little or no effect of change in O/F ratio. This series of tests indicated that the problem was in the injector manifolding and was not a result of the coupling of the spray to fuel manifold.

To insure that the use of the Moog valve had no effect on the problem, several tests (runs 23-116 through 23-120) were made with the valve removed. The test stand safety valves were used as start valves for this series of tests. Removal of the Moog valve from the system did not make any significant change in stability. For example, comparisons of the traces of runs 23-117 and 23-112, and runs 23-116 and 23-107 show similar results. A test with spray cooling, run 23-120, was also made and provided similar results to that obtained in runs 23-97 through 23-106 with the Moog valve.

A change was also made to the propellant feed system. Calibrated flow measurement orifices positioned in each supply line approximately 18 inches from the injector inlet were removed. This change was made to insure that the position of the orifices did not result in resonant line lengths and cause the chugging type instability. Run 23-121 pressure transients are shown in Figure 3.30. Random pressure peaks were somewhat higher in this firing compared to the previous run. However, the swirl cup and overall O/F ratios were increased which would tend to increase instability due to the increased momentum of the N_2O_4 swirl cup orifice exit stream.

D. Planned Revisions

The frequency of the combustion chamber pressure oscillation was in the order of 150-200 cps. The first longitudinal frequency of the WLR-23 combustion chamber is in the order of 4000 cps. The first tangential and radial modes are greater than 10,000 cps. It is therefore difficult to associate the instability experienced with the combustion chamber. It appears rather, that the problem is one of interaction of the feed system and combustion process. Since the stand feed system was the same as used during the ES156903N1 rig injector tests, it is thought that the differences must lie in the injector internal propellant manifolding.

The Reynolds Number in the fuel manifold is in the critical range of 2000 - 4000. (Note that the Reynolds Number in the oxidizer manifold is well out of this range.) This could result in unstable flow although the mechanism causing this instability to be magnified to the amplitude of pressure oscillations experienced during test is not known.

Another subtle possibility is the change that was made in the relation of the fuel manifold to the oxidizer manifold. The rig engine injector was run with Eckel solenoid start valves which were displaced by approximately 180°. The flight type injector was designed for the Moog bi-propellant valve and the angular spacing was approximately 55°. This change in relationship may be significant as the manifolds are tapered rather than of a constant area configuration and could produce a coupling effect.

Based on the above, the following changes are planned:

1. The fuel manifold flow passage area will be decreased; thus the Reynolds Number will be increased above the critical value and will insure turbulent flow.
2. The angular relationship between the propellant inlet ports and manifolding will be evaluated.

NASA - MSC HOUSTON ACE PROGRAM SCHEDULE

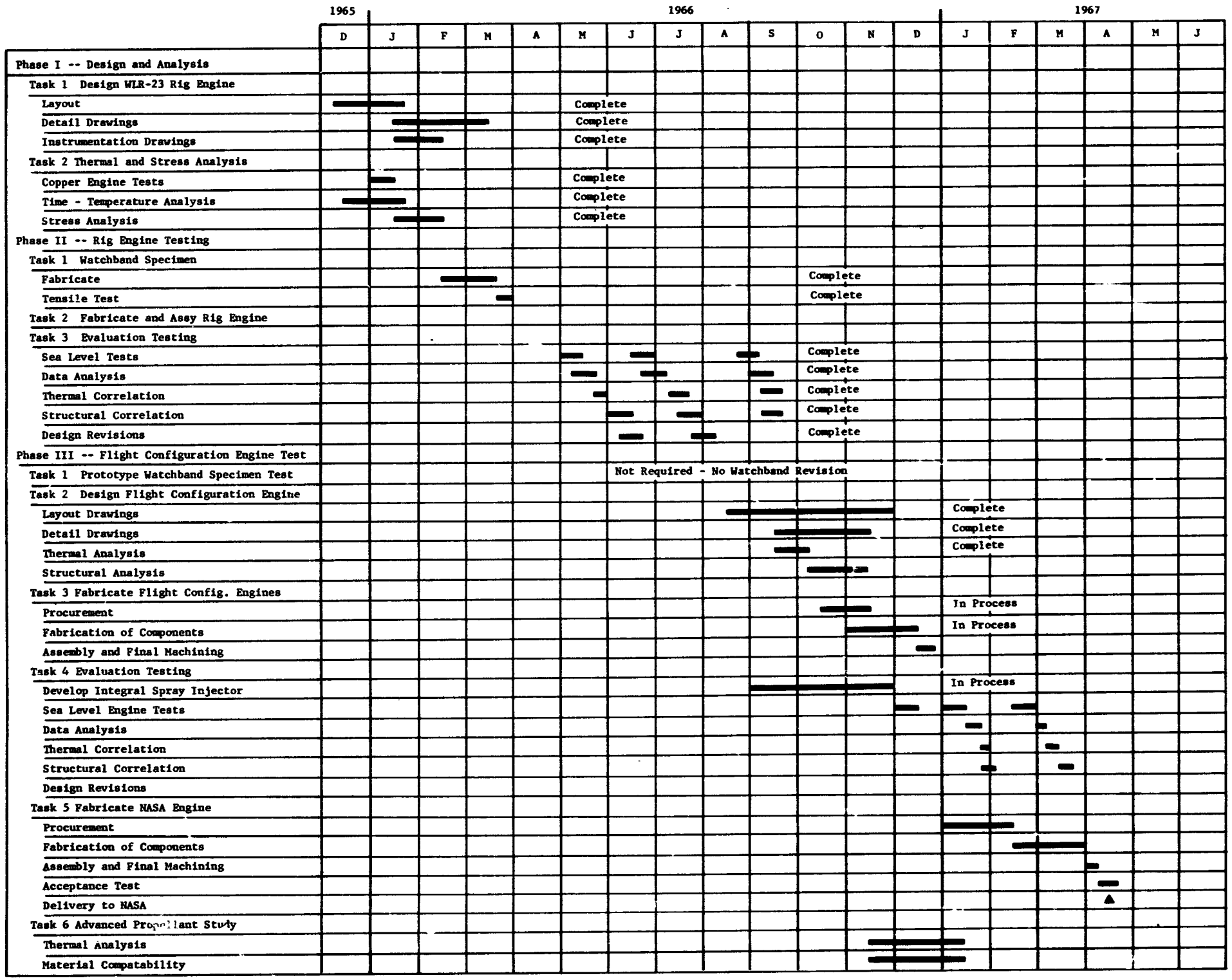

Note (*) Integral Injector With Ace Rig Engine

Revision No. 1
10-1-66

Figure 1.1

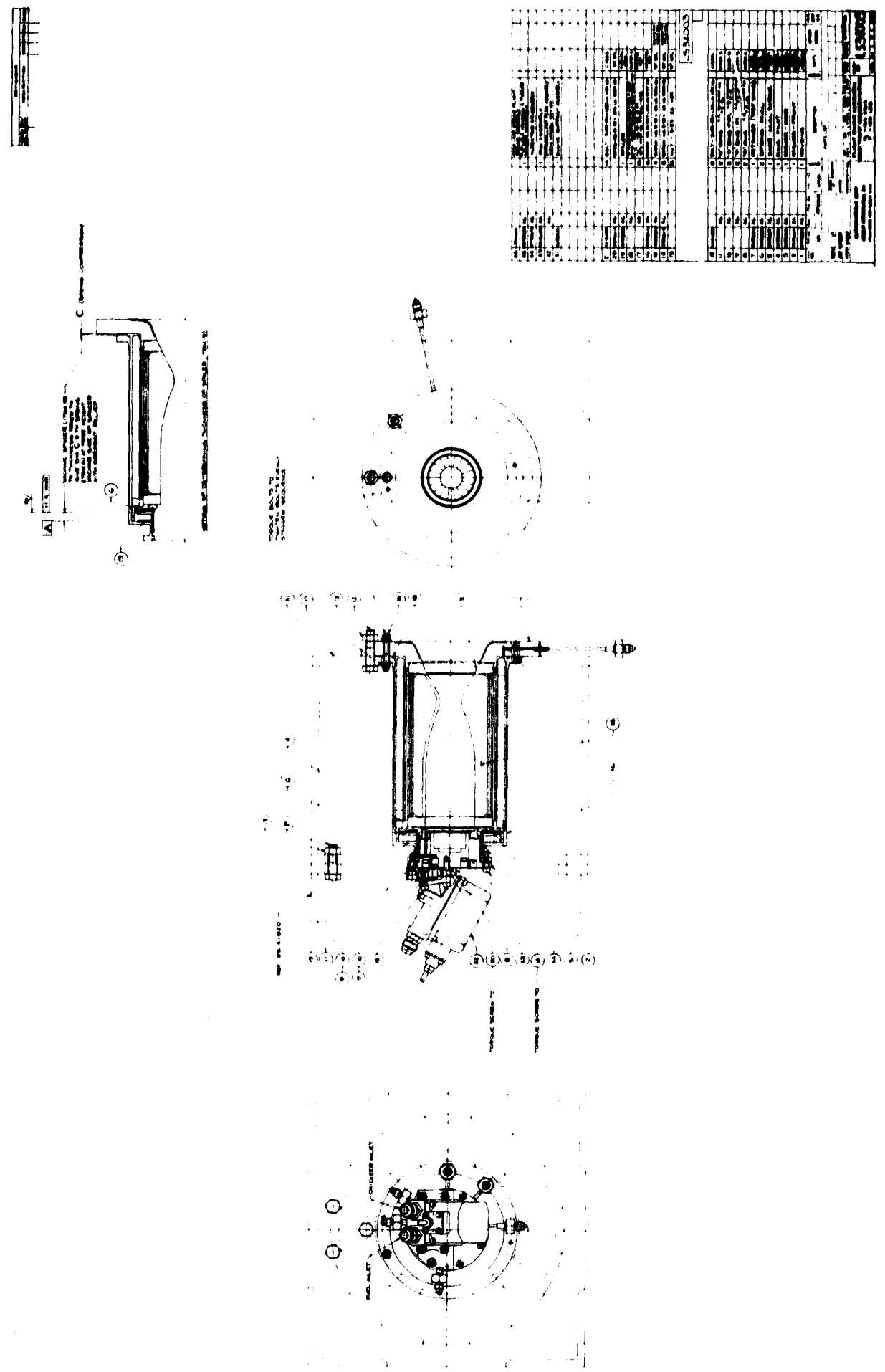

66-1034

Figure 2.1

FOLDOUT FRAME 1

INJECTOR ASSEMBLY WITH IN

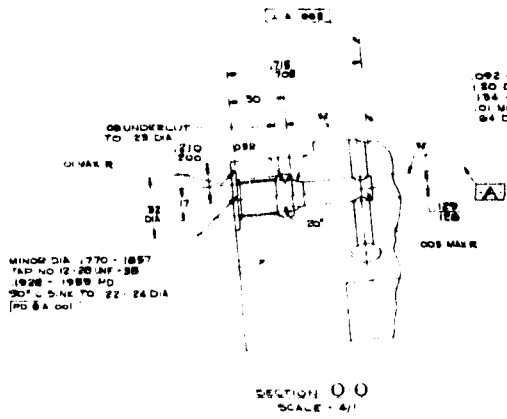

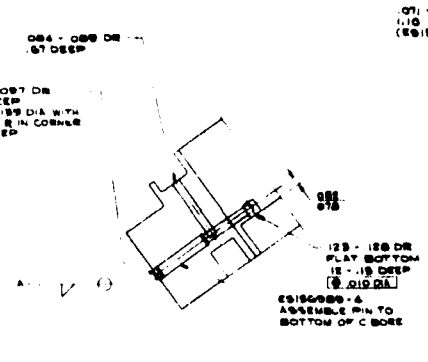

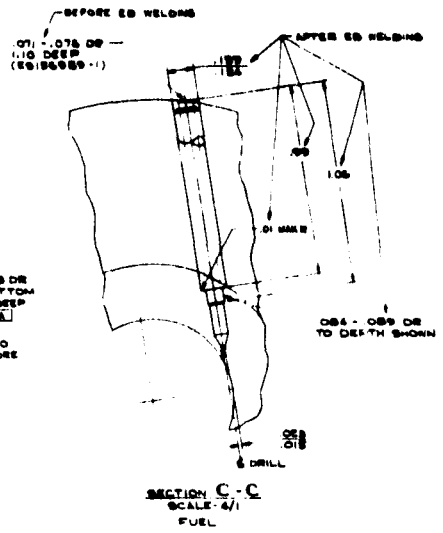

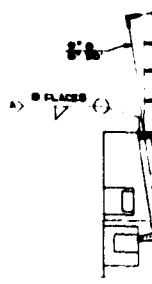

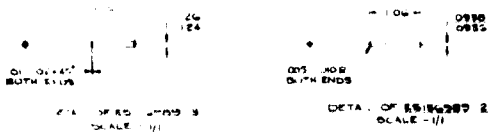

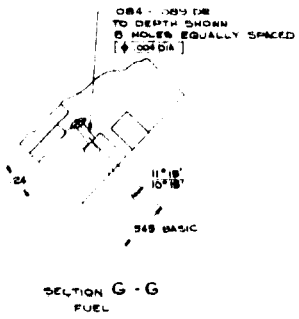

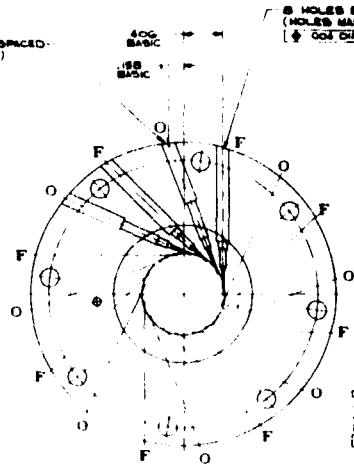

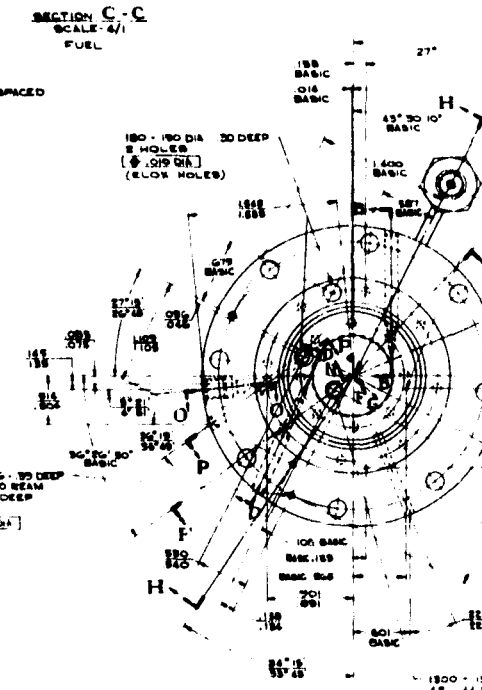

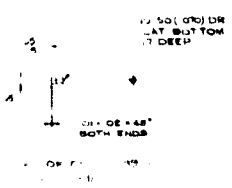

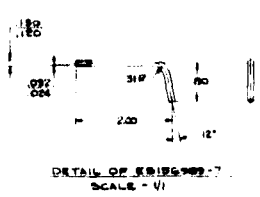

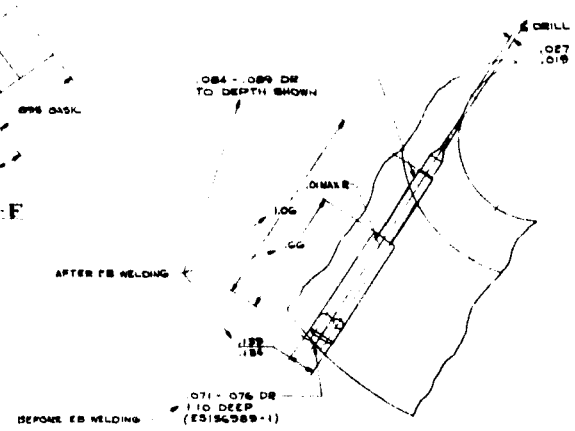

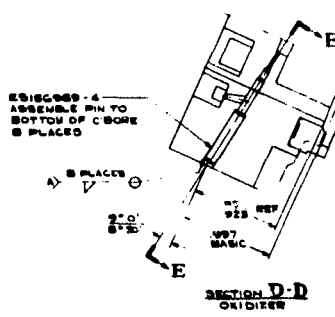

FOLDOUT FRAME 2

ITH INTEGRAL SPRAY (ES 156989)

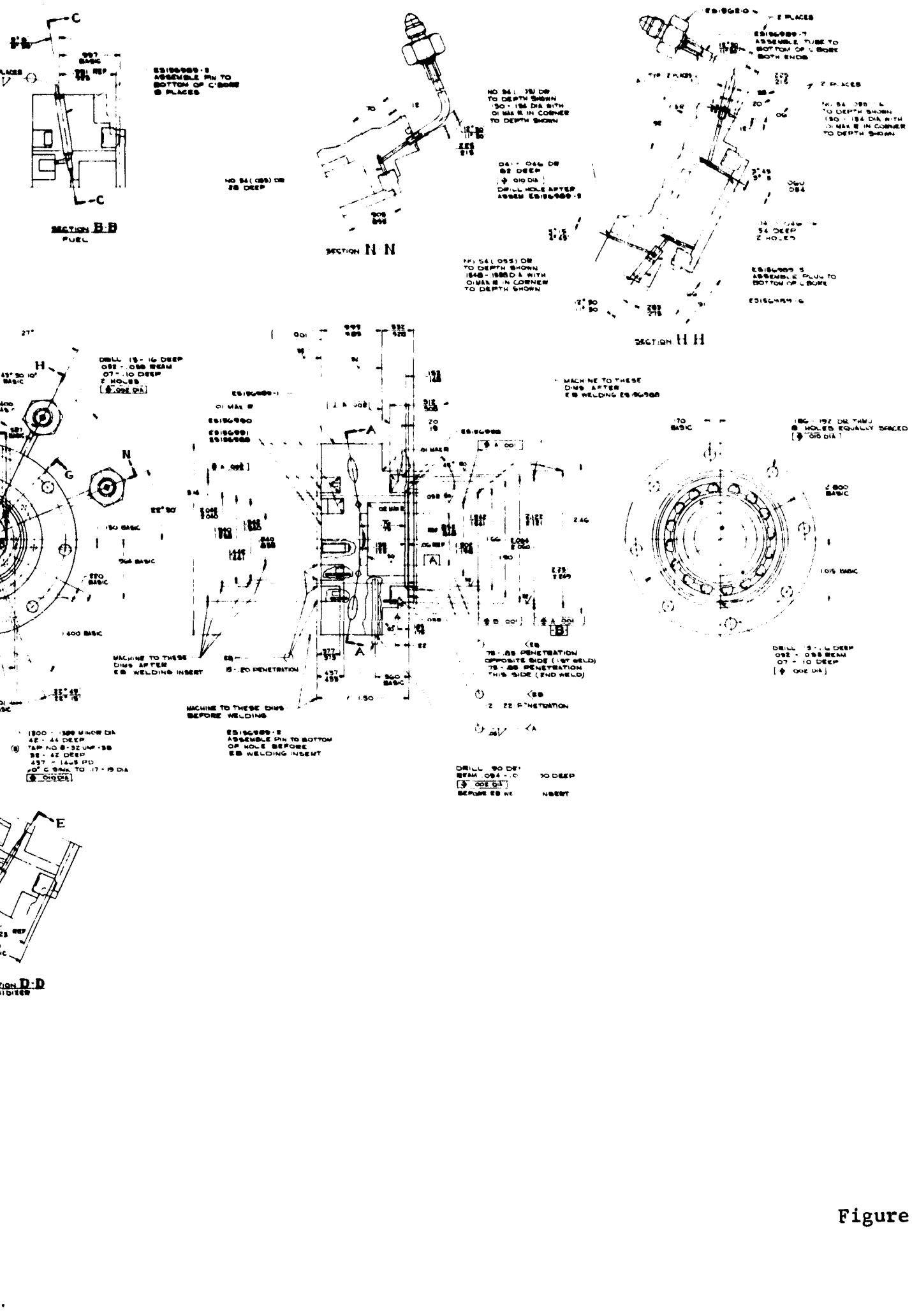

Figure 2.2

FLIGHT INJECTOR ASSEMBLY - REWORK (ES 158073)

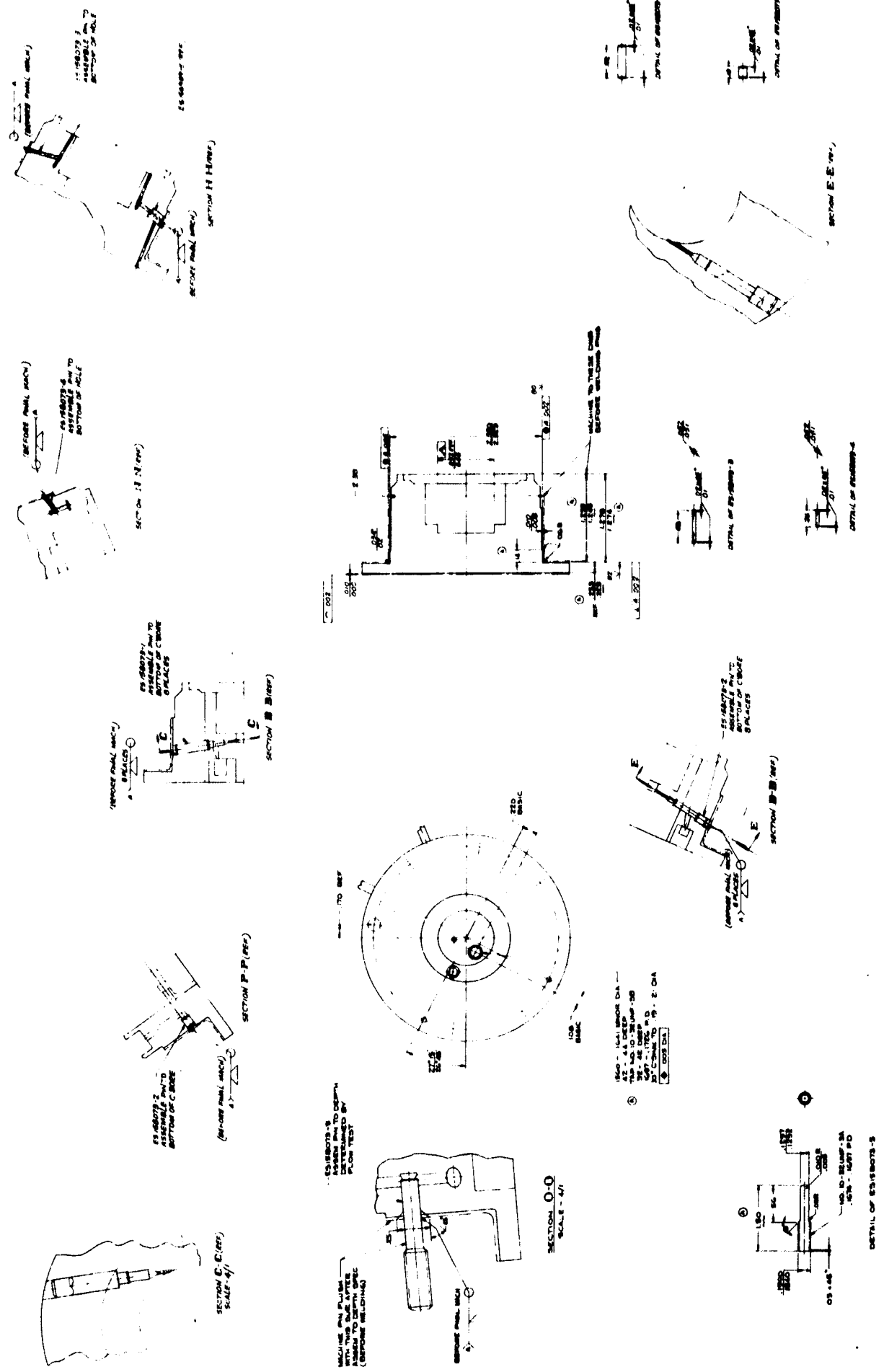

Figure 2.3

WLR-23 FLIGHT ENGINE

BELLEVILLE SPRING LOAD - STRESS - DEFLECTION CHARACTERISTICS

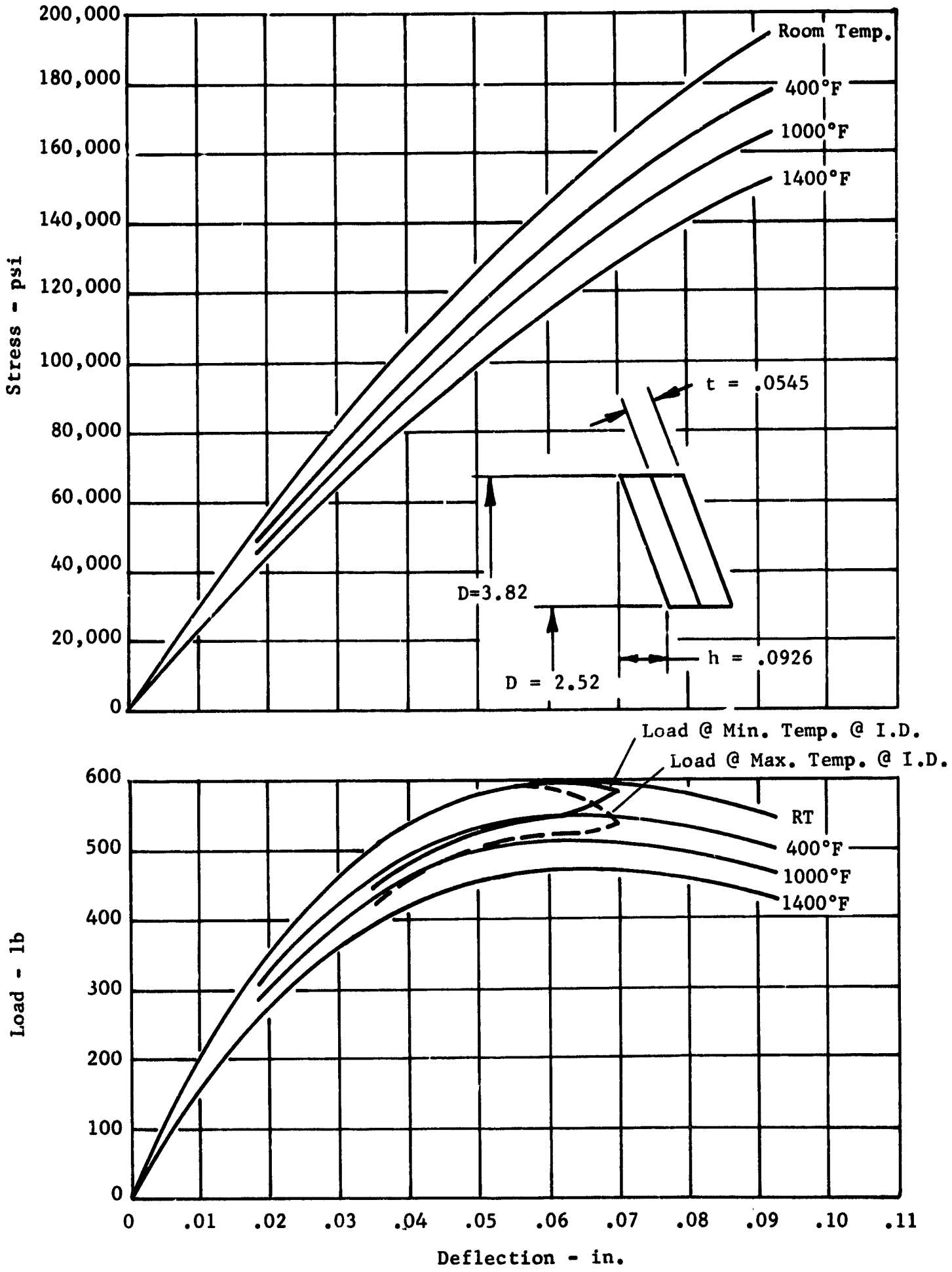

67-0020

Figure 2.4

WLR-23 FLIGHT ENGINE LOAD SUMMARY - SEA LEVEL

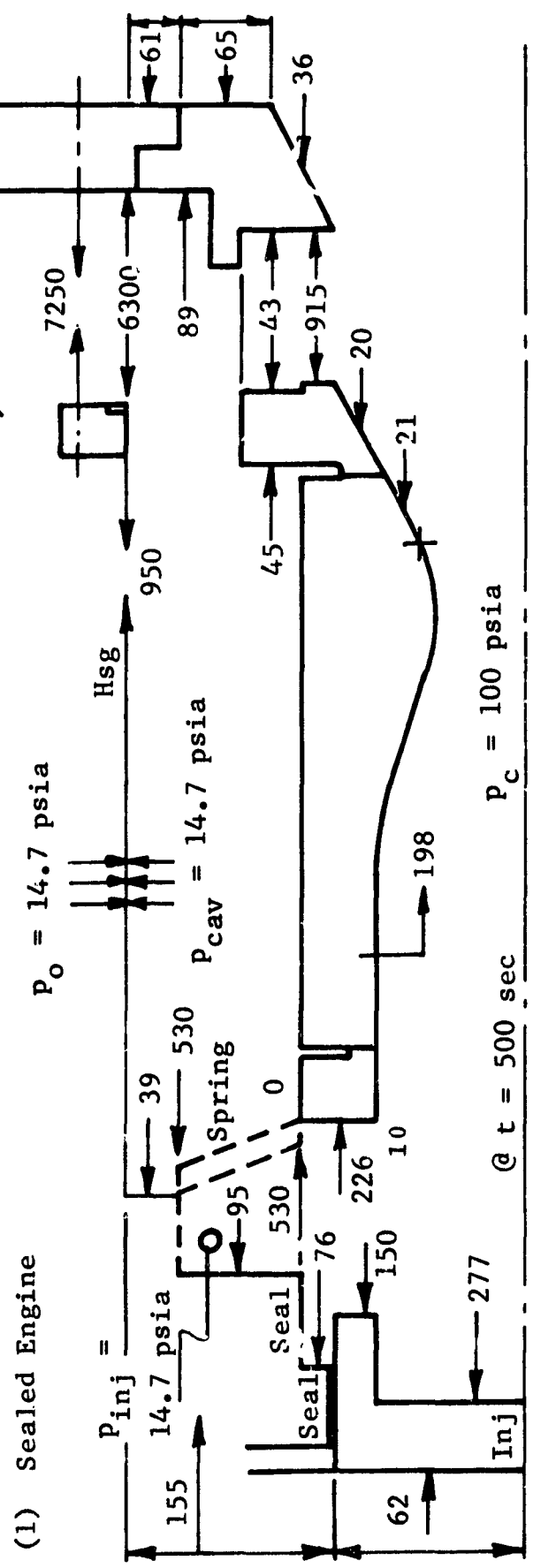

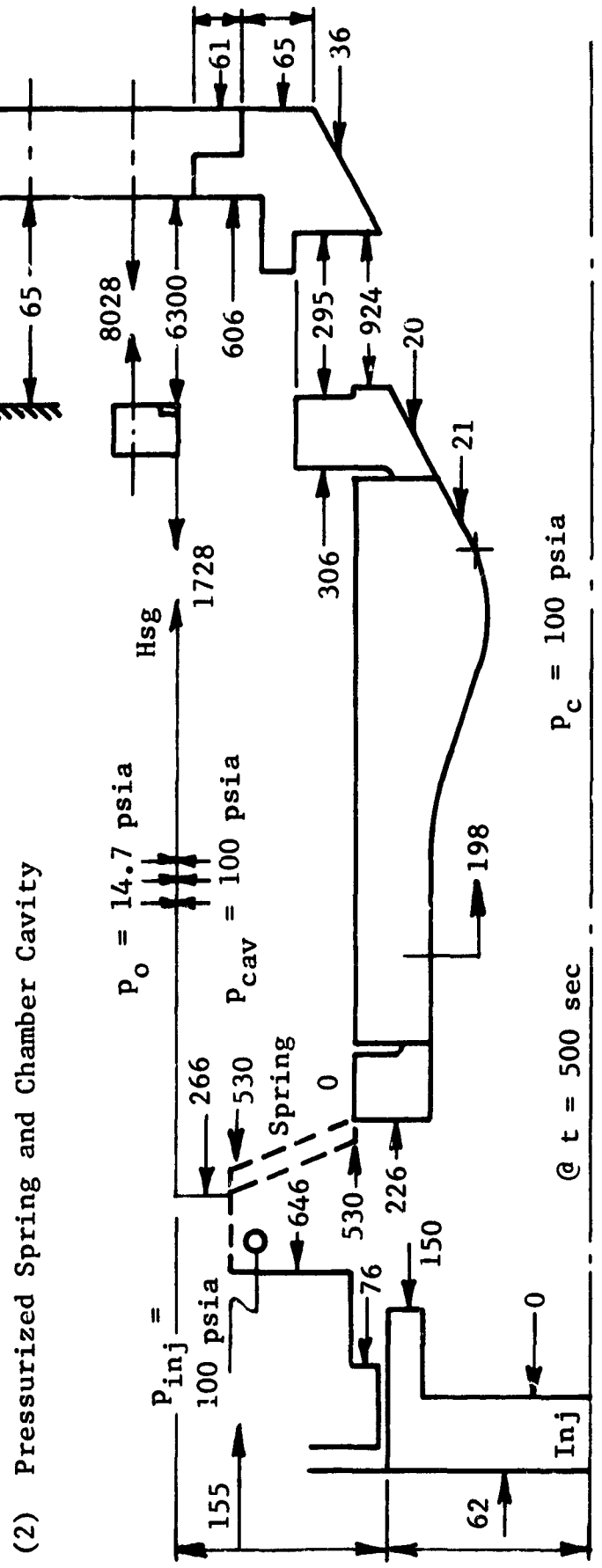

67-0018

Figure 2.5

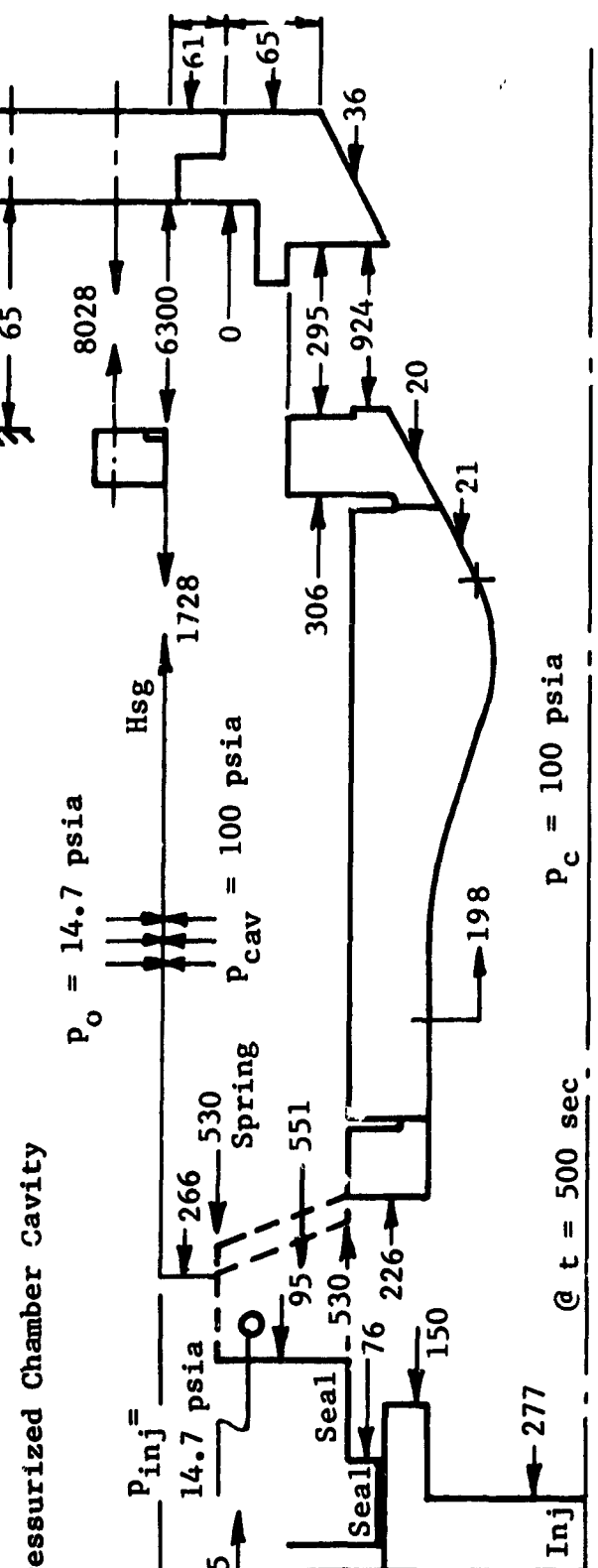

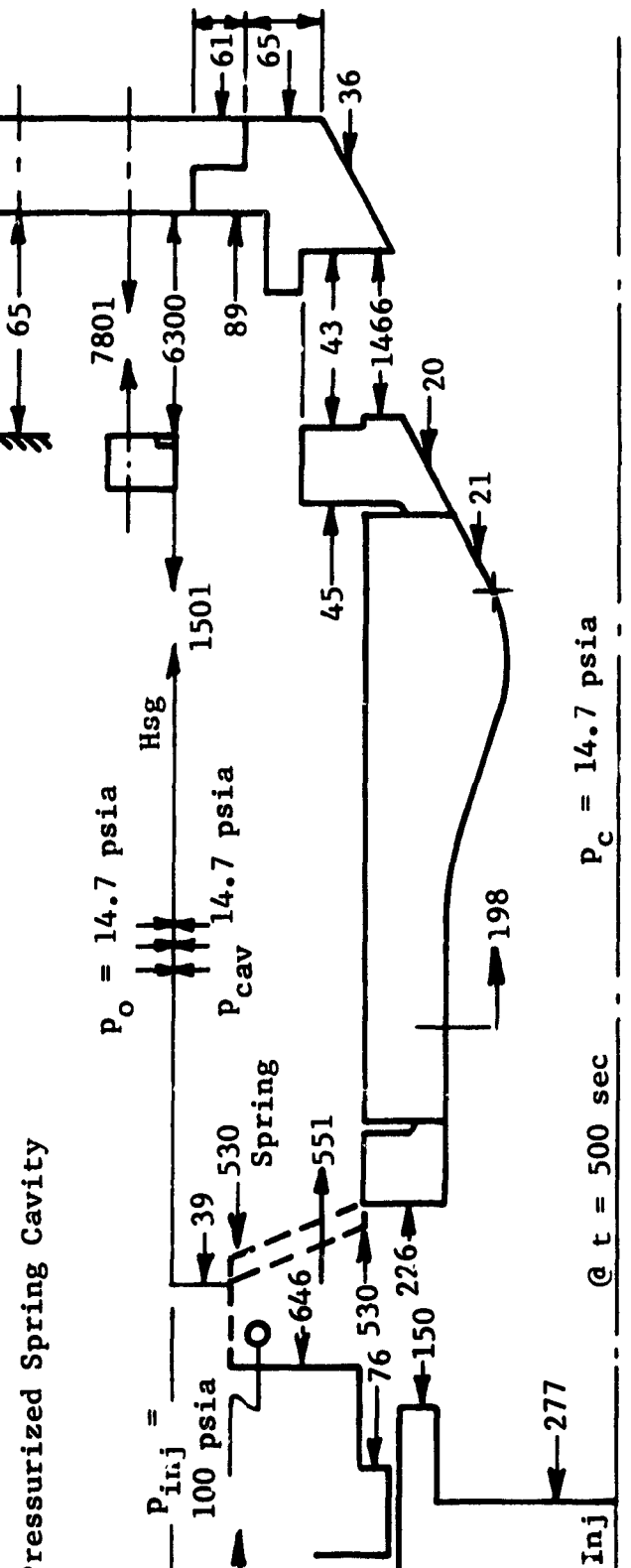

67-0006

Figure 2.6

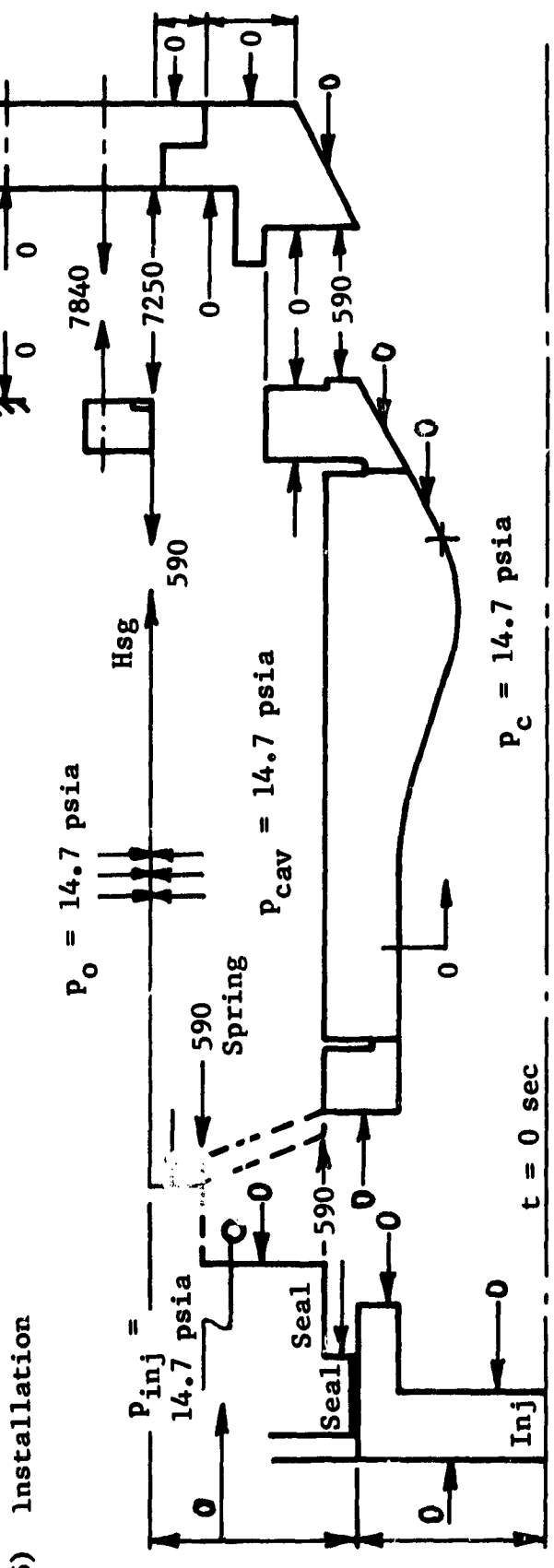

(5) Installation

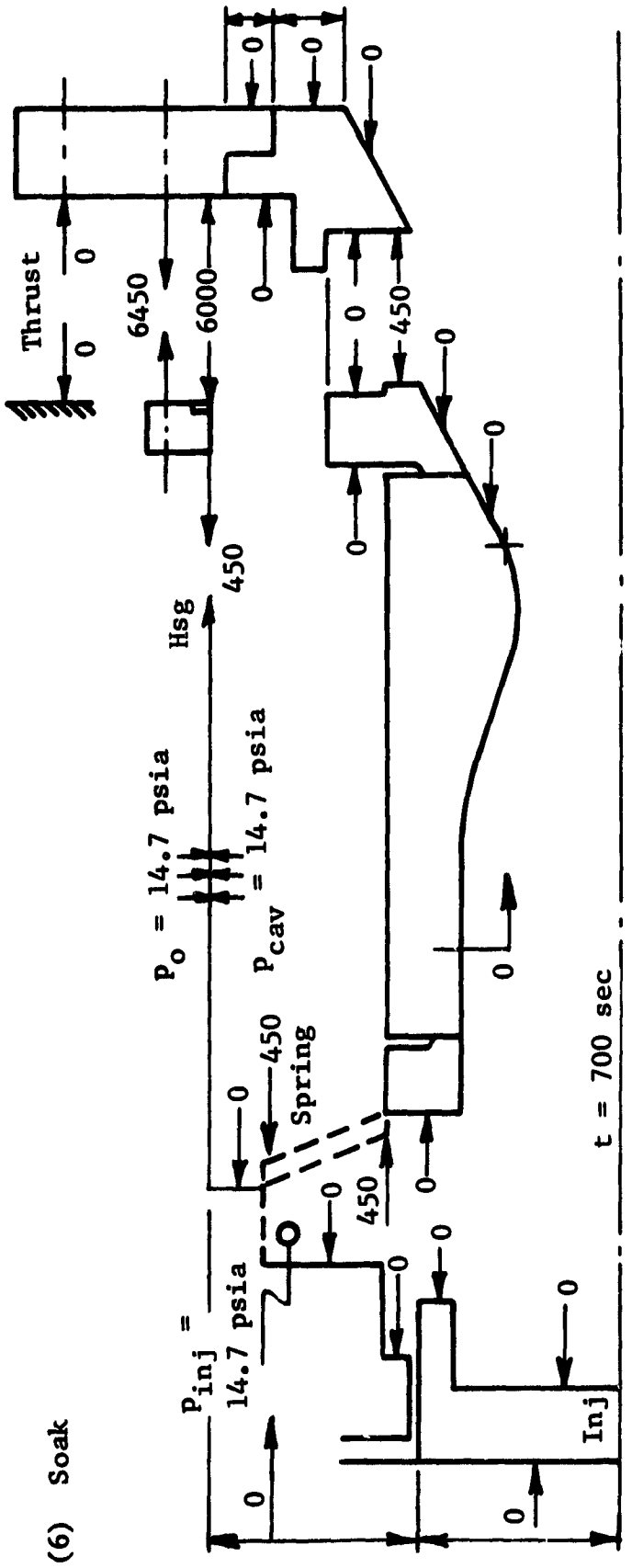

(6) Soak

67-0024

Figure 2.7

WLR-23 FLIGHT ENGINE LOAD SUMMARY - VACUUM, ϵ = 40

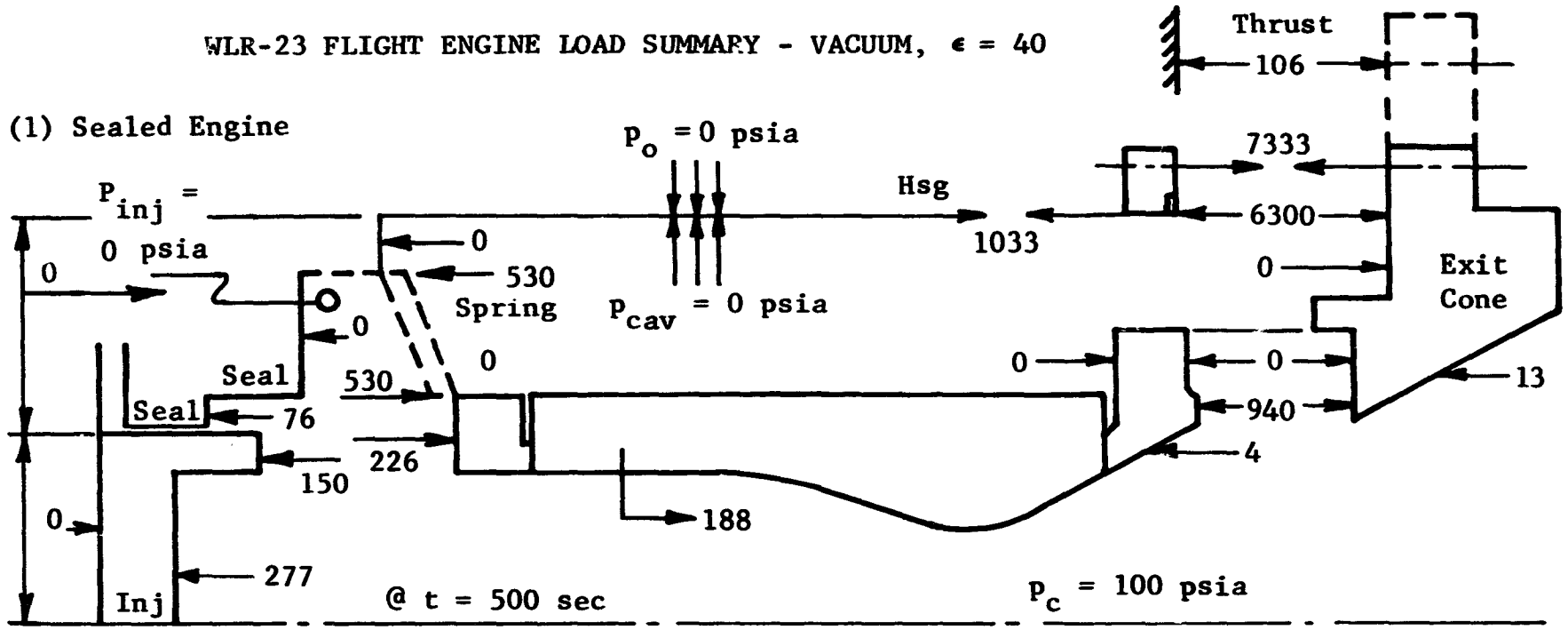

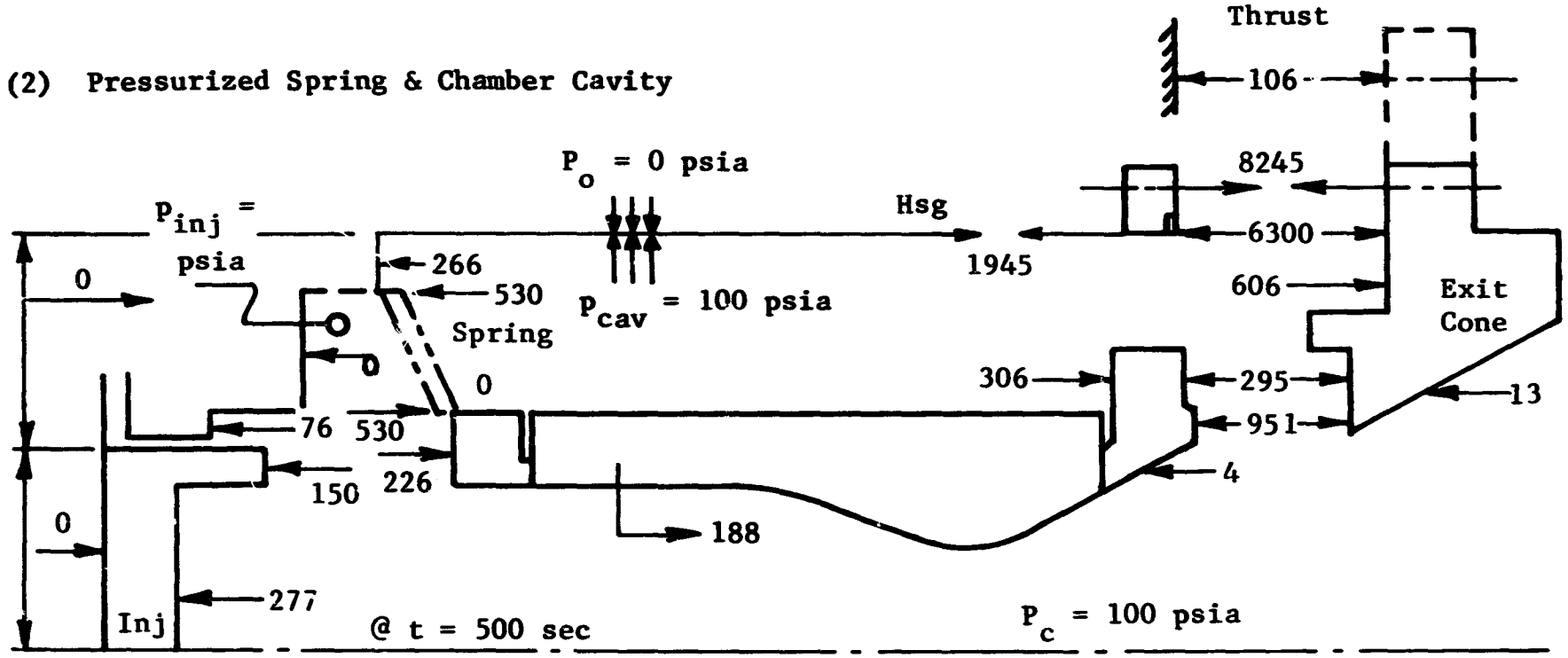

Figure 2.8

(3) Pressurized Chamber Cavity

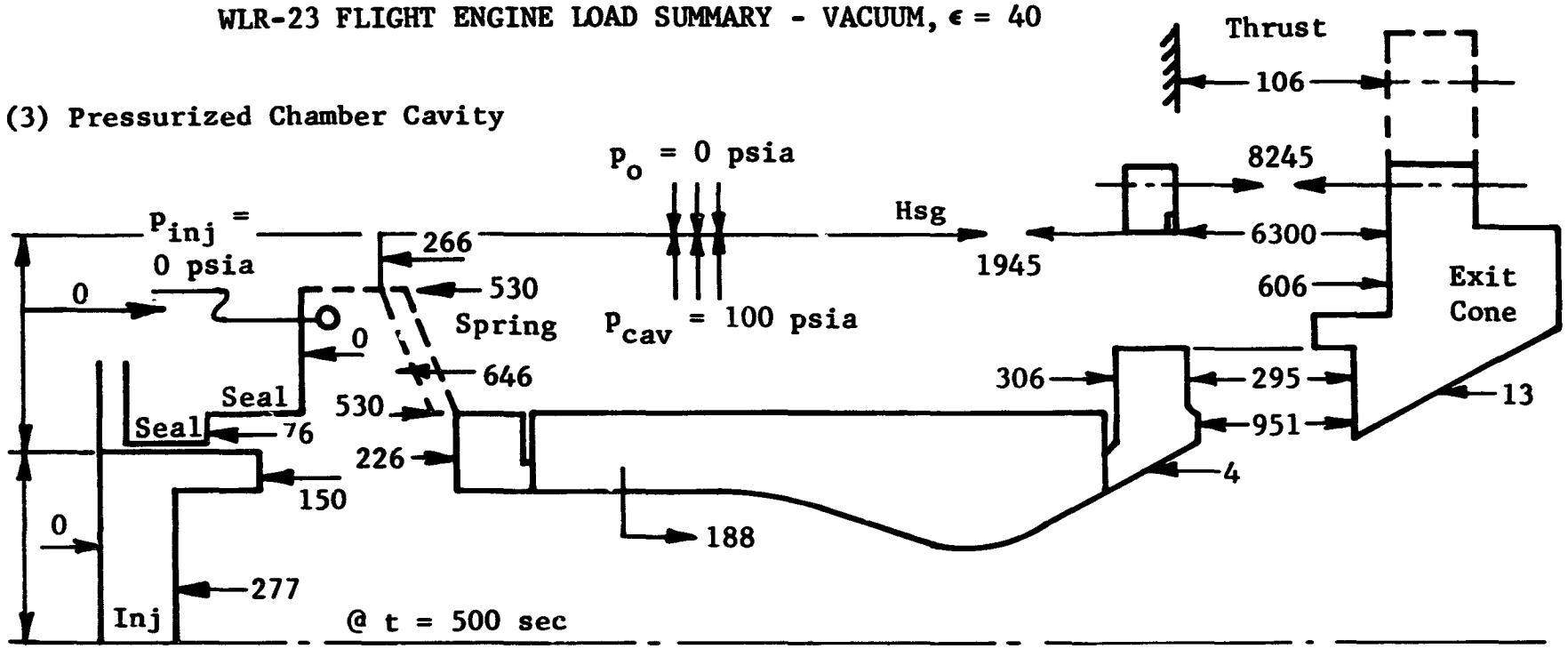

Figure 2.9

(4) Pressurized Spring Cavity

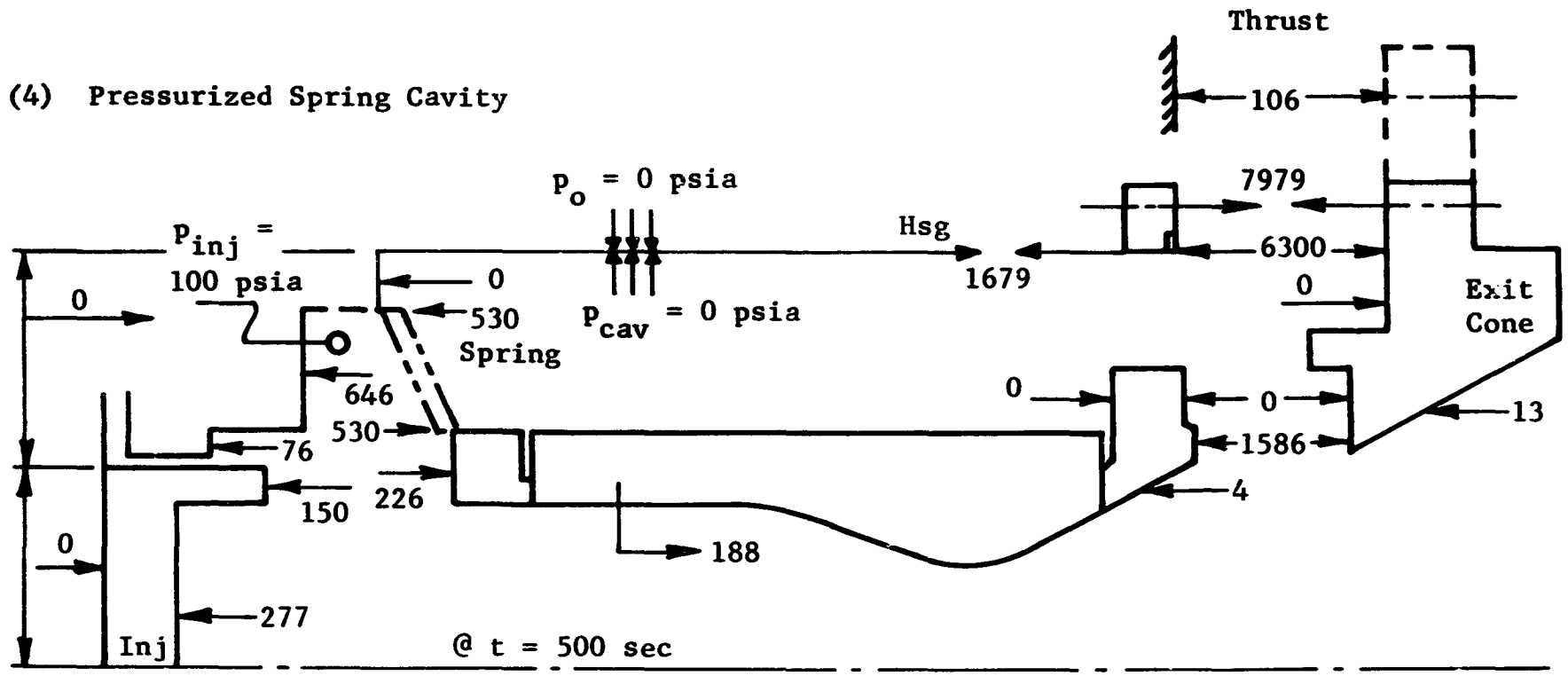

WLR-23 FLIGHT ENGINE LOAD SUMMARY - VACUUM, = 40

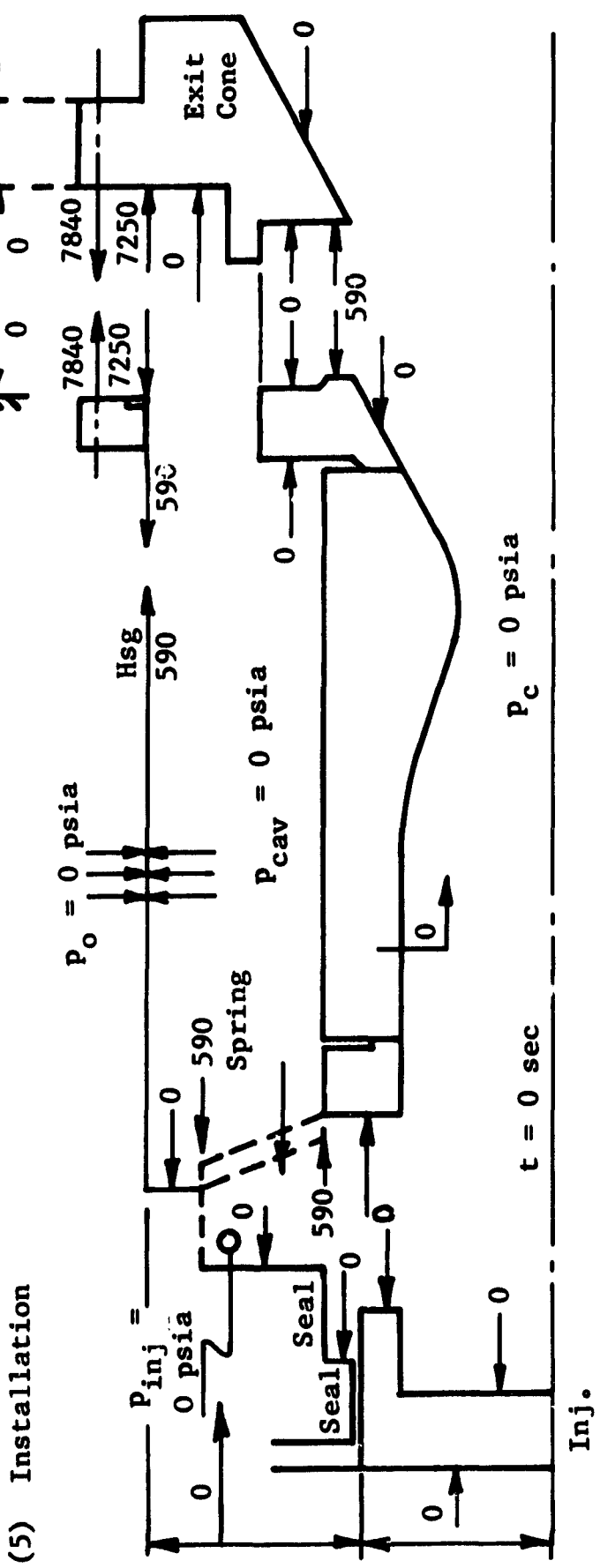

(5) Installation

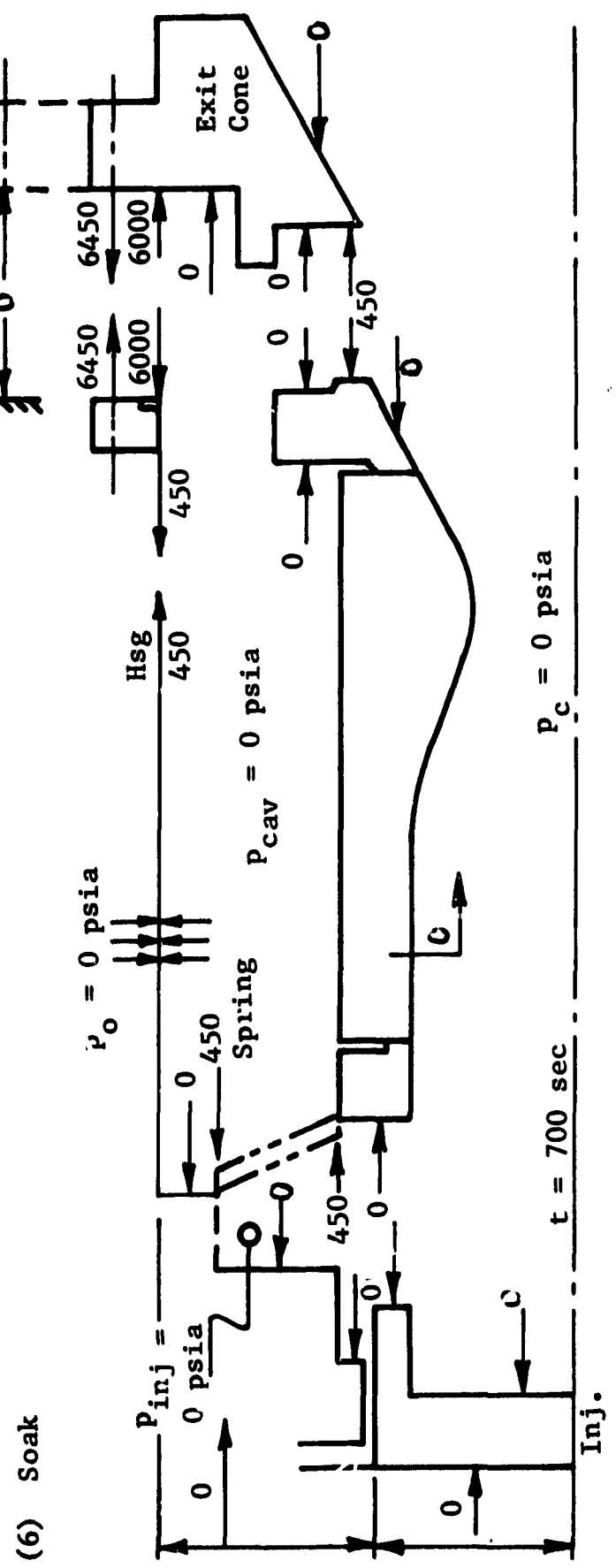

(6) Soak

67-0021

Figure 2.10

WLR-23 FLIGHT ENGINE

Aft Flange Metal O-Ring Clamp Load vs. Temp.

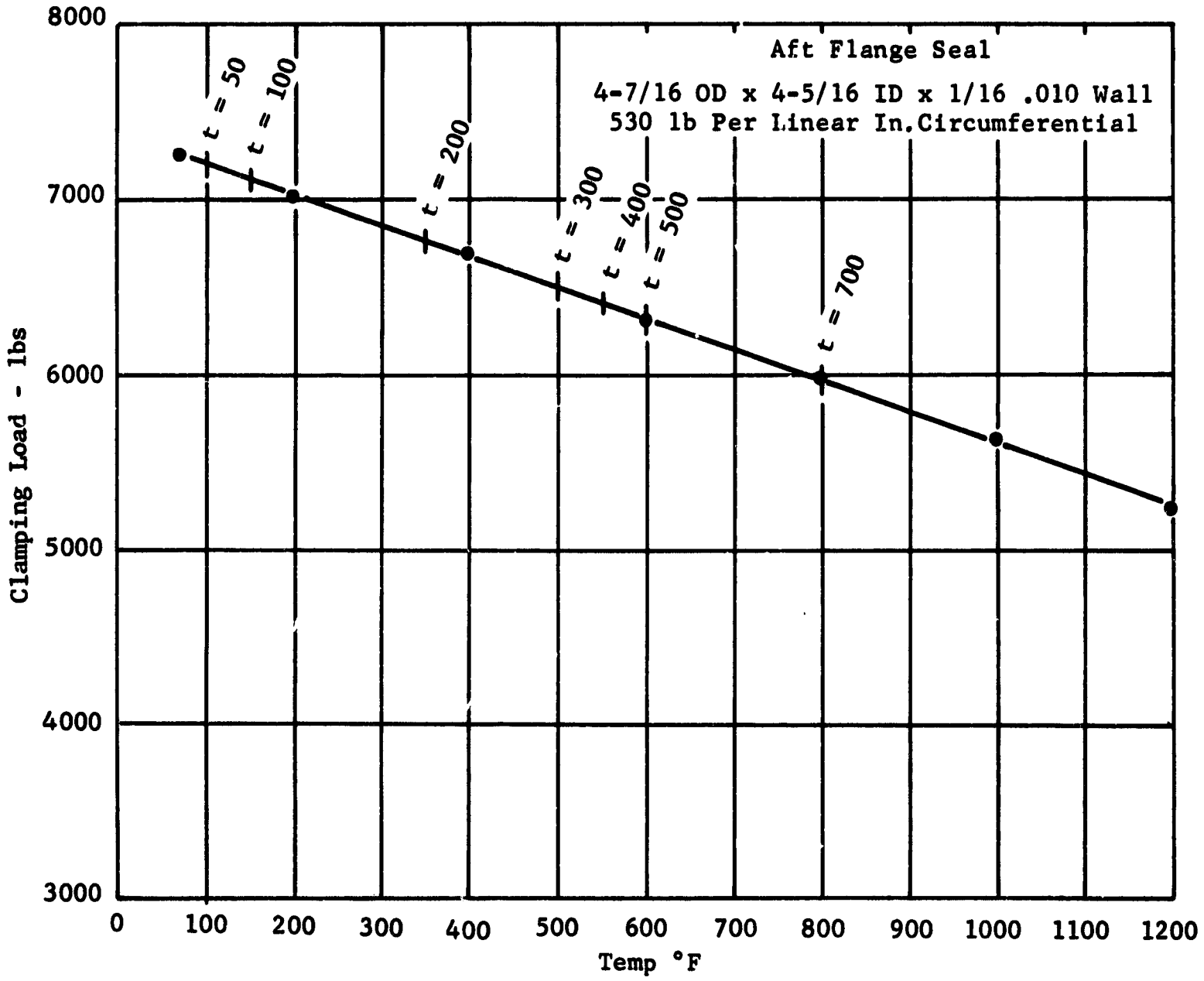

67-0010

Figure 2.11

WLR-23 FLIGHT ENGINE END SEAL LOADS - SEA LEVEL

Without Belleville Load

(1) Sealed Engine

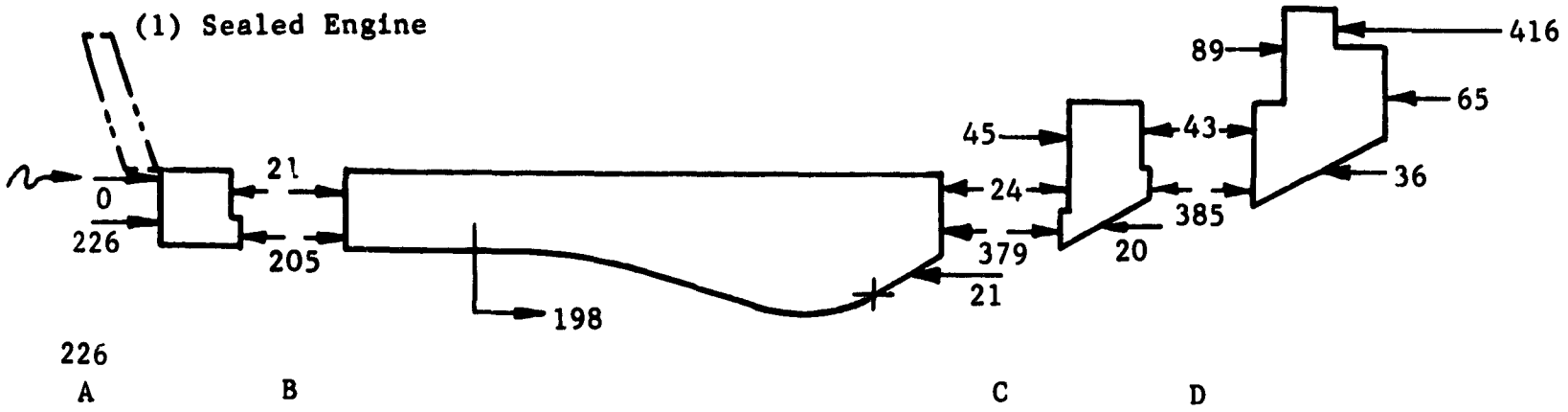

(2) Pressurized Spring and Chamber Cavity

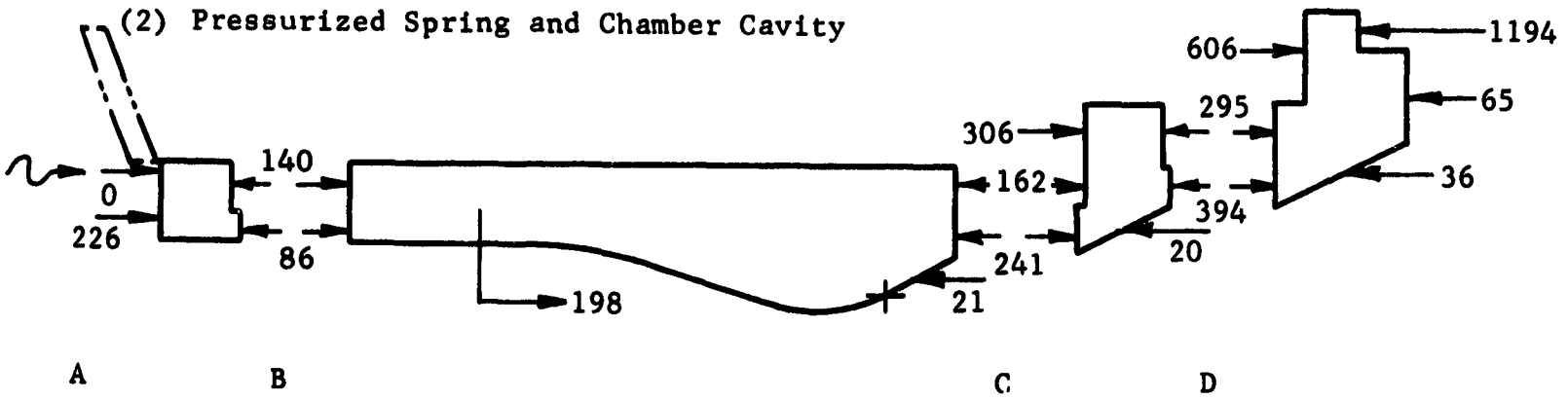

(3) Pressurized Chamber Cavity

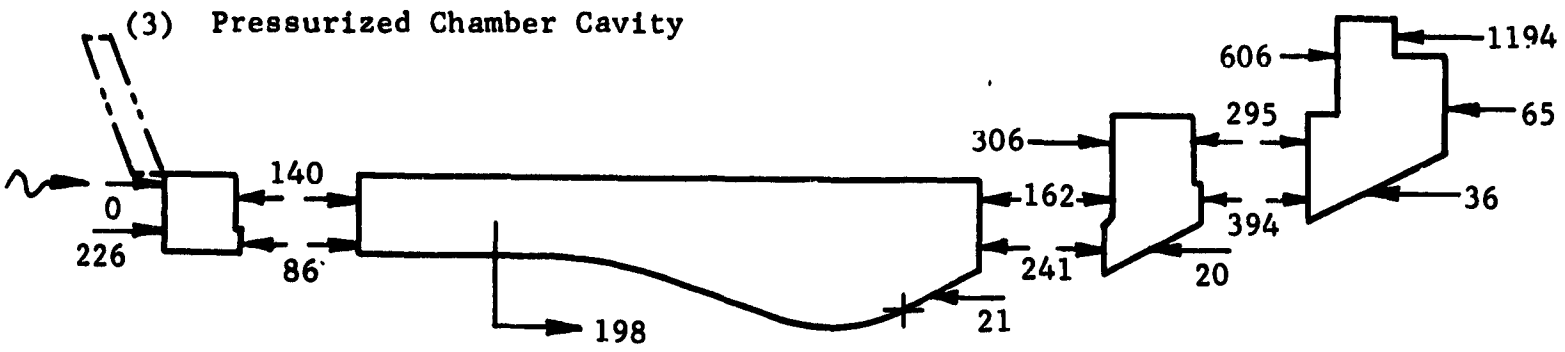

(4) Pressurized Spring Cavity

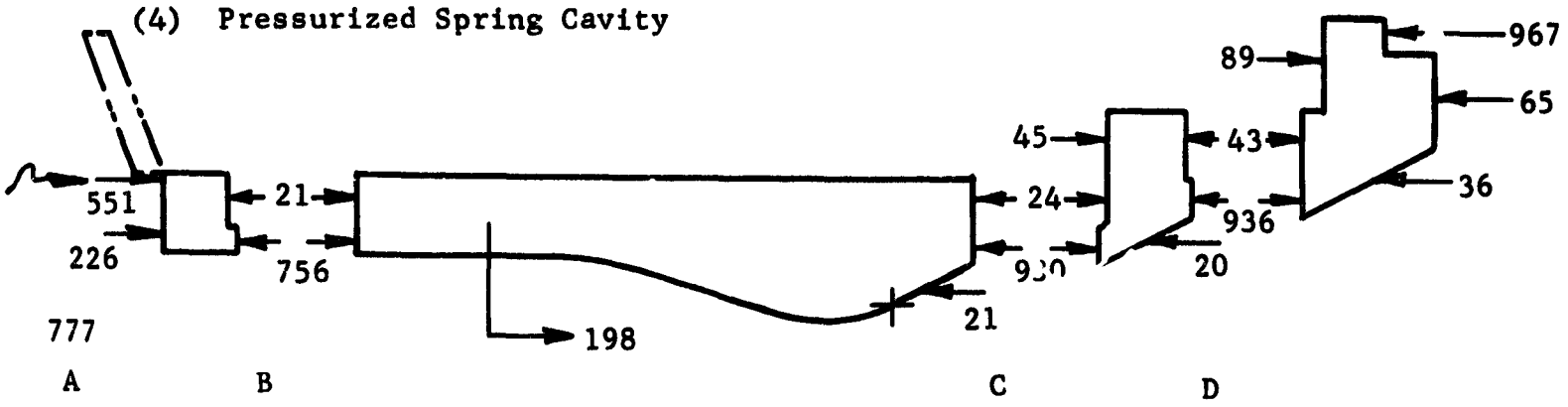

67-0014

Figure 2.12

WLR-23 FLIGHT ENGINE END SEAL LOADS - VACUUM, ϵ = 40

(Without Belleville Load)

(1) Sealed Engine

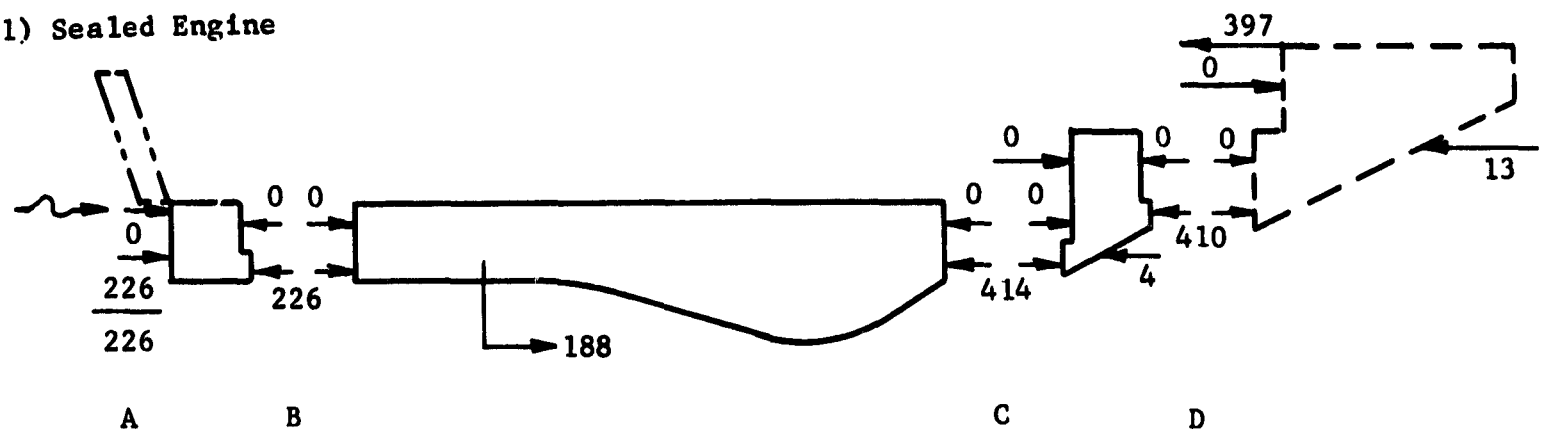

(2) Pressurized Spring and Chamber Cavity

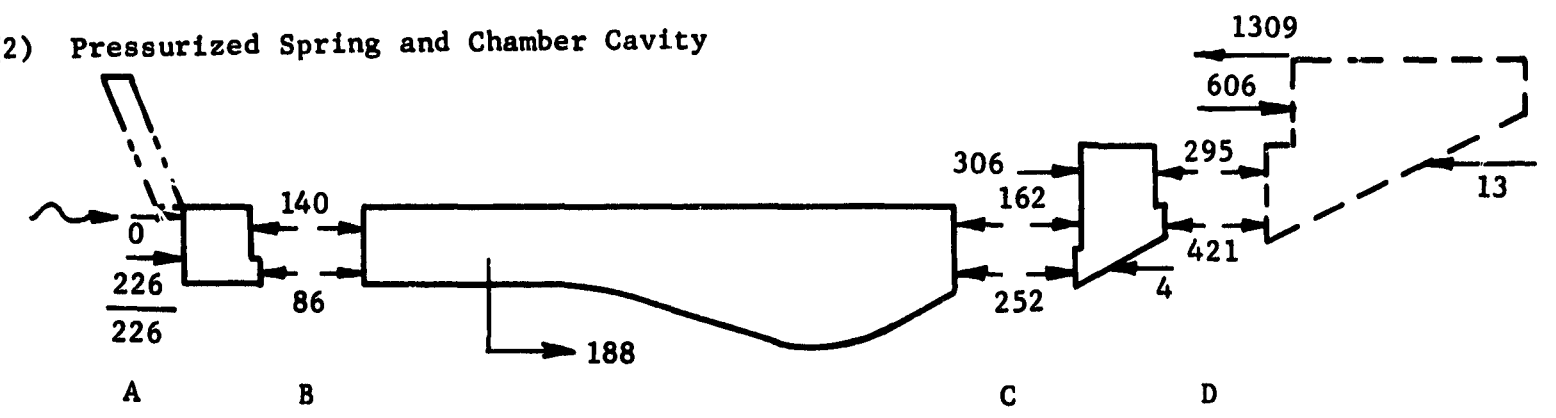

(3) Pressurized Chamber Cavity

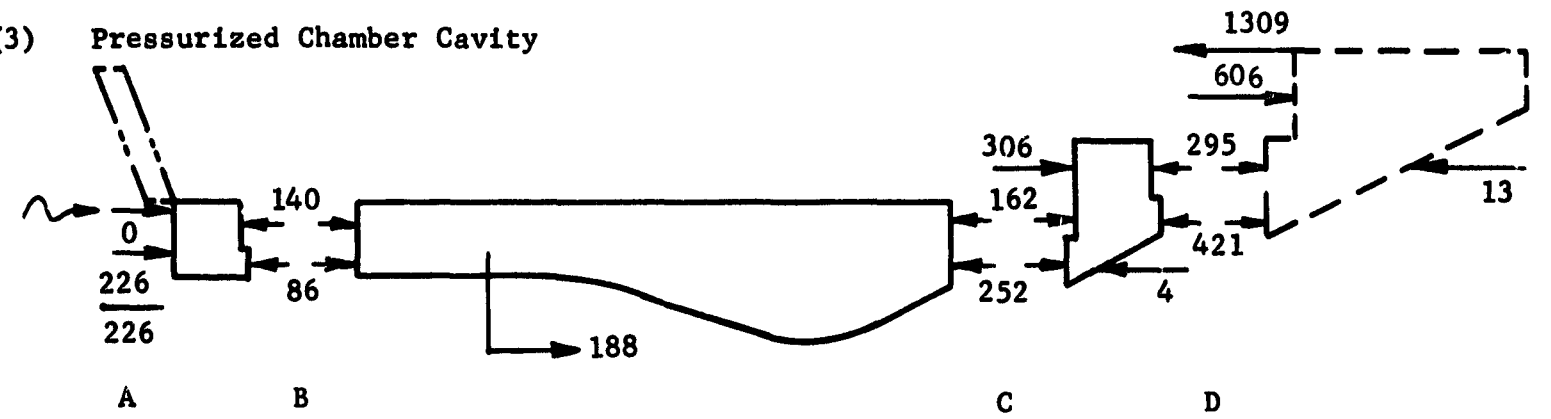

(4) Pressurized Spring Cavity

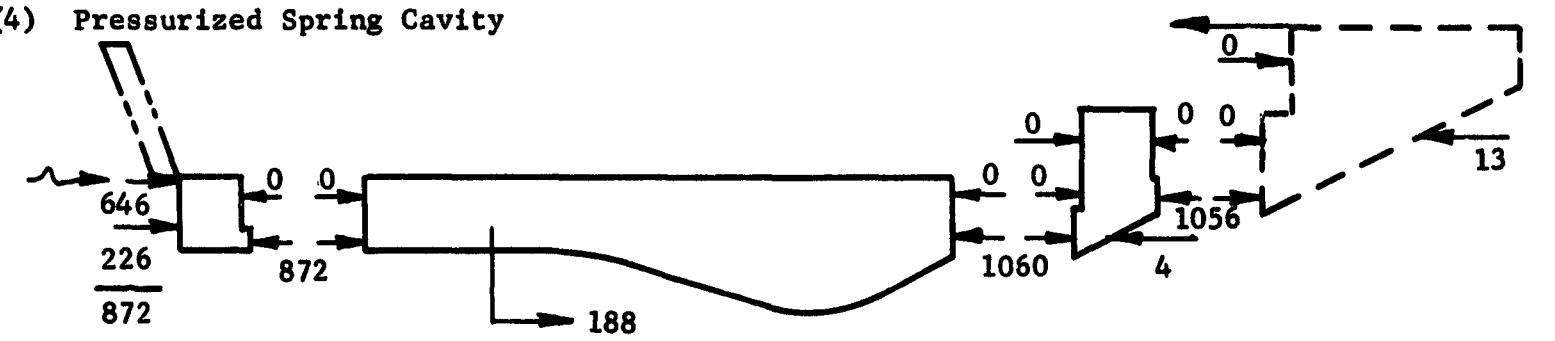

66-1082

Figure 2.13

WLR-23 FLIGHT ENGINE

AXIAL THERMAL GROWTH STUDY

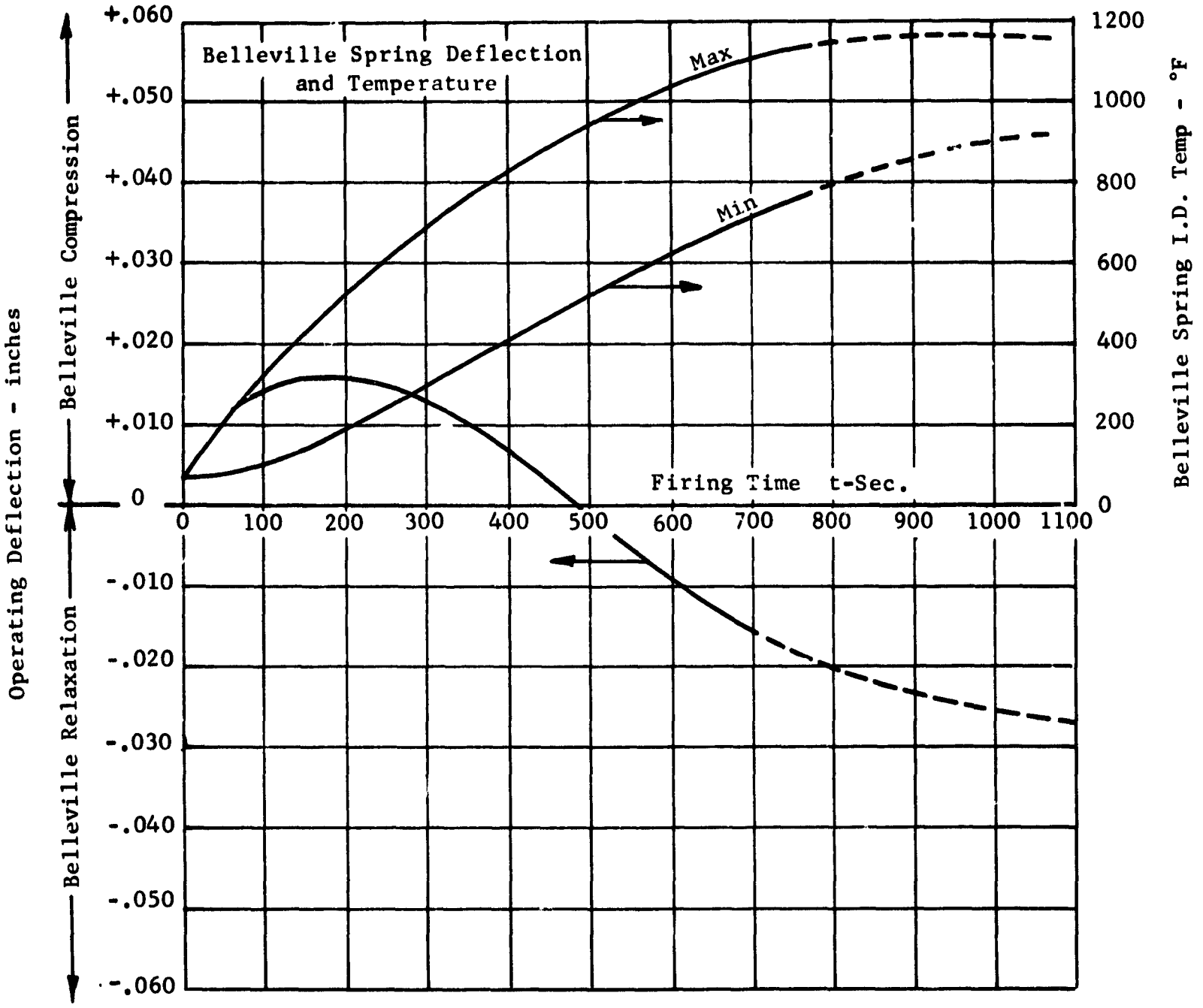

67-0022

Figure 2.14

WLR-23 FLIGHT ENGINE TEMPERATURE DISTRIBUTION

AT 50 SECONDS

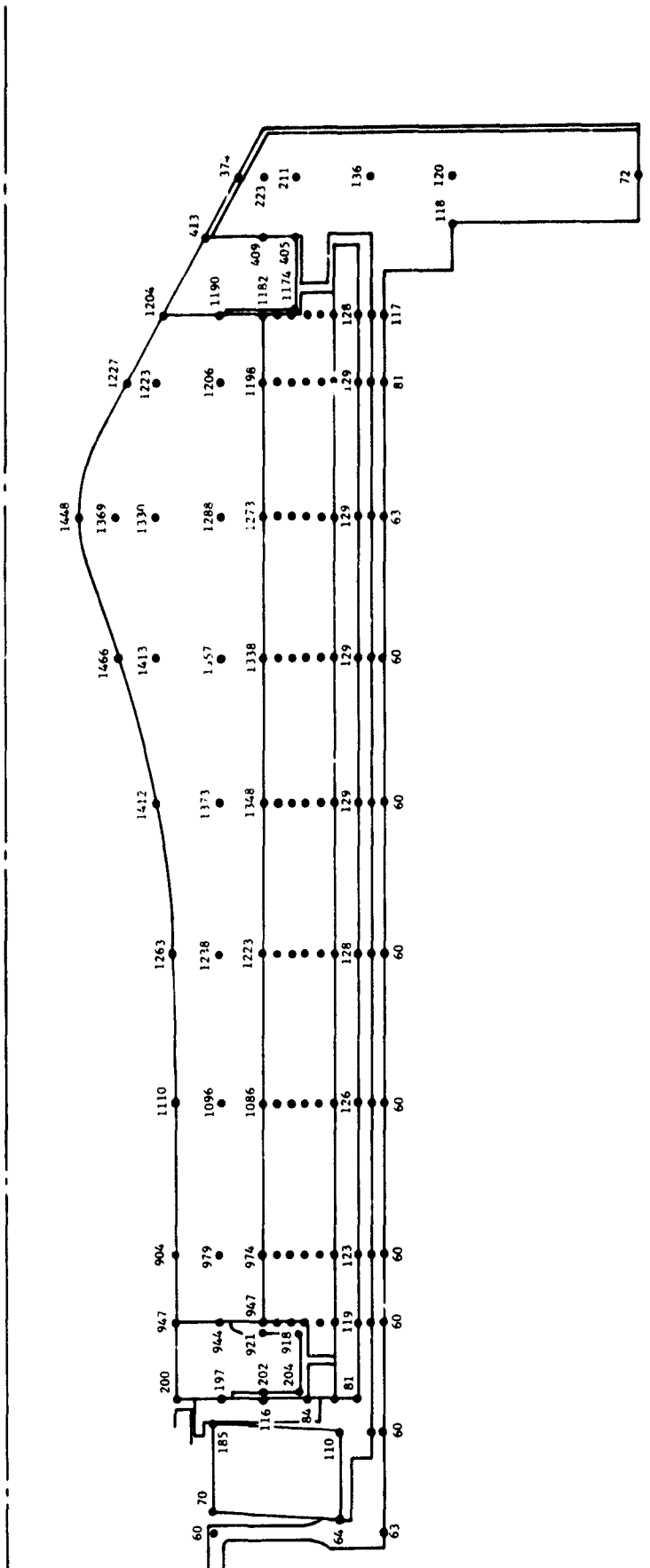

Figure 2.15

WLR-23 FLIGHT ENGINE TEMPERATURE DISTRIBUTION AT 100 SECONDS

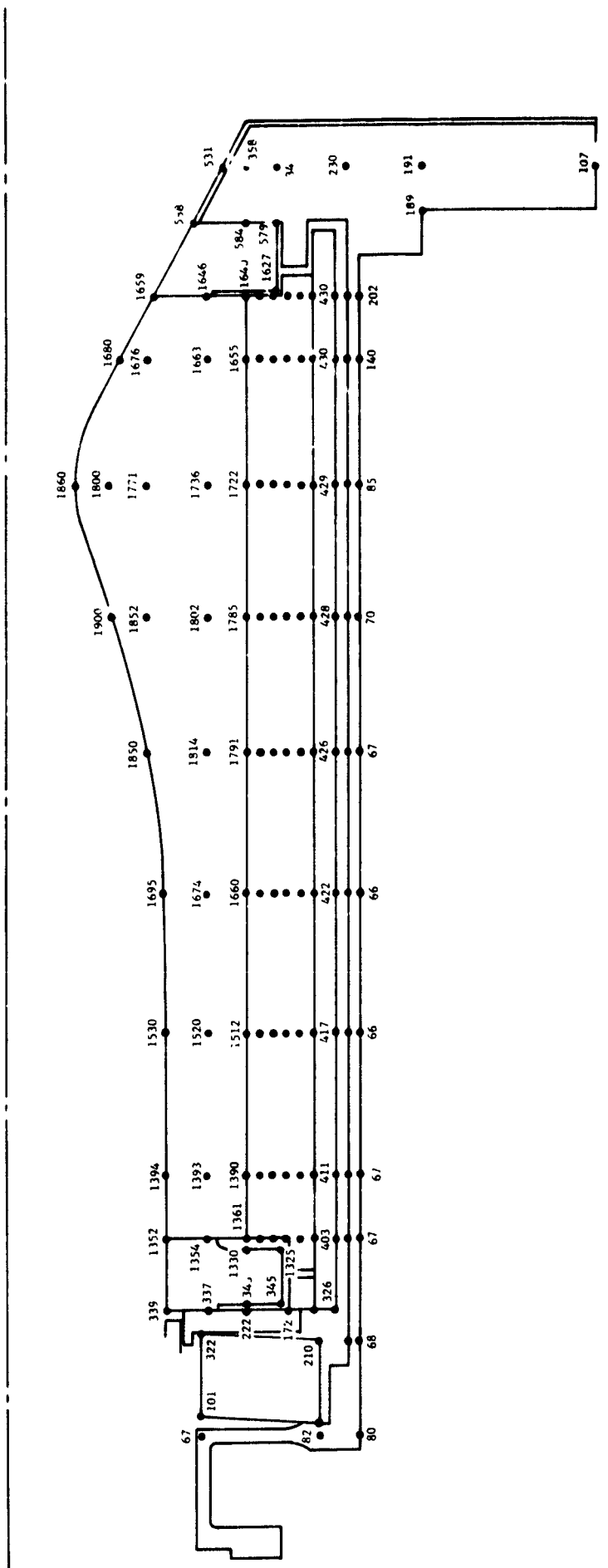

66-1100

Figure 2.16

WLR-23 FLIGHT ENGINE TEMPERATURE DISTRIBUTION

AT 200 SECONDS

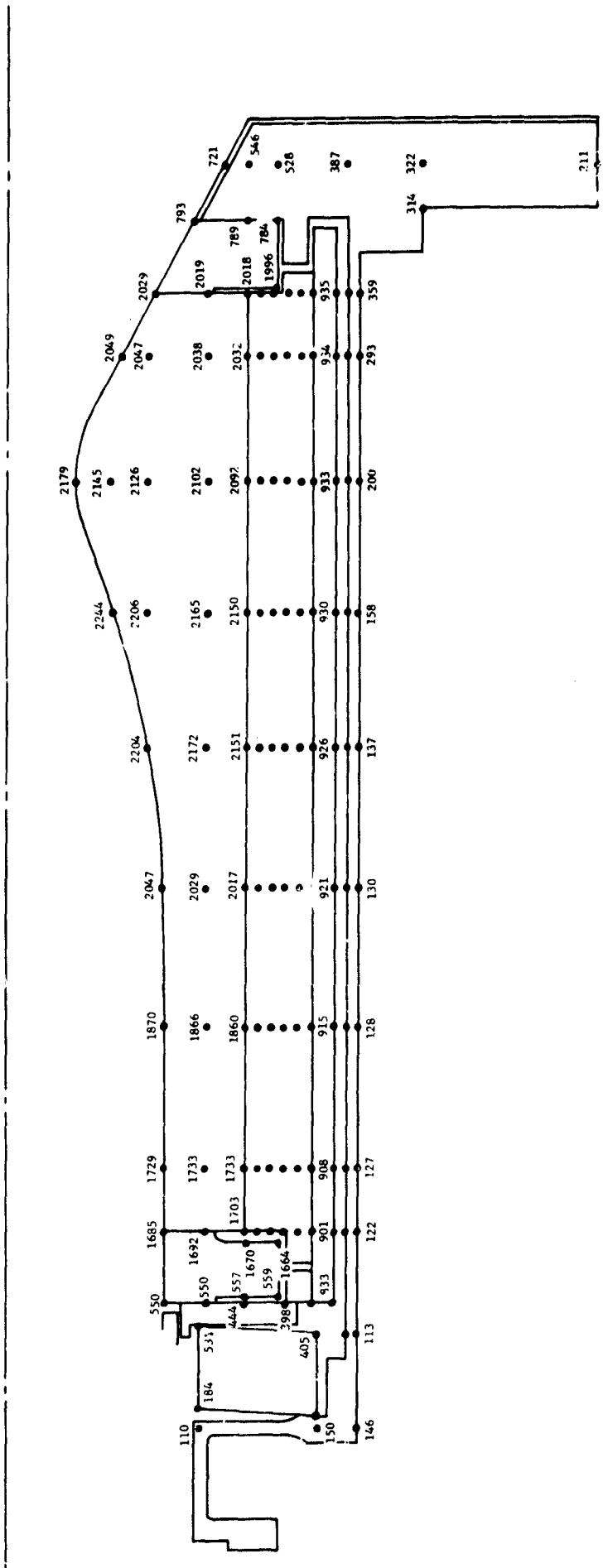

Figure 2.17

WLR-23 FLIGHT ENGINE TEMPERATURE DISTRIBUTION

AT 300 SECONDS

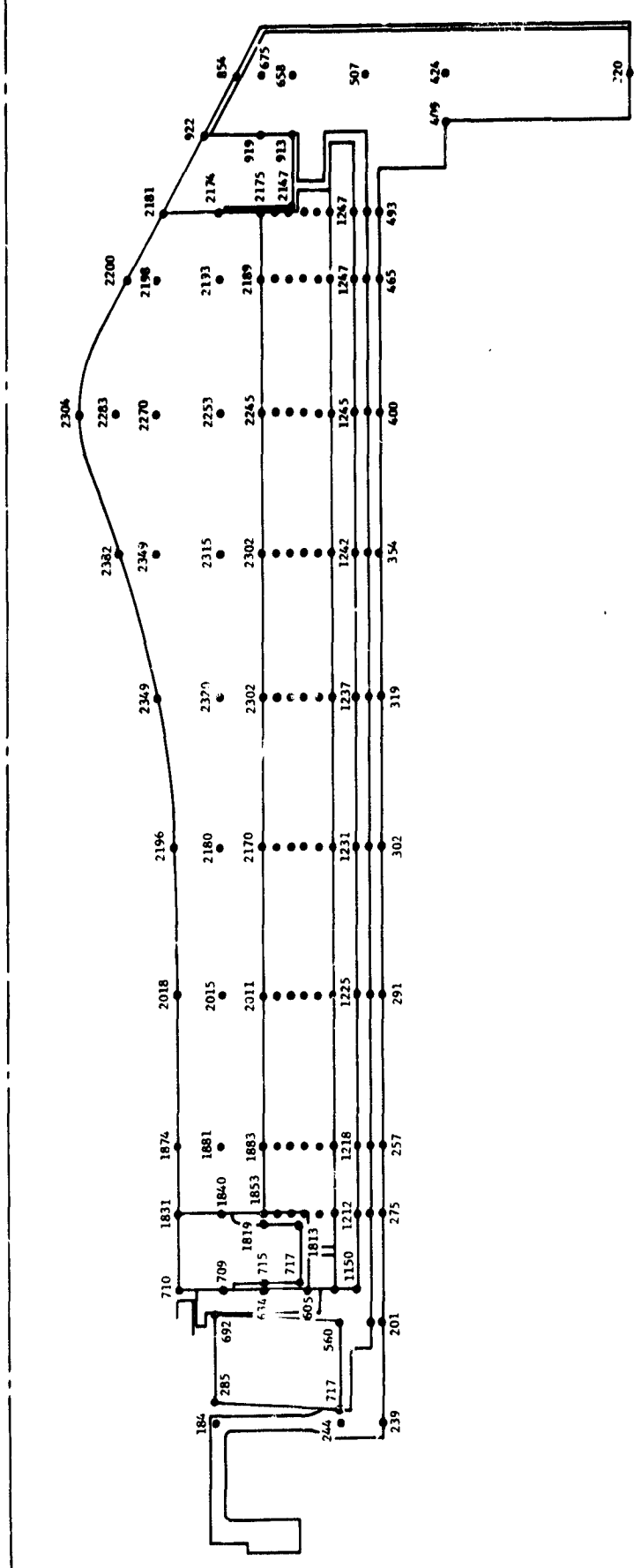

66-1052

Figure 2.18

WLR-23 FLIGHT ENGINE TEMPERATURE DISTRIB'TION AT 400 SECONDS

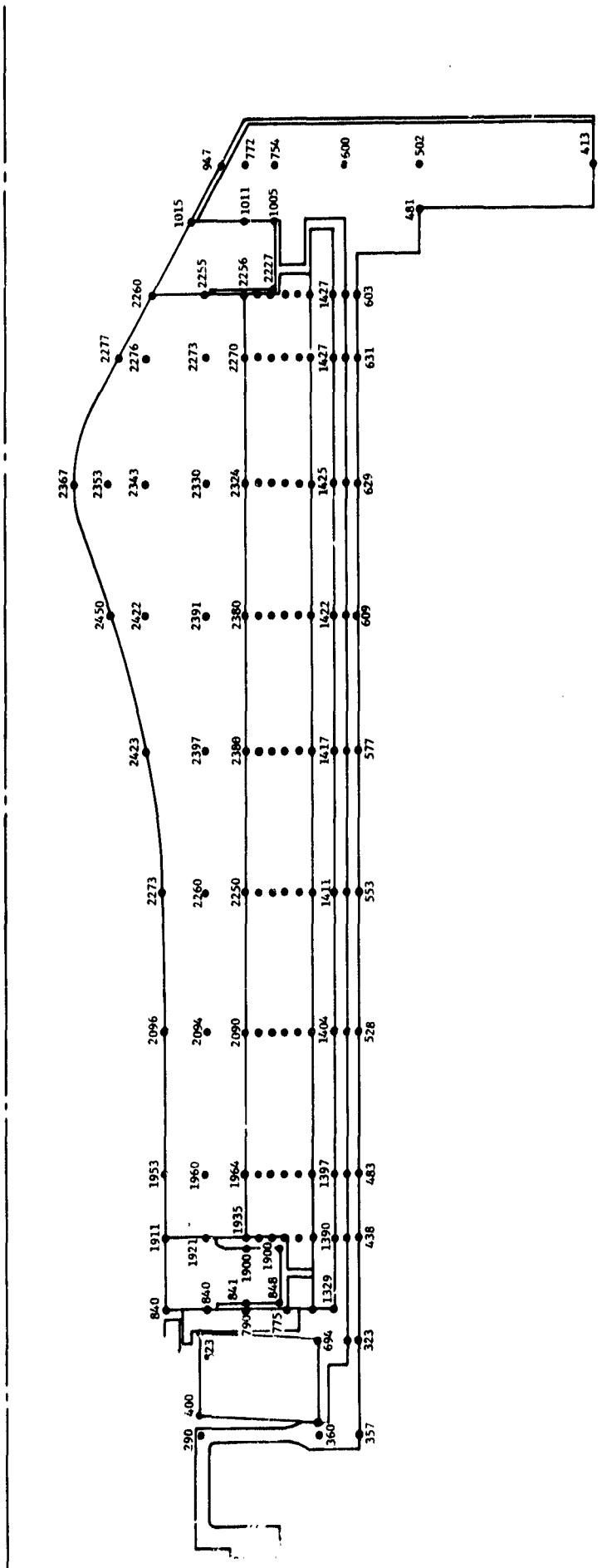

66-1070

Figure 2.19

WLR-23 FLIGHT ENGINE TEMPERATURE DISTRIBUTION AT 500 SECONDS

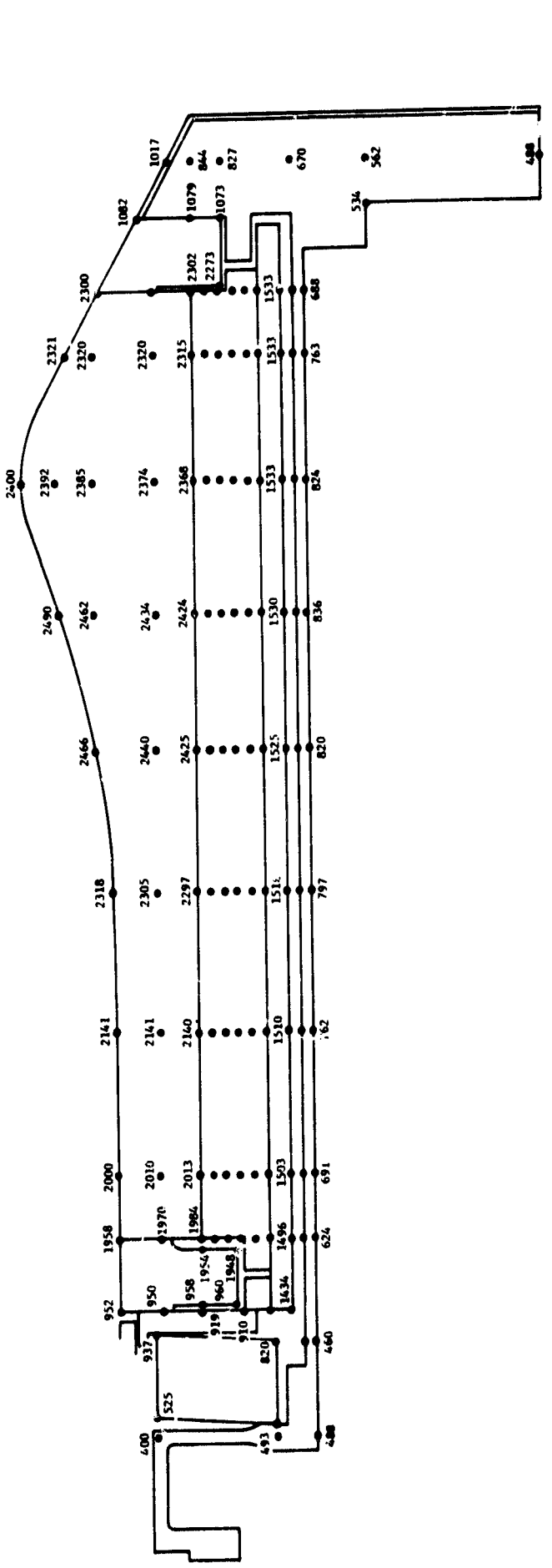

Figure 2.20

WLR-23 FLIGHT ENGINE TEMPERATURE DISTRIBUTION AT 700 SECONDS

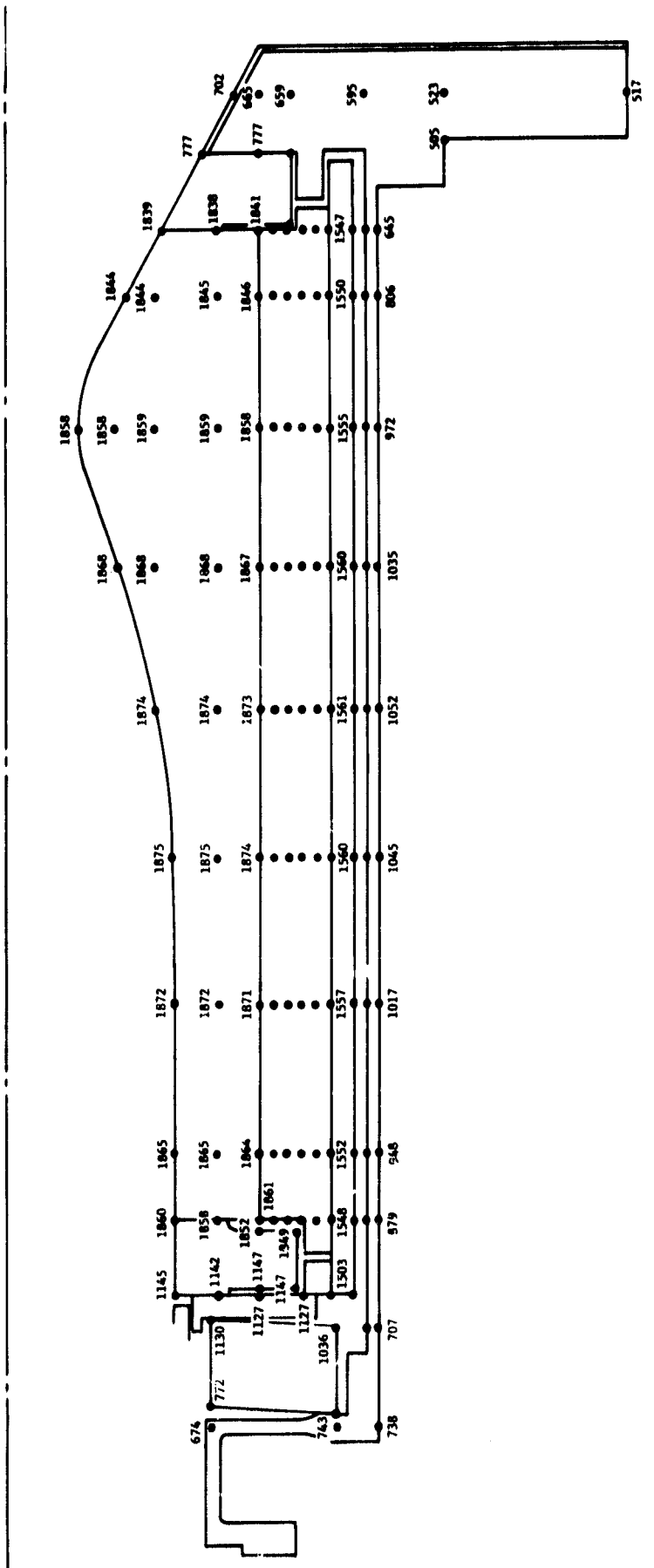

66-1088

Figure 2.21

WLR-23 FLIGHT HOUSING AND AFT RETAINER TEMPERATURES - °F

Time - Sec	1	2	3	4	5	6	7	8	9	10	11	12	13	14	15	16	17
0	60	60	60	60	60	60	60	60	60	60	60	60	60	60	60	60	60
50	60	60	64	63	60	60	60	60	60	60	60	63	81	117	72	120	300
100	67	67	82	80	68	67	67	66	66	67	70	85	140	202	107	190	420
200	80	110	140	130	100	100	100	100	100	100	120	160	250	310	211	320	600
300	100	160	220	210	180	230	250	270	270	290	320	360	425	450	320	420	750
400	190	290	360	357	323	400	430	440	450	480	510	530	530	500	413	500	850
500	250	350	493	488	460	600	650	650	700	720	740	840	660	590	488	540	900
700	500	570	640	640	600	780	900	900	900	900	900	900	806	645	507	520	700

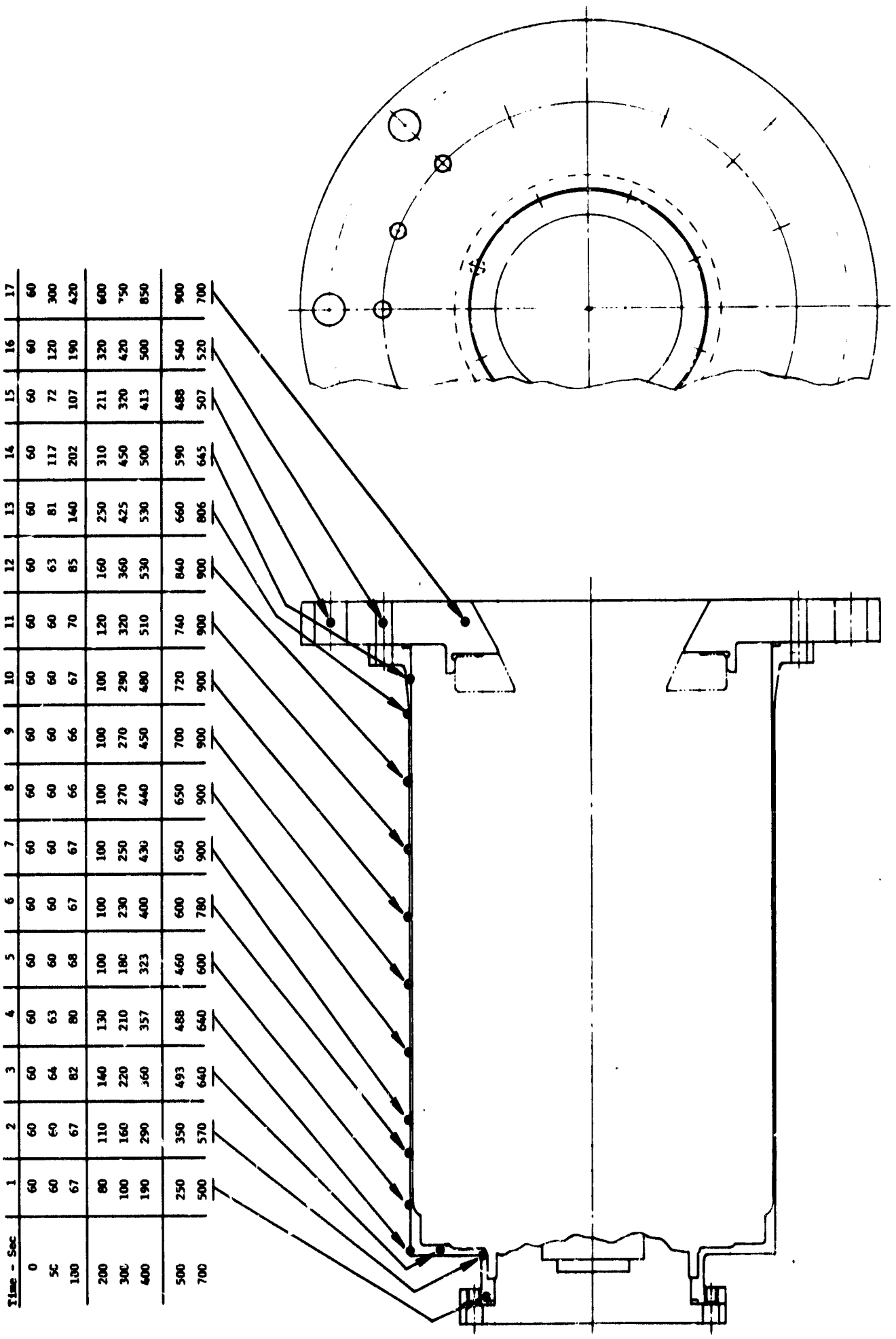

67-0015

Figure 2.22

FLIGHT ENGINE END SEAL LOAD AND STRESS SUMMARY - SEA LEVEL

1. Sealed Engine

Sealing Sect.	Shoe-Front Washer Interface					Front Washer Wedge Interface				
Time -sec	@ Inst.	@ Start-up	200	500	700 soak	@ Inst.	@ Start-up	200	500	700 soak
Aero Load lbs	0	118	118	118	0	0	205	205	205	0
B'ville Load -lbs	590	590	580	530	450	590	590	580	530	450
Total Load -lbs	590	708	698	648	450	590	795	785	735	450
Seal Height -in	.092	.092	.092	.092	.092	.125	.125	.104	.100	.125/.100
Bear. Area $-in^2$	.708	.708	.708	.708	.708	.795	.795	.666	.641	.795/.641
Bearing Stress-psi	832	1000	985	915	636	744	1000	1175	1145	566/701

Sealing Sect.	Wedge-Rear Washer Interface					Rear Washer-Aft Retainer Interface				
Time -sec	@ Inst.	@ Start-up	200	500	700	@ Inst.	@ Start-up	200	500	700
Aero Load -lbs	0	379	379	379	0	0	385	385	385	0
B'ville Load -lbs	590	590	580	530	450	590	590	580	530	450
Total Load -lbs	590	969	959	909	450	590	975	965	915	450
Seal Height -in	.157	.157	.136	.132	.157/.132	.126	.126	.126	.126	.126
Bearing Area $-in^2$	.969	.969	.844	.820	.969/.820	.975	.975	.975	.975	.975
Bearing Stress-psi	609	1000	1136	1109	465/549	605	1000	991	939	461

Figure 2.23

WLR23

FLIGHT ENGINE END SEAL LOAD AND STRESS SUMMARY - SEA LEVEL

2. Pressurized Spring and Chamber Cavity
3. Pressurized Chamber Cavity

Sealing Sect.		Shoe-Front Washer Interface					Front Washer Wedge Interface				
Time	-sec	@ Inst.	@ Start-up	200	500	700	@ Inst.	@ Start-up	200	500	700
Aero Load	-lbs	0	118	118	118	0	0	86	86	86	0
B'ville Load	-lbs	590	590	580	530	450	590	590	580	530	450
Total Load	-lbs	590	708	698	648	450	590	676	666	616	450
Seal Height	-in	.092	.092	.092	.092	.092	.125	.125	.104	.100	.125/.100
Bear. Area	-in^2	.708	.708	.708	.708	.708	.795	.795	.666	.641	.795/.641
Bearing Stress	-psi	832	1000	986	915	636	744	850	1000	960	576/702

Sealing Sect.		Wedge-Rear Washer Interface					Rear Washer-Aft Retainer Interface				
Time	-sec	Inst.	Start-up	200	500	700	Inst.	Start-up	200	500	700
Aero Load	-lbs	0	241	241	241	0	0	394	394	394	0
B'ville Load	-lbs	590	590	580	530	450	590	590	580	530	450
Total Load	-lbs	590	831	821	771	450	590	984	974	924	450
Seal Height	-in	.157	.157	.136	.132	.157/.132	.126	.126	.126	.126	.126
Bear. Area	-in^2	.969	.969	.844	.820	.969/.820	.975	.975	.975	.975	.975
Bearing Stress	-psi	610	860	974	941	465/549	605	1010	999	947	461

Figure 2.24

WLR23

FLIGHT ENGINE END SEAL LOAD AND STRESS SUMMARY - SEA LEVEL

4. Pressurized Spring Cavity

Sealing Sect.		Shoe-Front Washer Interface					Front Washer - Wedge Interface				
Time	-sec	@ Inst.	@ Start-up 551	200	500	700	@ Inst.	@ Start-up	200	500	700
Aero Load	-lbs	0	118	669	669	0	0	756	756	756	0
B'ville Load	-lbs	590	590	580	530	450	590	590	580	530	450
Total Load	-lbs	590	1259	1249	1199	450	590	1346	1336	1286	450
Seal Height	-in	.092	.092	.092	.092	.092	.125	.125	.104	.100	.125/.100
Bear. Area	-in^2	.708	.708	.708	.708	.708	.795	.795	.666	.641	.795/.641
Bearing Stress	-psi	835	1780	1765	1695	636	742	1690	2000	2000	566/701

Sealing Sect		Wedge-Rear Washer Interface					Rear Washer-Aft Retainer Interface				
Time	-sec	@ Inst.	@ Start-up	200	500	700	@ Inst.	@ Start-up	200	500	700
Aero Load	-lbs	0	930	930	930	0	0	936	936	936	0
B'ville Load	-lbs	590	590	580	530	450	590	590	580	530	450
Total Load	-lbs	590	1520	1510	1460	450	590	1526	1516	1466	450
Seal Height	-in	.157	.157	.136	.132	.157/.132	.126	.126	.126	.126	.126
Bear. Area	-in^2	.969	.969	.844	.820	.969/.820	.975	.975	.975	.975	.975
Bearing Stress	-psi	610	1570	1790	1820	469/550	606	1555	1552	1510	462

Figure 2.25

WLR23

FLIGHT ENGINE END SEAL LOAD AND STRESS SUMMARY - VACUUM, $\epsilon = 40$

1. Sealed Engine

Sealing Sect.	Shoe-Front Washer Interfacc					Front Washer - Wedge Interface				
Time -sec	@ Inst.	@ Start-up	200	500	700	@ Inst.	@ Start-up	200	500	700
Aero Load -lbs	0	118	118	118	0	0	226	226	226	0
B'ville Load -lbs	590	590	580	530	450	590	590	580	530	450
Total Load -lbs	590	708	698	648	450	590	816	806	756	450
Seal Height -in	.092	.092	.092	.092	.092	.125	.125	.104	.100	.125/.100
Bear. Area -in^2	.708	.708	.708	.708	.708	.795	.795	.666	.641	.795/.641
Bearing Stress-psi	832	1000	986	915	636	744	1028	1210	1180	566/702

Sealing Sect.	Wedge-Rear Washer Interface					Rear-Washer - Exit Cone Interface				
Time -sec	@ Inst.	@ Start-up	200	500	700	@ Inst.	@ Start-up	200	500	700
Aero Load -lbs	0	414	414	414	0	0	410	410	410	0
B'ville Load -lbs	590	590	580	530	450	590	590	580	530	450
Total Load -lbs	590	1004	994	944	450	590	1000	990	940	450
Seal Height -in	.157	.157	.136	.132	.157/.132	.126	.126	.126	.126	.126
Bear. Area -in^2	.969	.969	.844	.820	.969/.820	.975	.975	.975	.975	.975
Bearing Stress-psi	610	1038	1180	1150	465/550	605	1028	1015	965	461

Figure 2.26

FLIGHT ENGINE END SEAL LOAD AND STRESS SUMMARY - VACUUM. $\epsilon = 40$

2. Pressurized Spring and Chamber Cavity
3. Pressurized Chamber Cavity

Sealing Sect.		Shoe-Front Washer Interface					Front Washer - Wedge Interface				
Time	-sec	@ Inst.	@ Start-up	200	500	700	@ Inst.	@ Start-up	200	500	700
Aero Load	-lbs	0	118	118	118	0	0	86	86	86	0
B'ville Load	-lbs	590	590	580	530	450	590	590	580	530	450
Total Load	-lbs	590	708	698	648	450	590	676	666	616	450
Seal Height	-in	.092	.092	.092	.092	.092	.125	.125	.104	.100	.125/.100
Bear. Area	-in^2	.708	.708	.708	.708	.708	.795	.795	.666	.641	.795/.641
Bearing Stress	-psi	832	1000	986	915	636	744	850	1000	960	561/702

Sealing Sect.		Wedge-Rear Washer Interface					Rear Washer - Exit Cone Interface				
Time	-sec	@ Inst.	@ Start-up	200	500	700	@ Inst.	@ Start-up	200	500	700
Aero Load	-lbs	0	252	252	252	0	0	421	421	421	0
B'ville Load	-lbs	590	590	580	530	450	590	590	580	530	450
Total Load	-lbs	590	812	832	782	450	590	1011	1001	951	450
Seal Height	-in	.157	.157	.136	.132	.157/.132	.126	.126	.126	.126	.126
Bear. Area	-in^2	.969	.969	.844	.820	.969/.820	.975	.975	.975	.975	.975
Bearing Stress	-psi	610	839	986	955	465/550	605	1038	1028	976	461

Figure 2.27

FLIGHT ENGINE END SEAL LOAD AND STRESS SUMMARY - VACUUM, ϵ = 40

4. Pressurized Spring Cavity

Sealing Sect.		Shoe-Front Washer Interface					Front Washer - Wedge Interface				
Time	-sec	@ Inst.	@ Start-up	200	500	700	@ Inst.	@ Start-up	200	500	700
Aero Load	-lbs	0	118	118	118	0	0	872	872	872	0
B'ville Load	-lbs	590	590	580	530	450	590	590	580	530	450
Total Load	-lbs	590	708	698	648	450	590	1462	1452	1402	450
Seal Height	-in	.092	.092	.092	.092	.092	.125	.125	.104	.100	.125/.104
Bear. Area	-in^2	.708	.708	.708	.708	.708	.795	.795	.666	.641	.795/.641
Bearing Stress	-psi	832	1000	986	915	636	744	1840	2200	2190	561/702

Sealing Sect		Wedge-Rear Washer Interface					Rear Washer - Exit Cone Interface				
Time	-sec	@ Inst.	@ Start-up	200	500	700	@ Inst.	@ Start-up	200	500	700
Aero Load	-lbs	0	1060	1060	1060	0	0	1056	1056	1056	0
B'ville Load	-lbs	590	590	580	530	450	450	590	580	530	450
Total Load	-lbs	590	1650	1640	1590	450	590	1646	1636	1586	450
Seal Height	-in	.157	.157	.136	.132	.157/.132	.126	.126	.126	.126	.126
Bear. Area	-in^2	.969	.969	.844	.820	1969/.820	.975	.975	.975	.975	.975
Bearing Stress	-psi	610	1700	1950	1940	465/550	605	1690	1680	1630	465

Figure 2.28

WLR23 FLIGHT ENGINE

BASED ON LOADS FOR A SEALED ENGINE OPERATING AT SEA LEVEL

Time -sec	Front Sealing Washer					Rear Sealing Washer				
	@ Inst.	@ Start-up	200	500	700 (Soak)	@ Inst.	@ Start-up	20	5	(Soak)
Out-of-plane moment lb-in/in-circum	16.05	18.95	18.70	17.30	11.81	17.21	27.20	27.00	25.5	3.
Bending Stress-psi	1265	1490	1470	1360	930	1360	2160	2140	2030	1030
Transverse Shear-psi	-	315	-	-	-	-	653	-		
Comparable Transverse Shear in Rig Engine -psi		NONE					650			

Figure 2.29

FLIGHT HOUSING STRESS MODEL

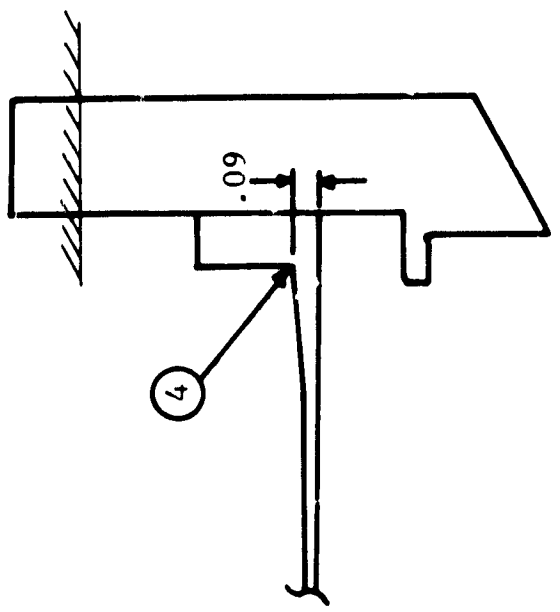

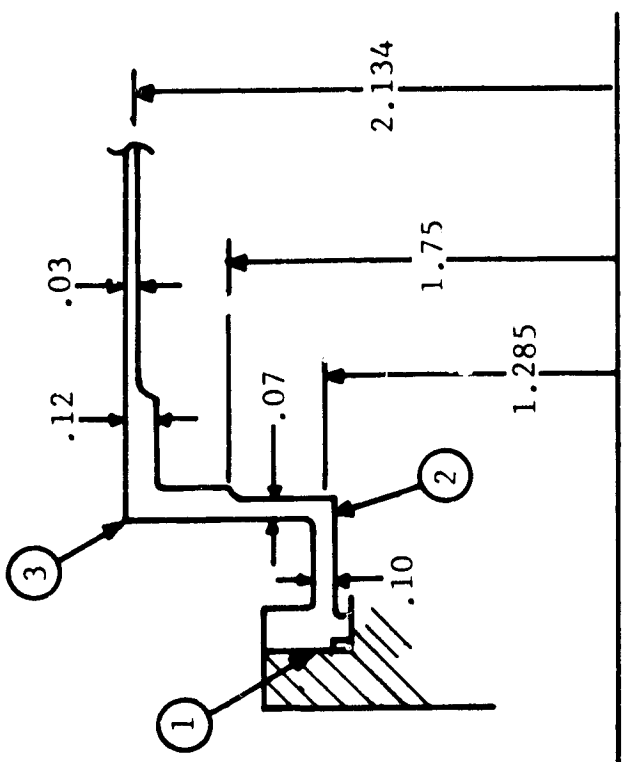

Figure 2.30

SWIRL CUP ORIFICE CALIBRATION

INJECTOR ES156989

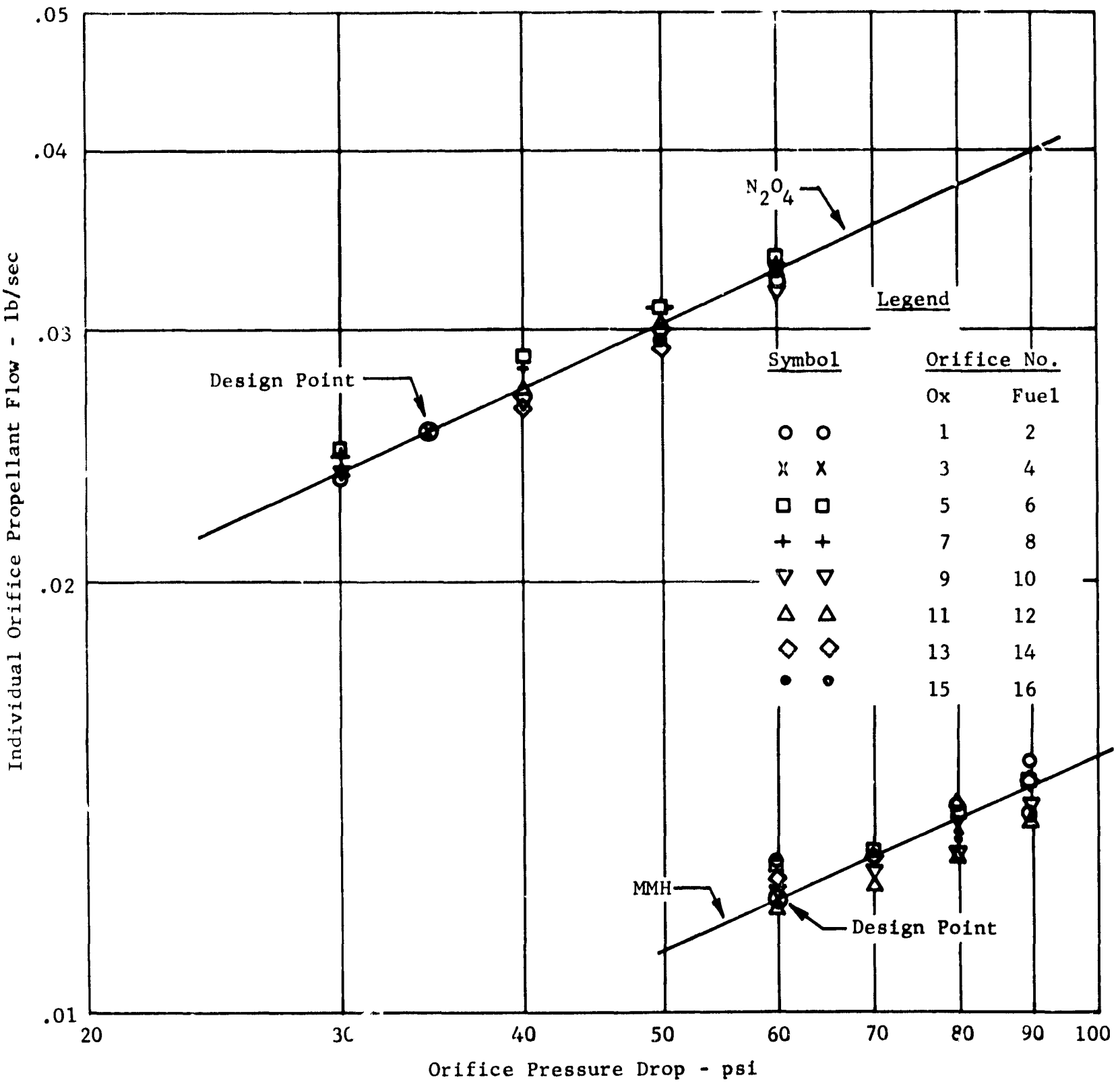

66-1004

Figure 3.1

SWIRL CUP ORIFICE AND MANIFOLD CALIBRATION

INJECTOR ES156989

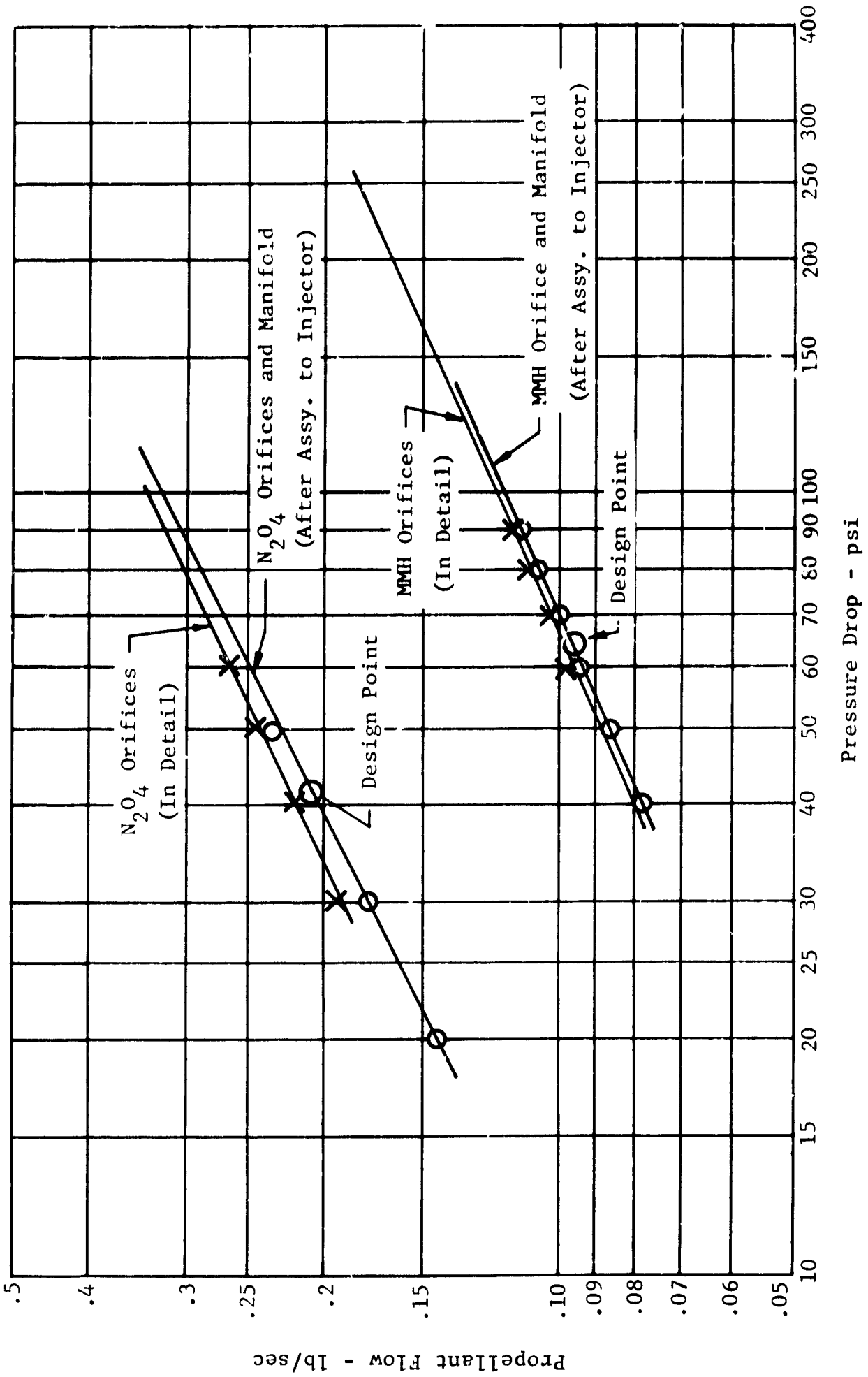

Figure 3.2

SPRAY COOLING CALIBRATIONS

INJECTOR ES156989

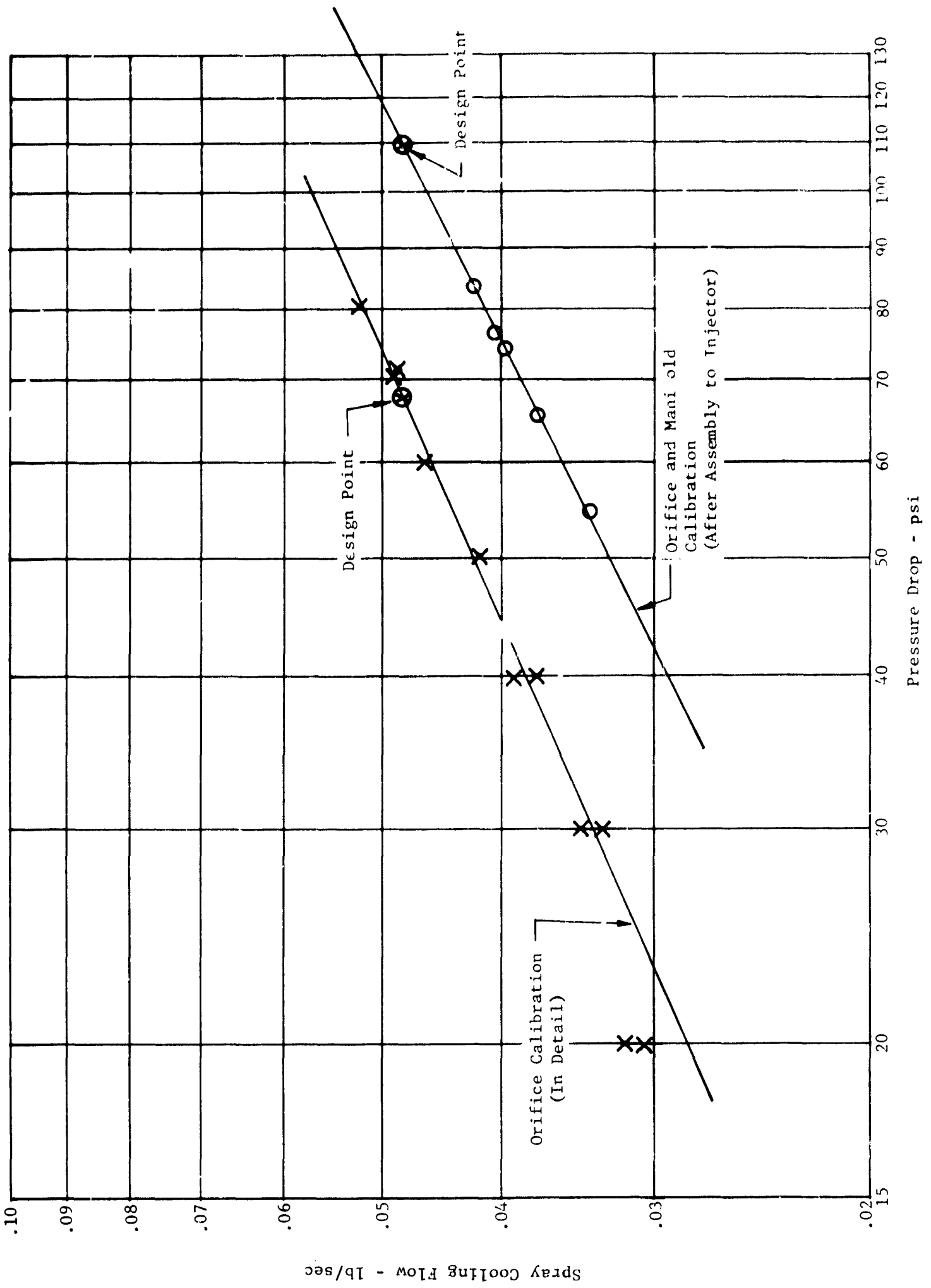

66-1022

Figure 3.3

TEST STAND INSTALLATION AND INSTRUMENTATION

SCHEMATIC

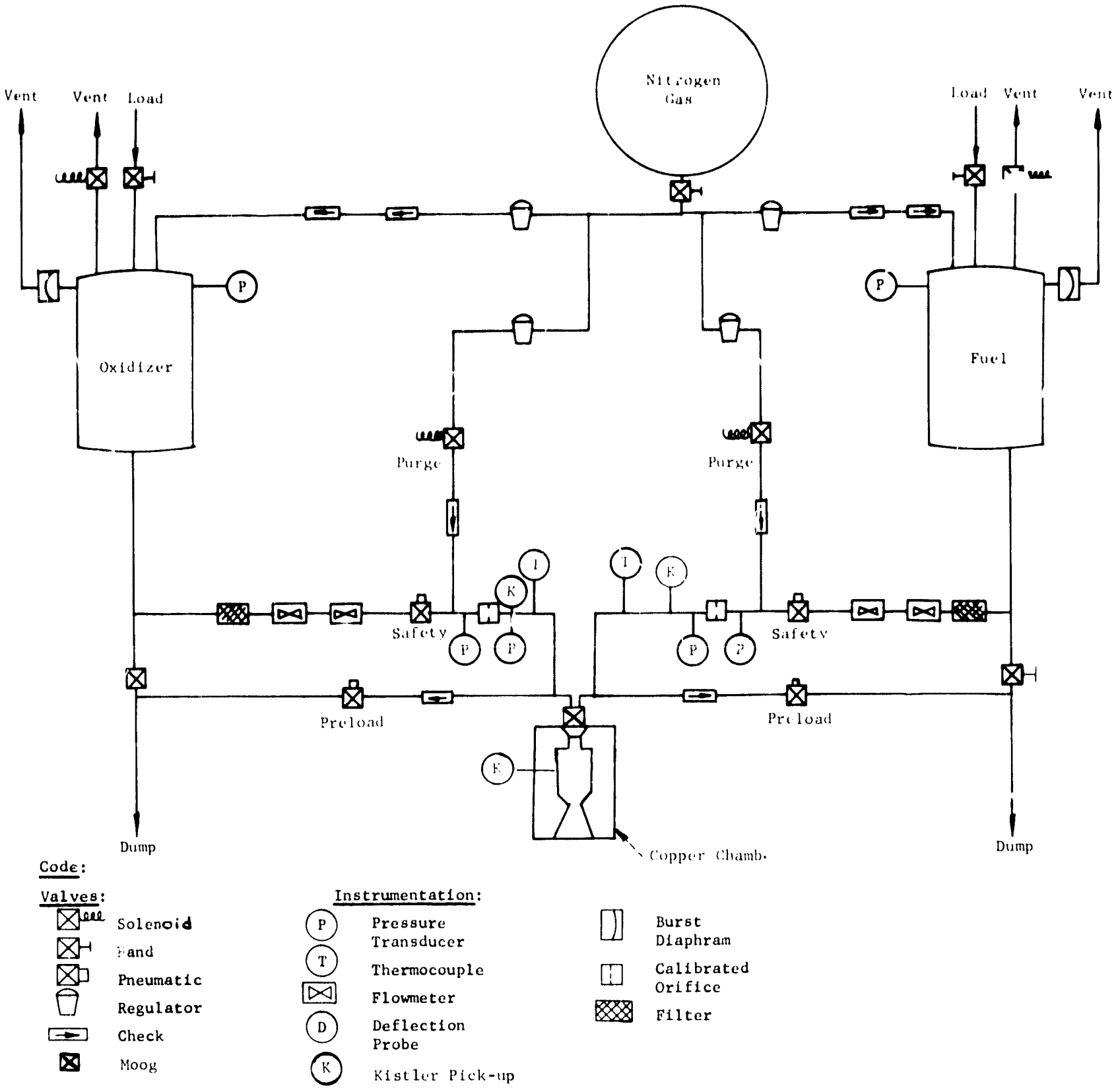

66-1028

Figure 3.4

INJECTOR INSTRUMENTATION

SCHEMATIC

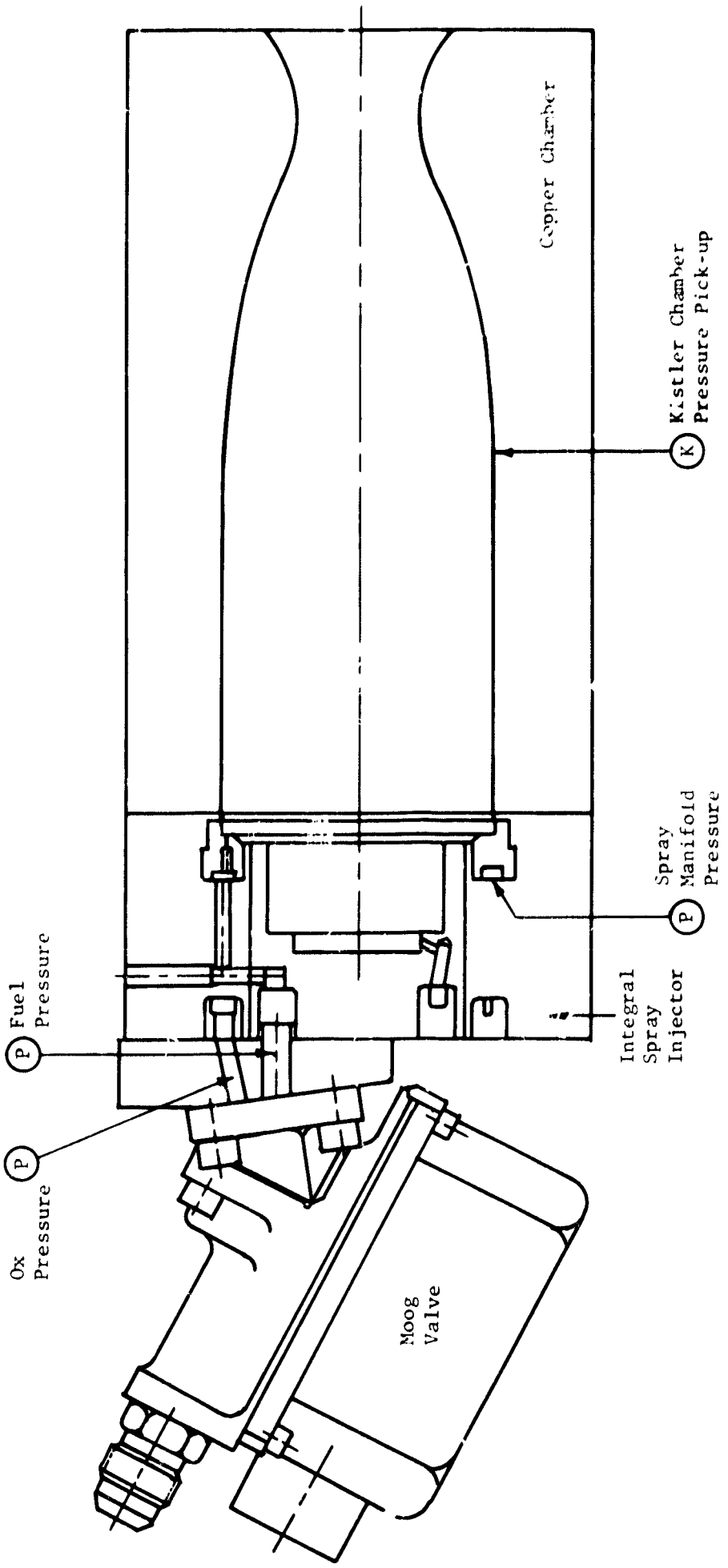

66-1076

Figure 3.5

WLR23 INTEGRAL SPRAY
INJECTOR ES156989
Run No. 23-97

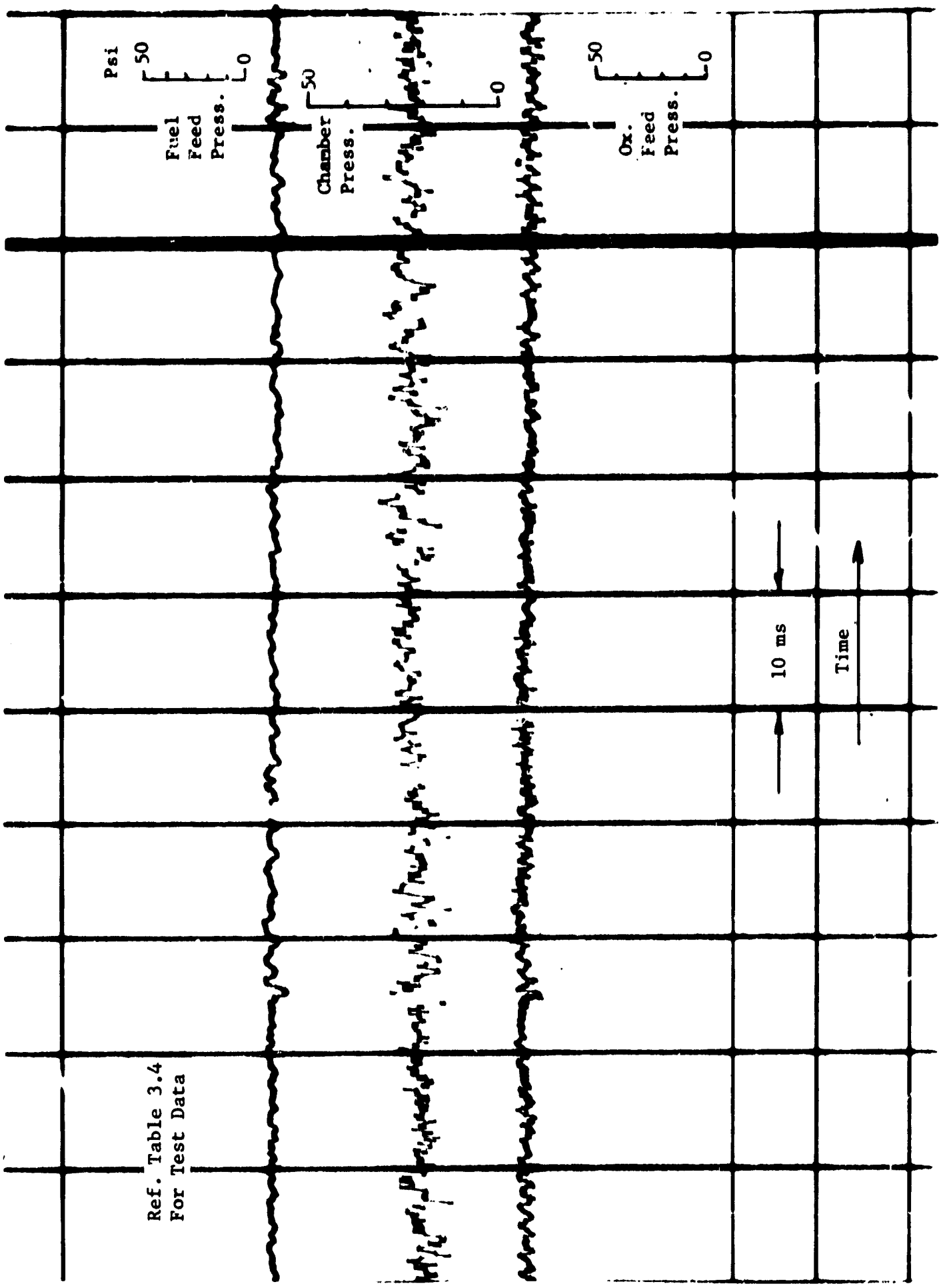

67-0067

Figure 3.6

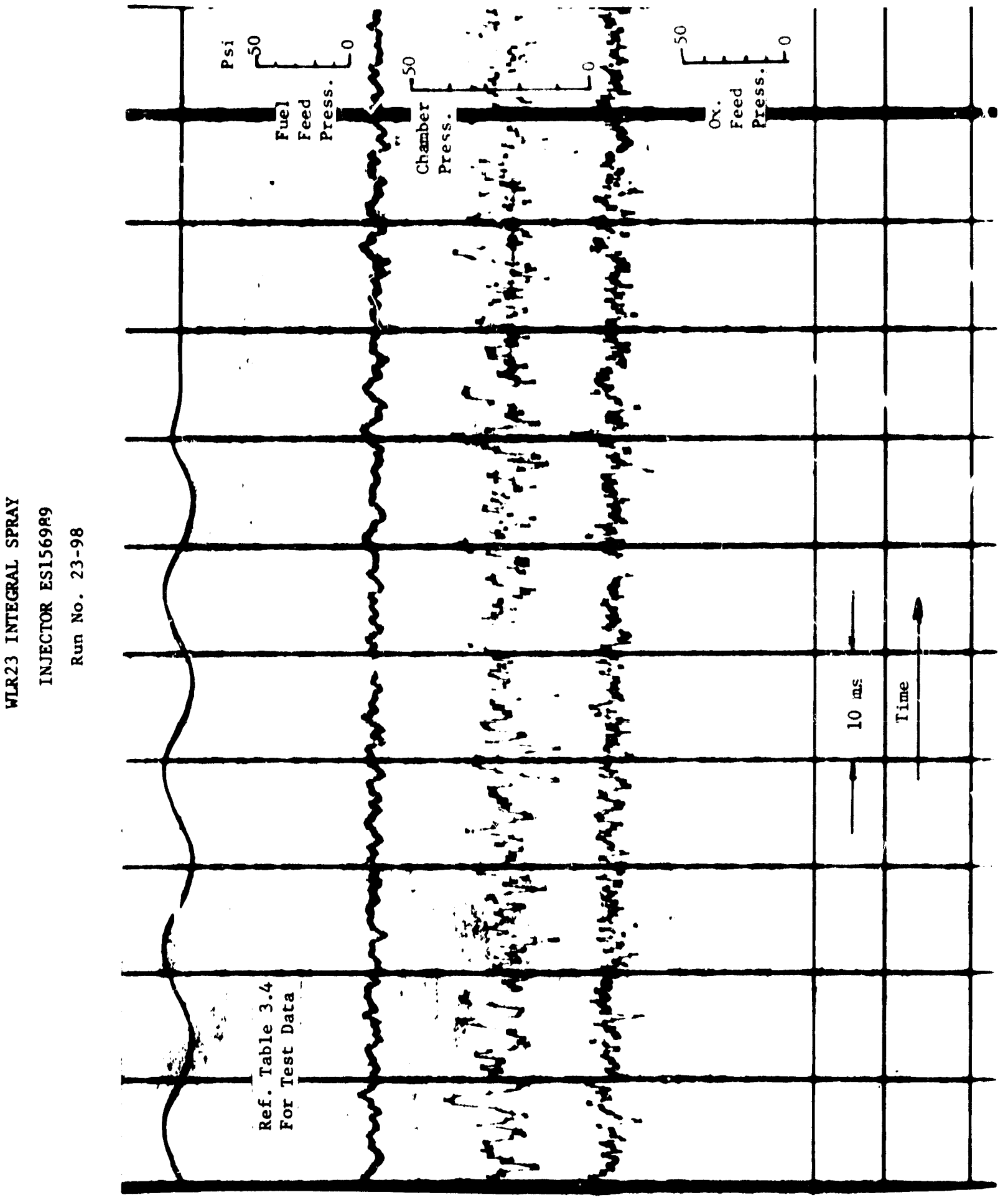
WLR23 INTEGRAL SPRAY
INJECTOR ES15698
Run No. 23-98
Psi
50
0
Fuel Feed Press.
Chamber Press.
Ox. Feed Press.
10 ms
Time
Ref. Table 3.4
For Test Data

Figure 3.7

WLR23 INTEGRAL SPRAY

INJECTOR ES156989

Run No. 23-99

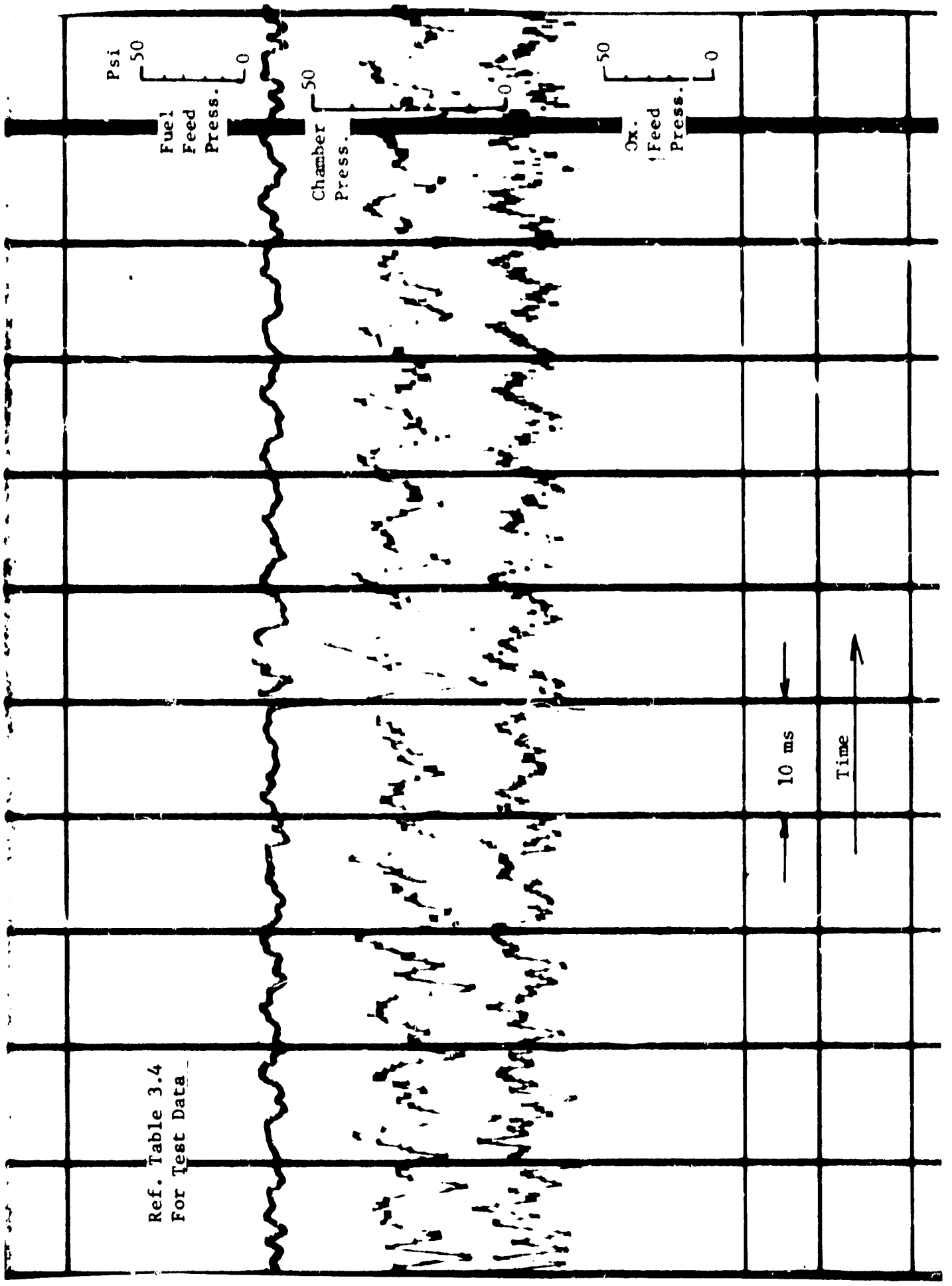

67-0026

Figure 3.8

WLR23 INTEGRAL SPRAY
INJECTOR ES156989
Run No. 23-100

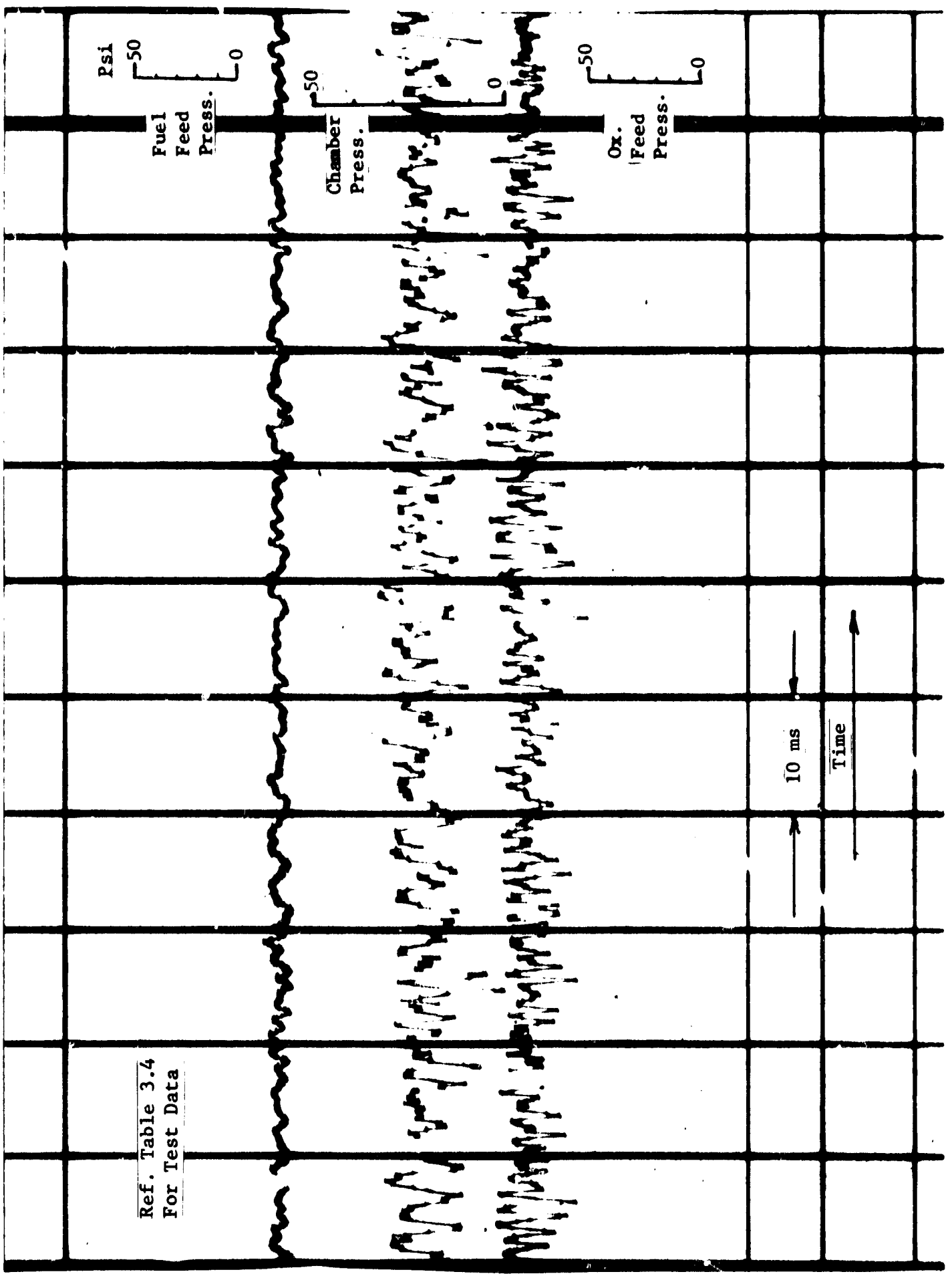

67-0080

Figure 3.9

WLR23 INTEGRAL SPRAY
INJECTOR ES156989
Run No. 23-101

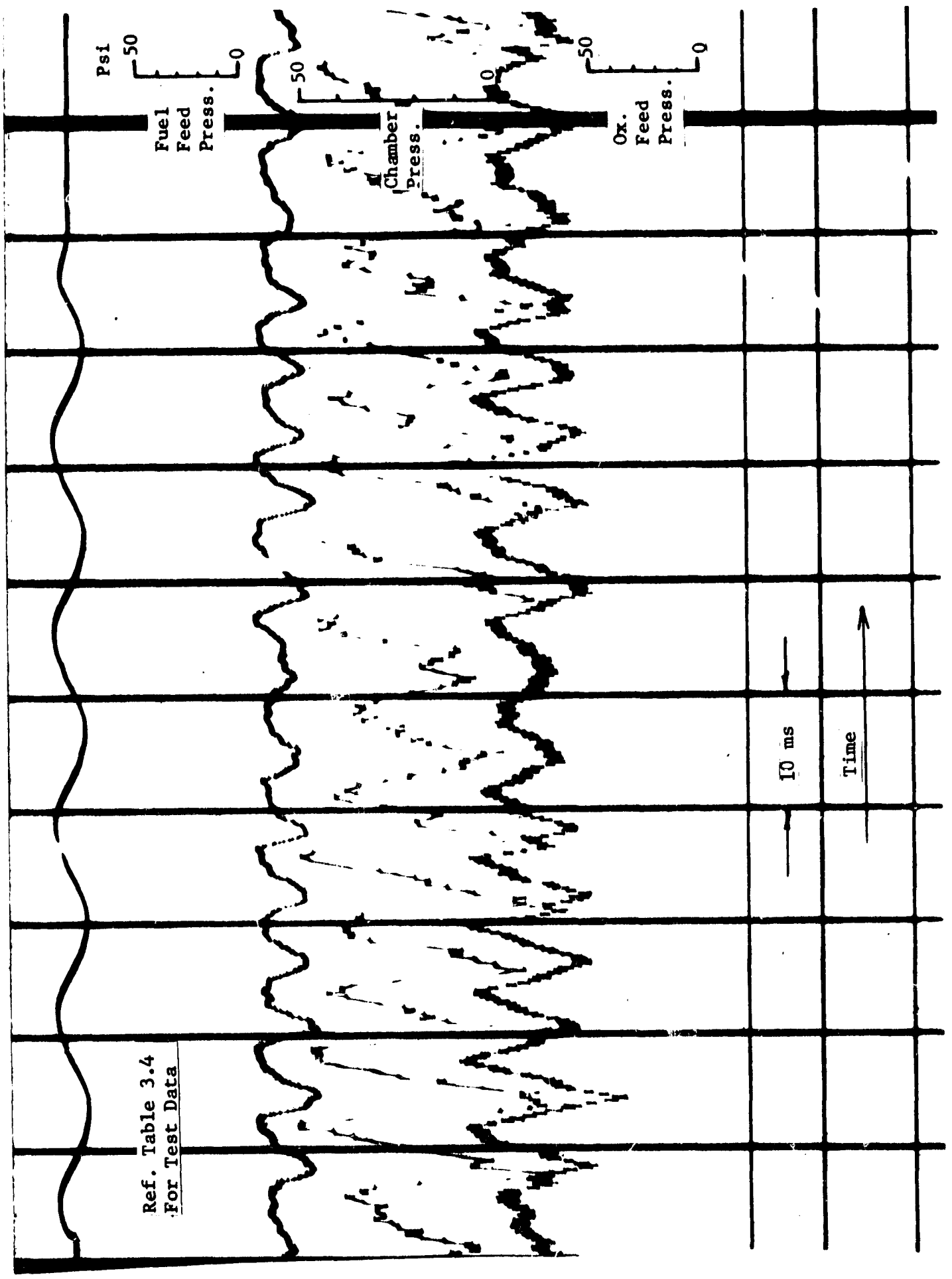

67-0079

Figure 3.10

WLR23 INTEGRAL SPRAY

INJECTOR ES156989

Run No. 23-102

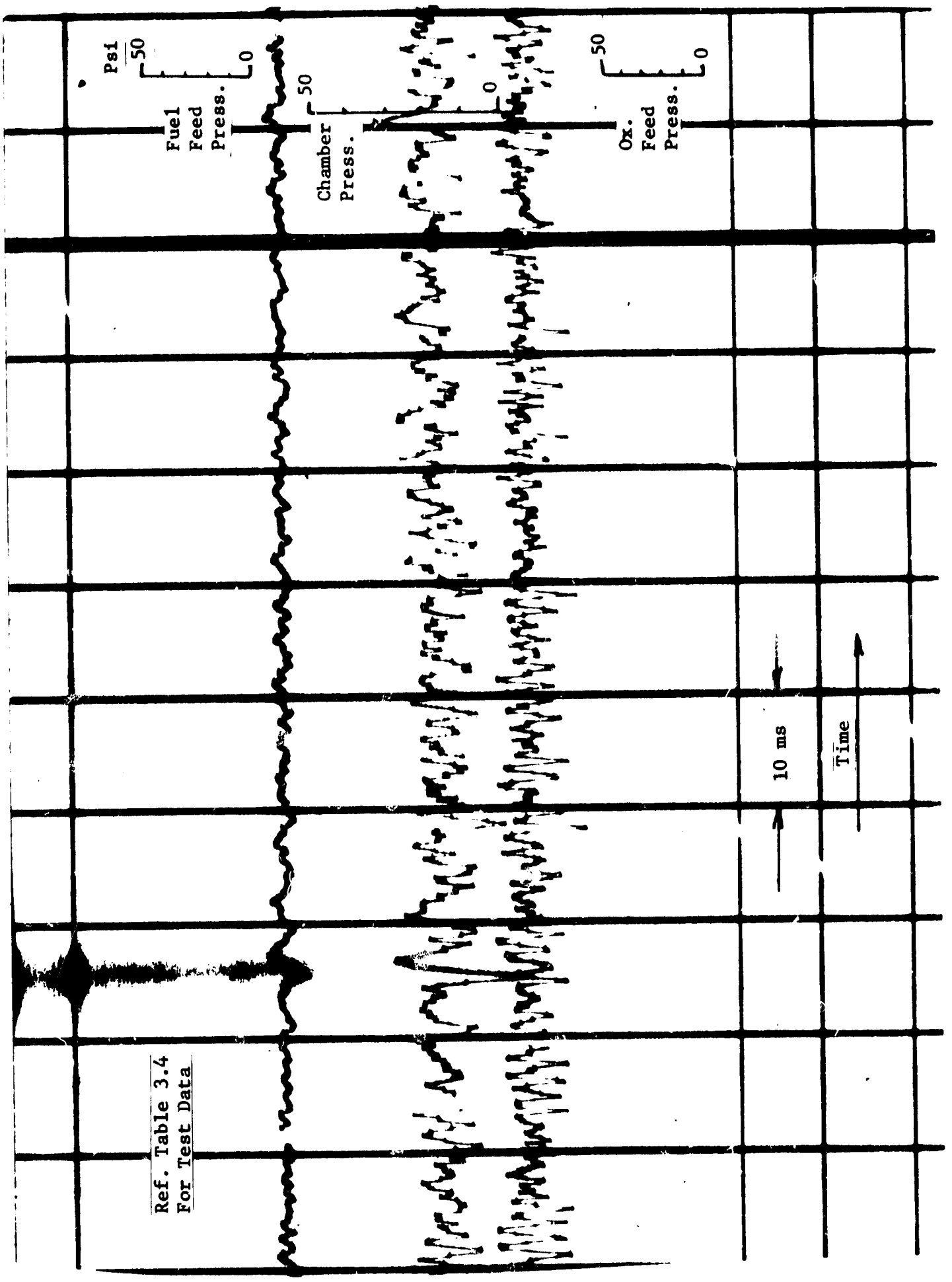

67-0084

Figure 3.11

WLR23 INTEGRAL SPRAY
INJECTOR ES156989
Run No. 23-103

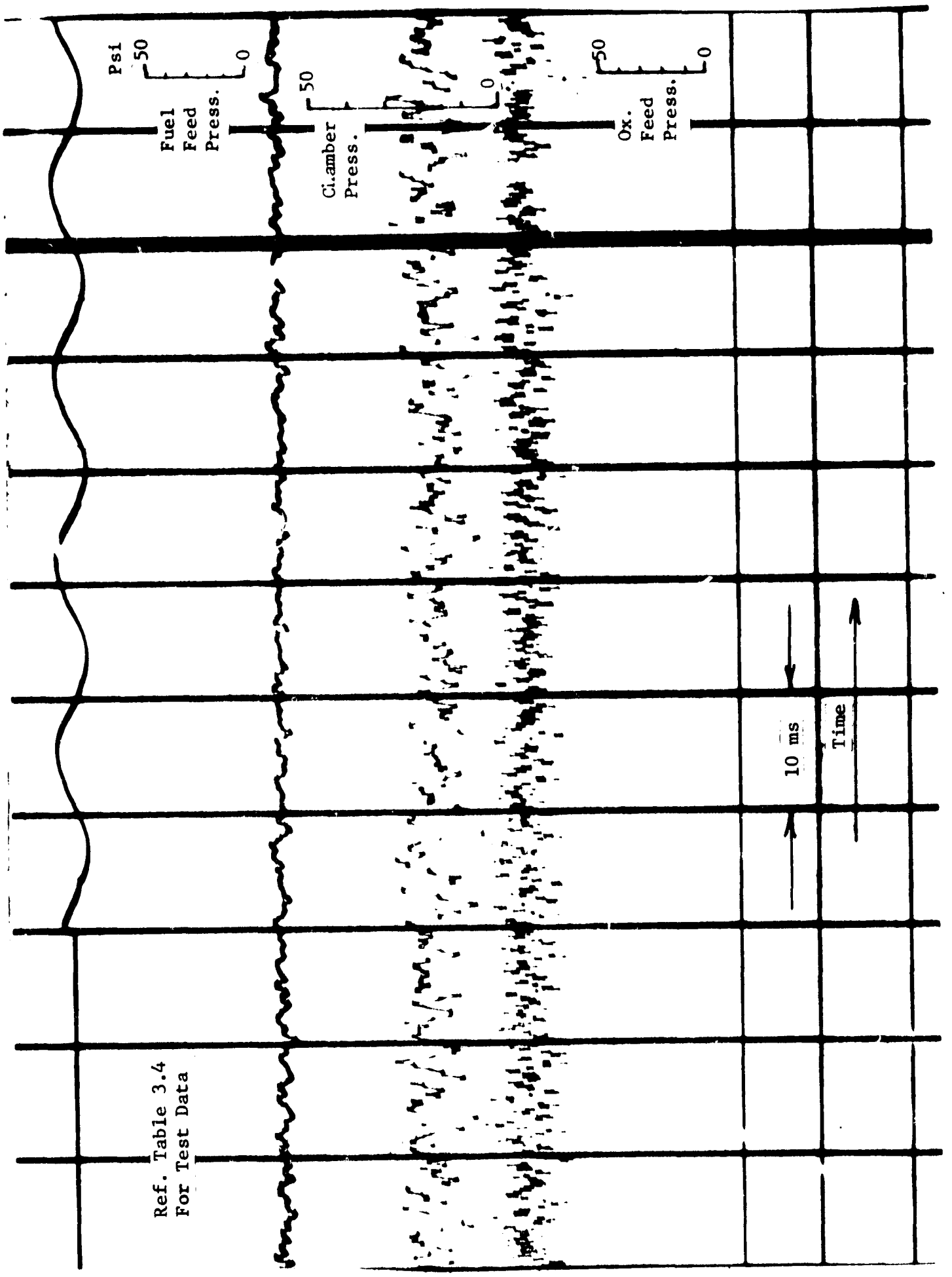

67-0096

Figure 3.12

WLR23 INTEGRAL SPRAY

INJECTOR ES156969

Run No. 23-104

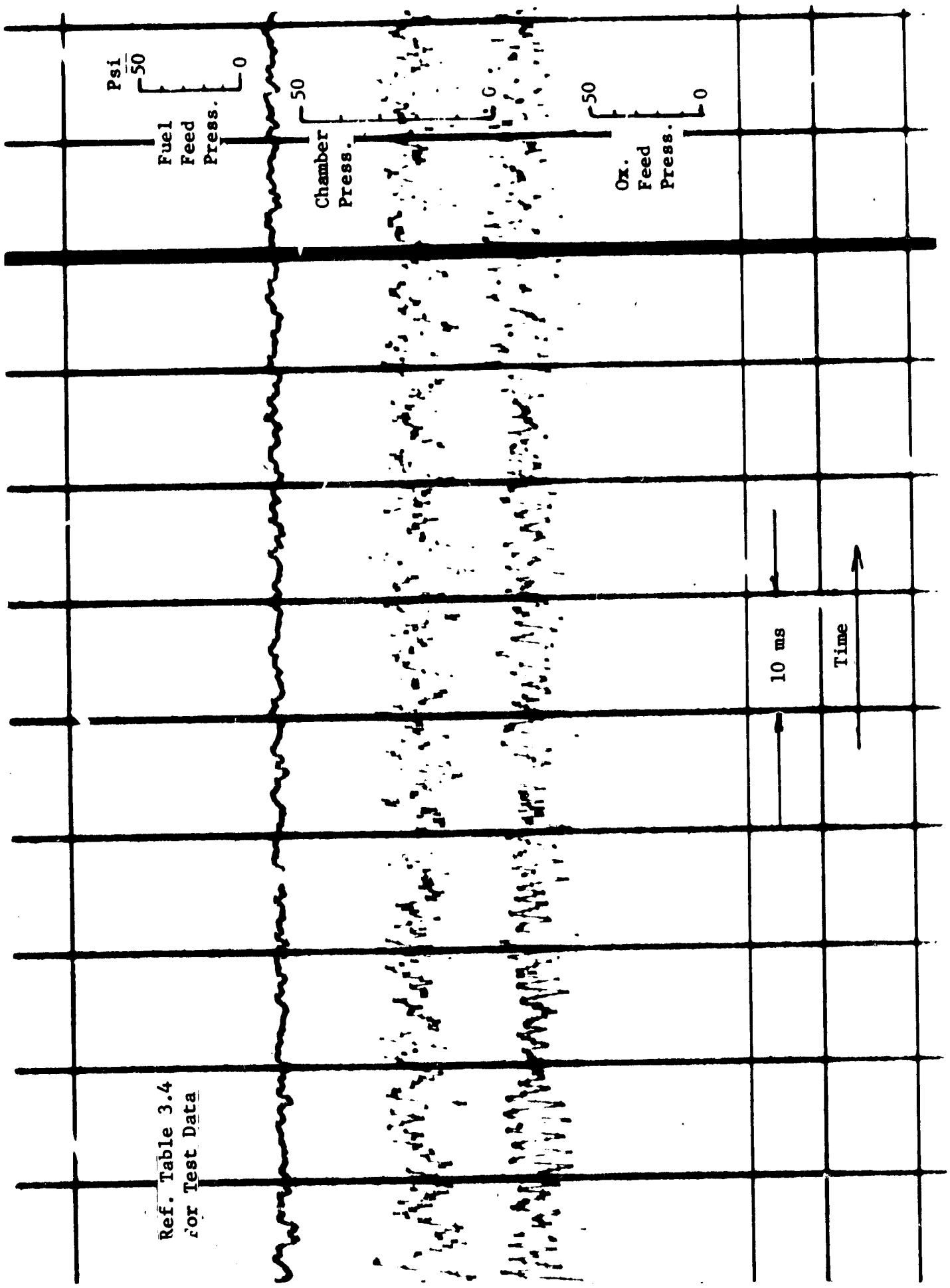

67-0070

Figure 3.13

WLR23 INTEGRAL SPRAY

INJECTOR ES156989

Run No. 23-105

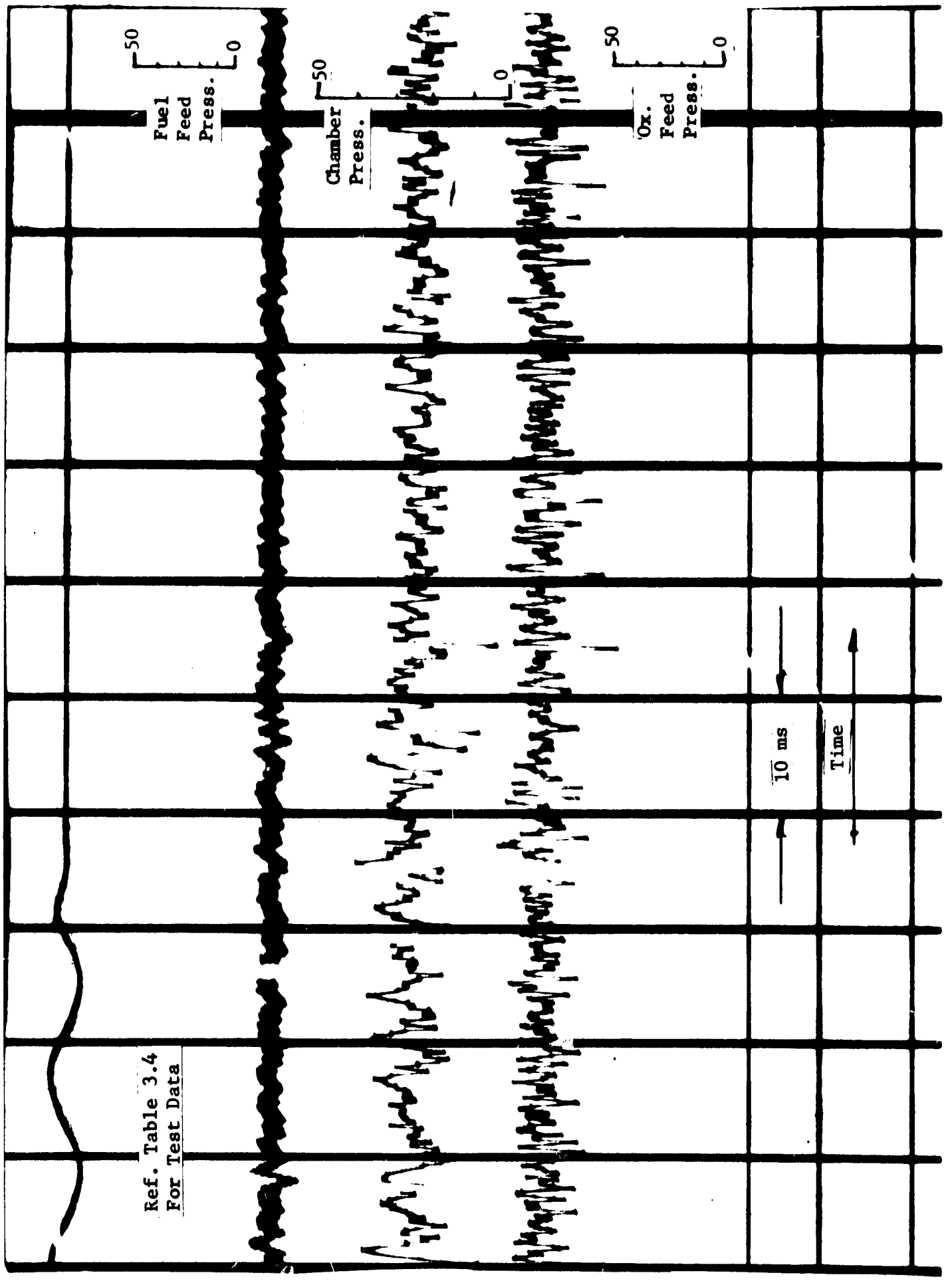

67-0082

Figure 3.14

WLR23 INTEGRAL SPRAY

INJECTOR ES156989

Run No. 23-106

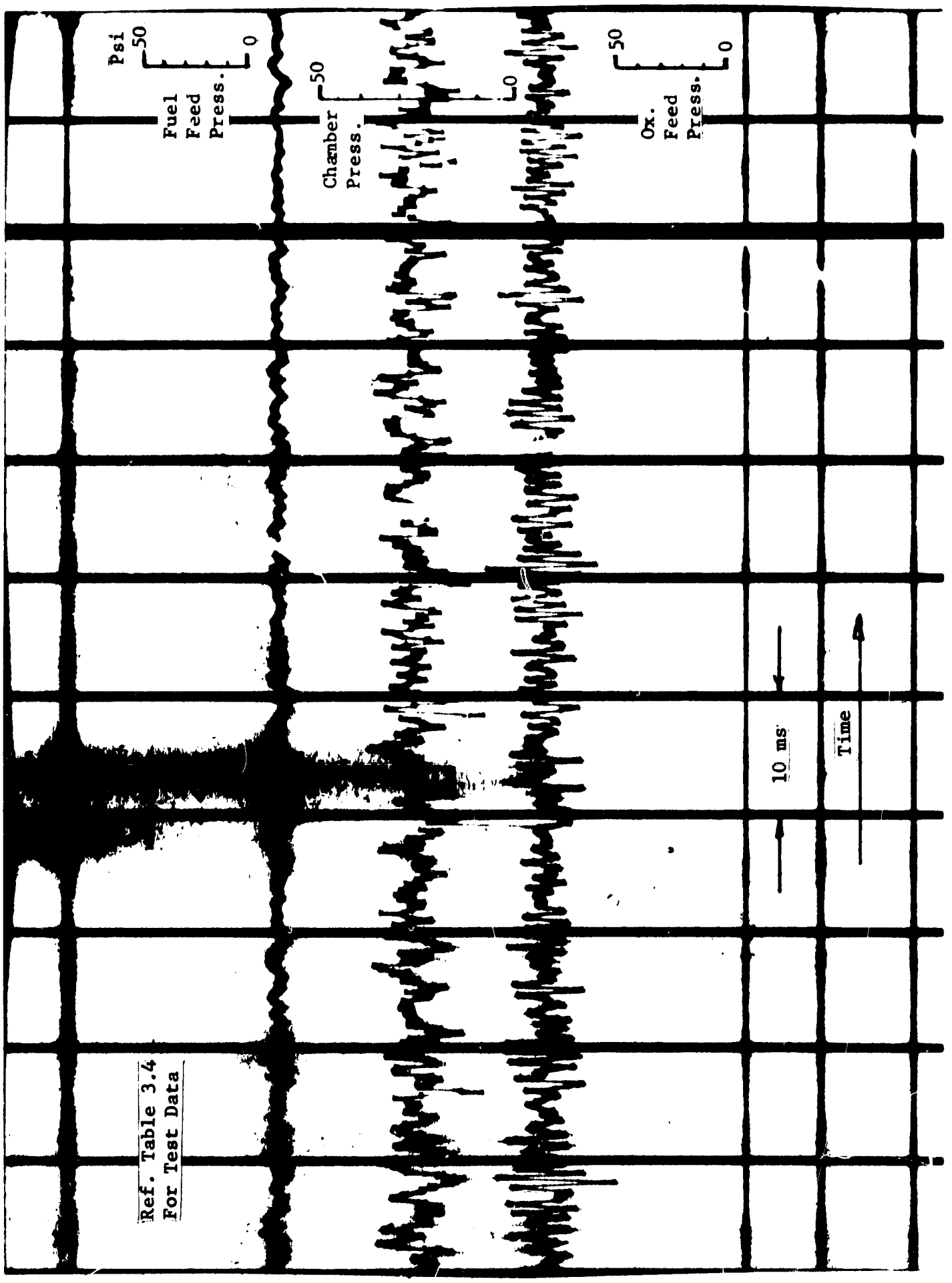

67-0081

Figure 3.15

WLR23 INTEGRAL SPRAY
INJECTOR ES156989
Run No. 23-107

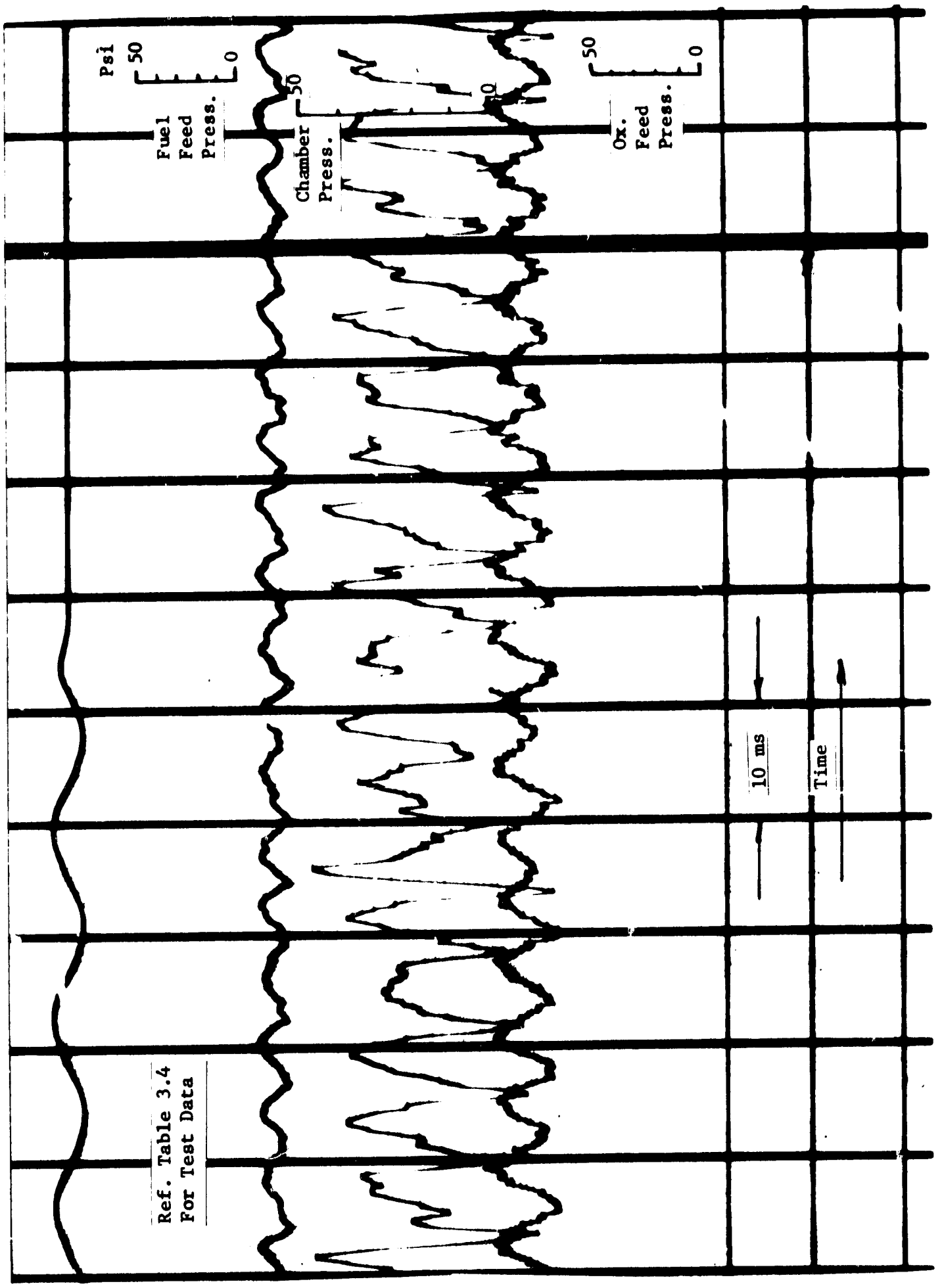

67-0088

Figure 3.16

WLR23 INTEGRAL SPRAY

INJECTOR ES156989

Run No. 23-108

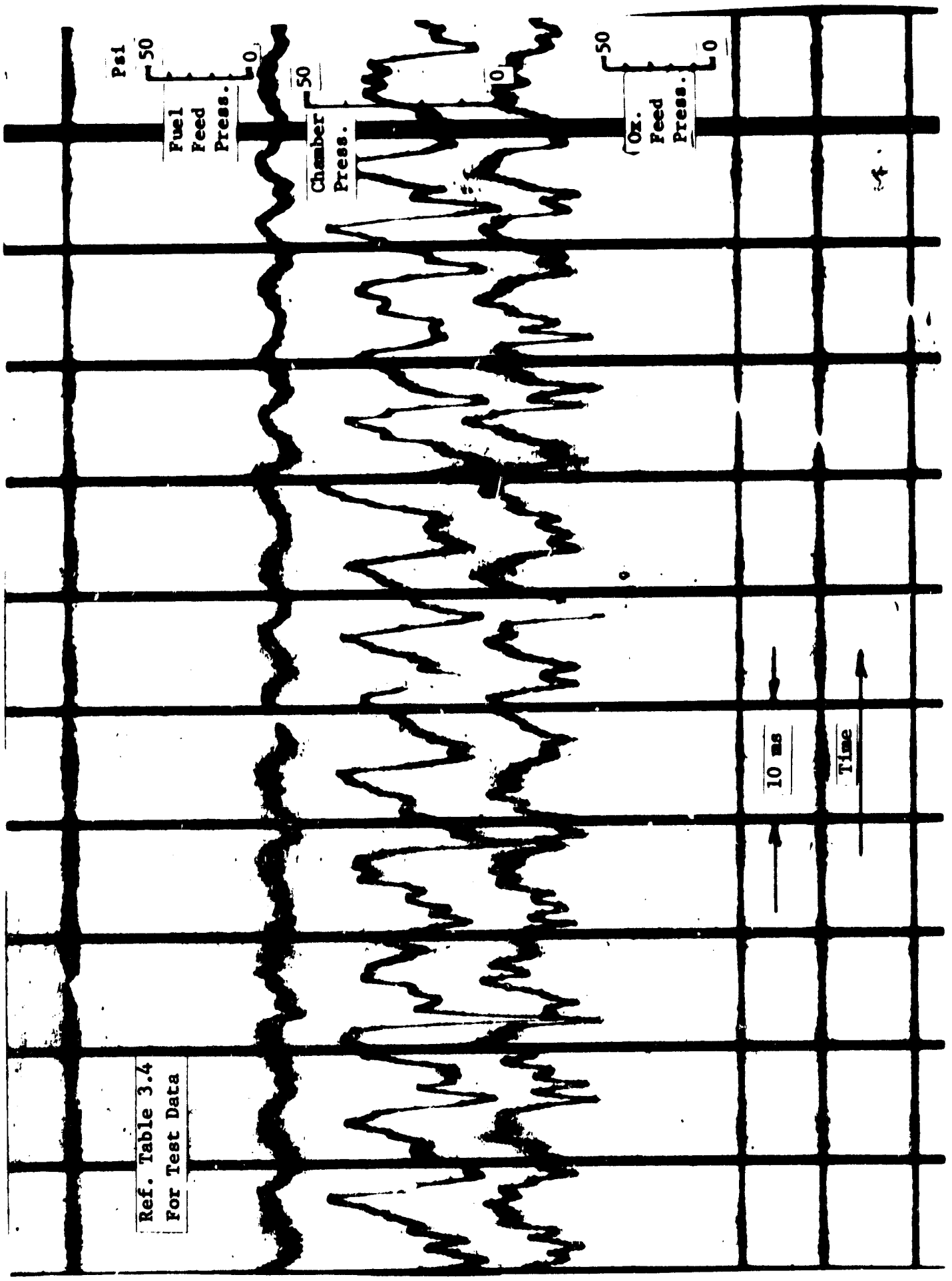

67-0009

Figure 3.17

WLR23 INTEGRAL SPRAY
INJECTOR ES156989
Run No. 23-109

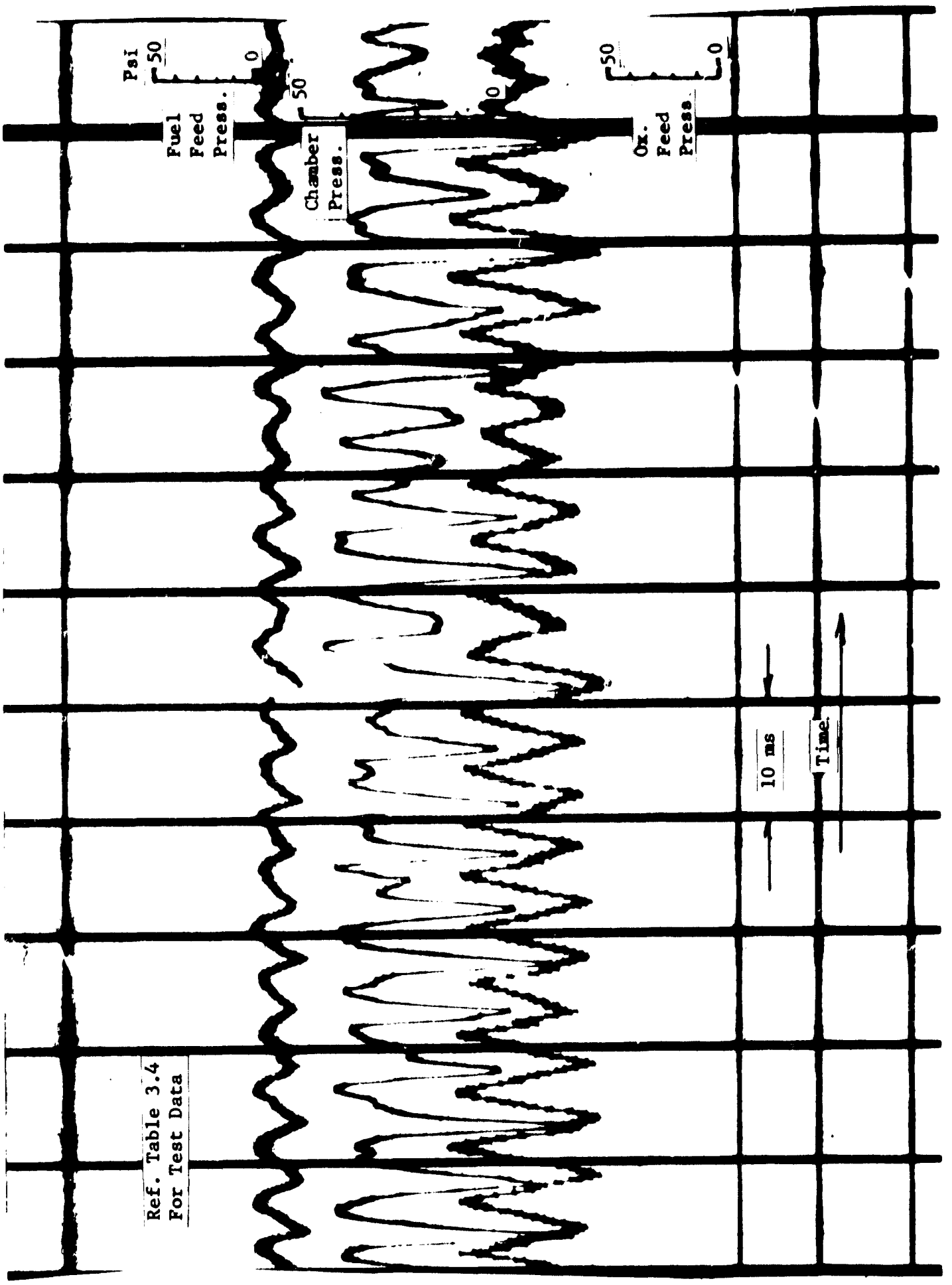

67-0008

Figure 3.18

WLR23 INTEGRAL SPRAY
INJECTOR ES156989
Run No. 23-110

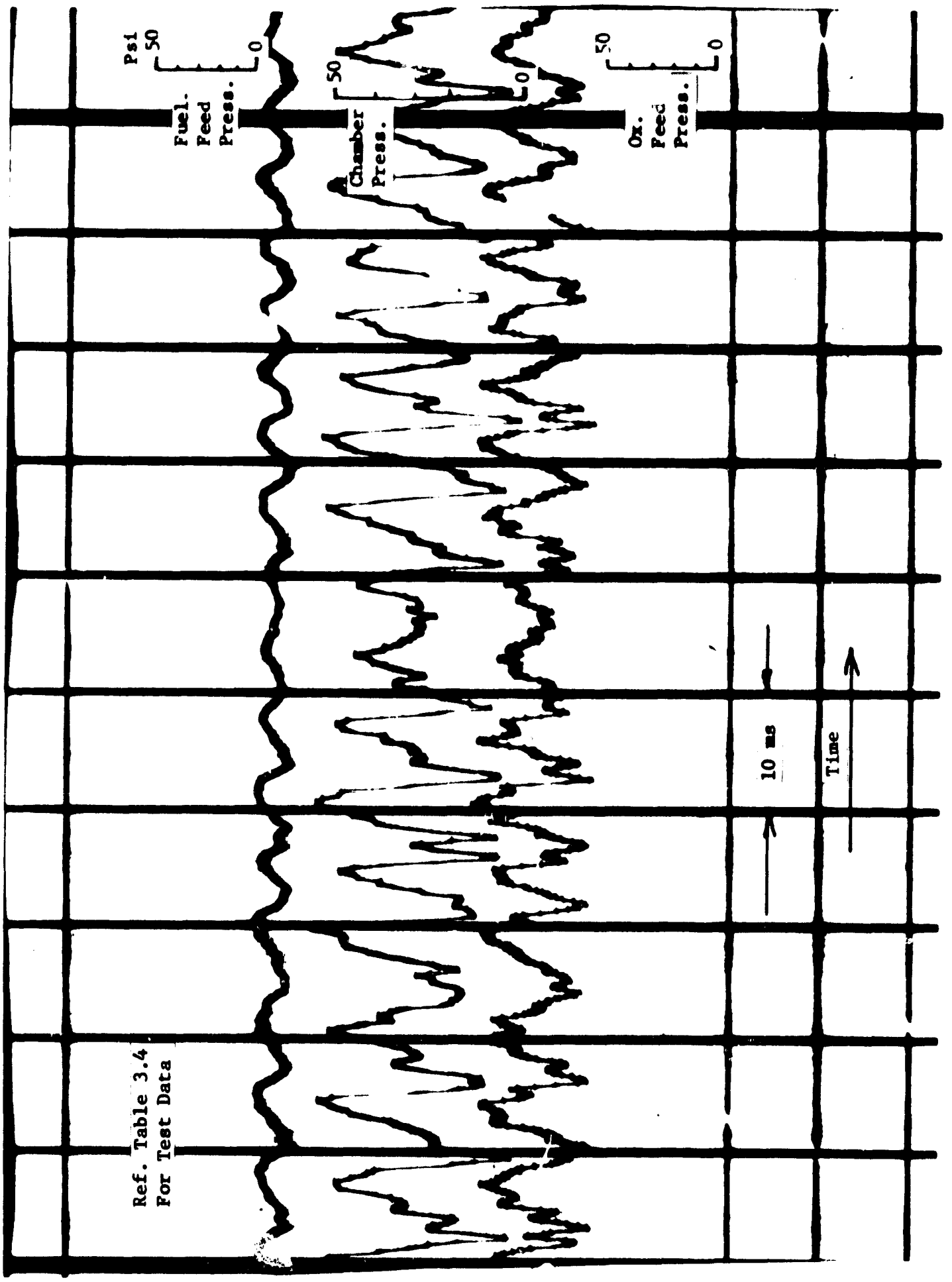

67-0095

Figure 3.19

WLR23 INTEGRAL SPRAY
INJECTOR ES156989
Run No. 23-111

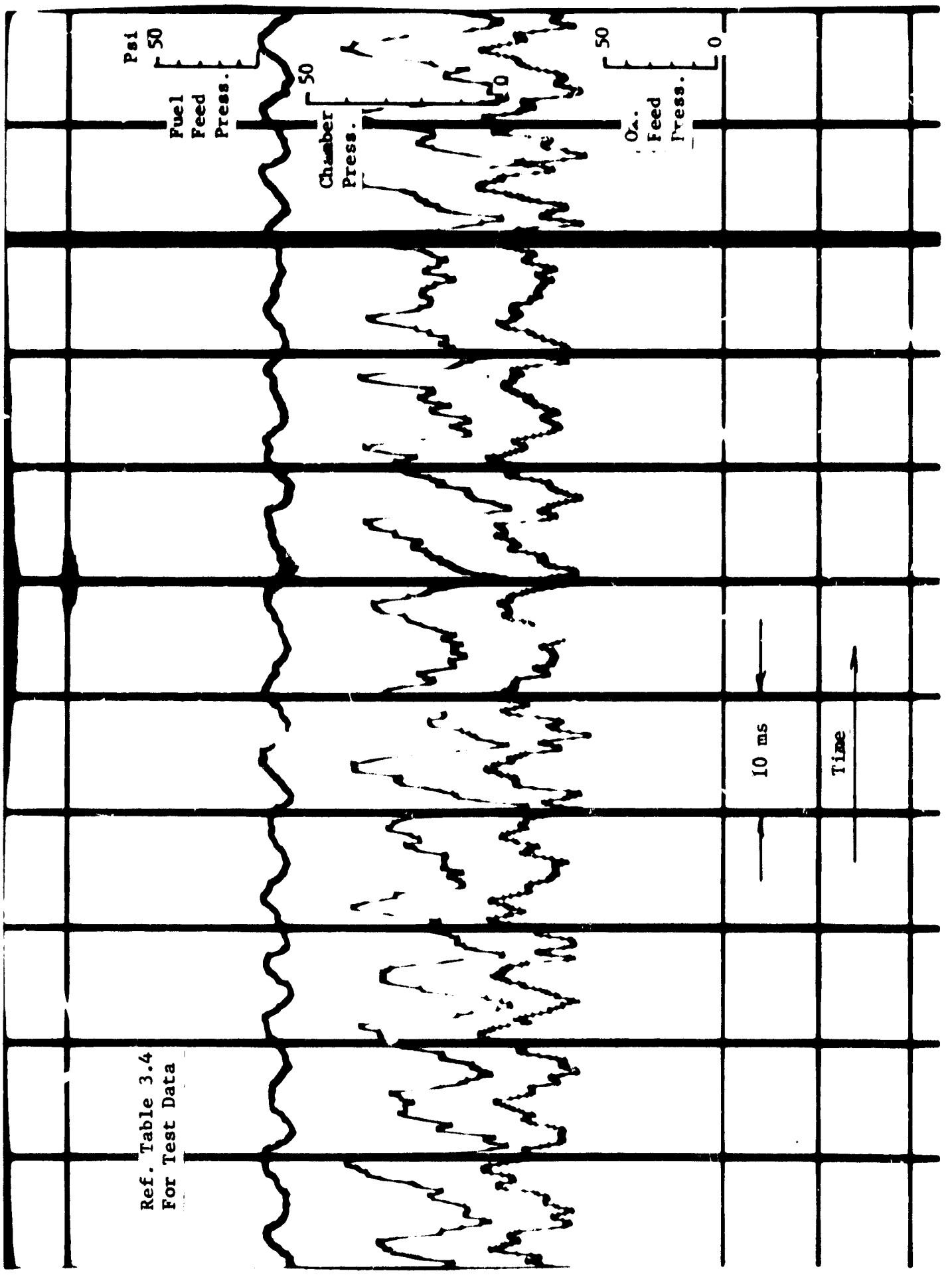

67-0078

Figure 3.20

WLR23 INTEGRAL SPRAY

INJECTOR ES156989

Run No. 23-112

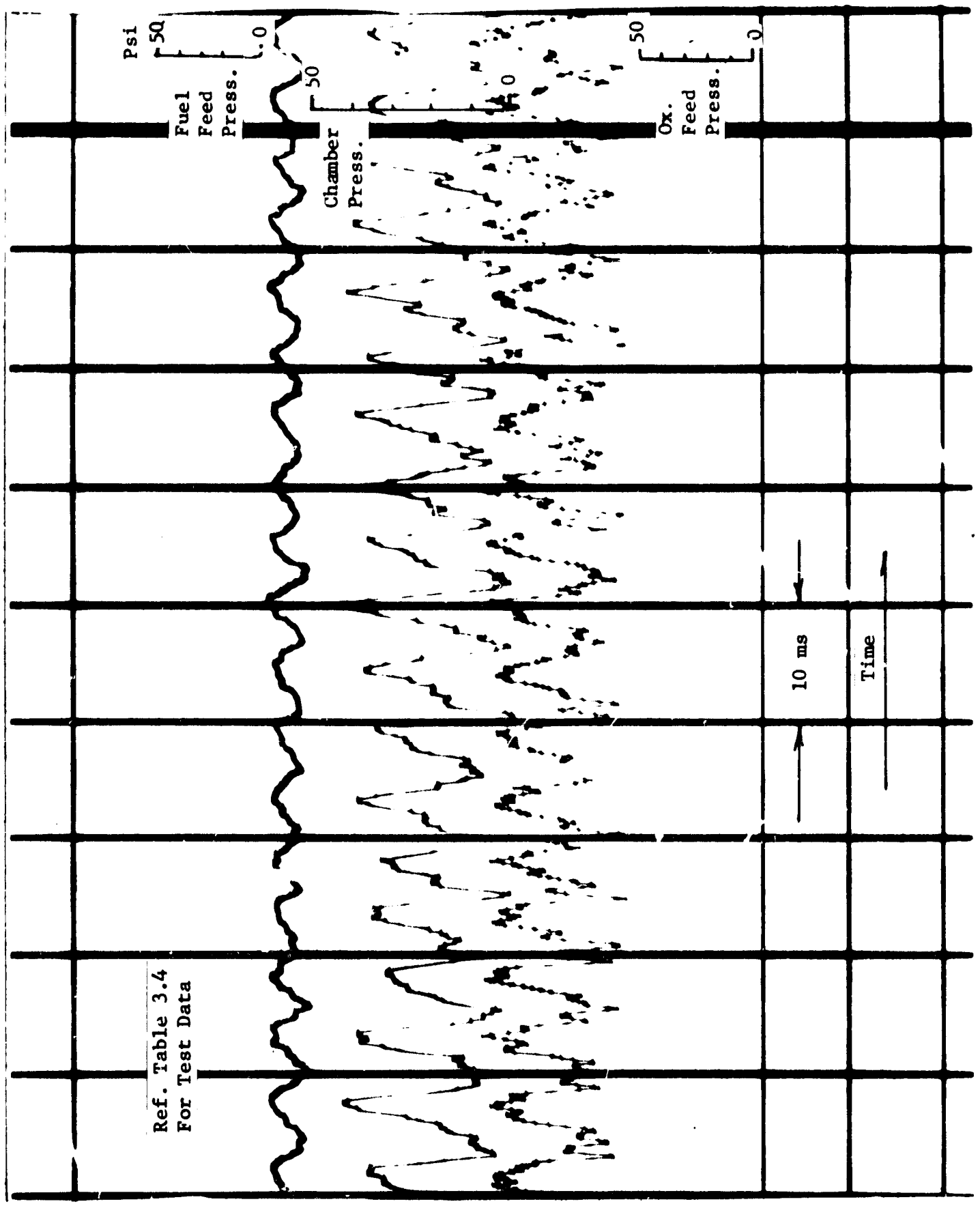

67-0091

Figure 3.21

WLR23 INTEGRAL SPRAY
INJECTOR ES156989
Run No. 23-113

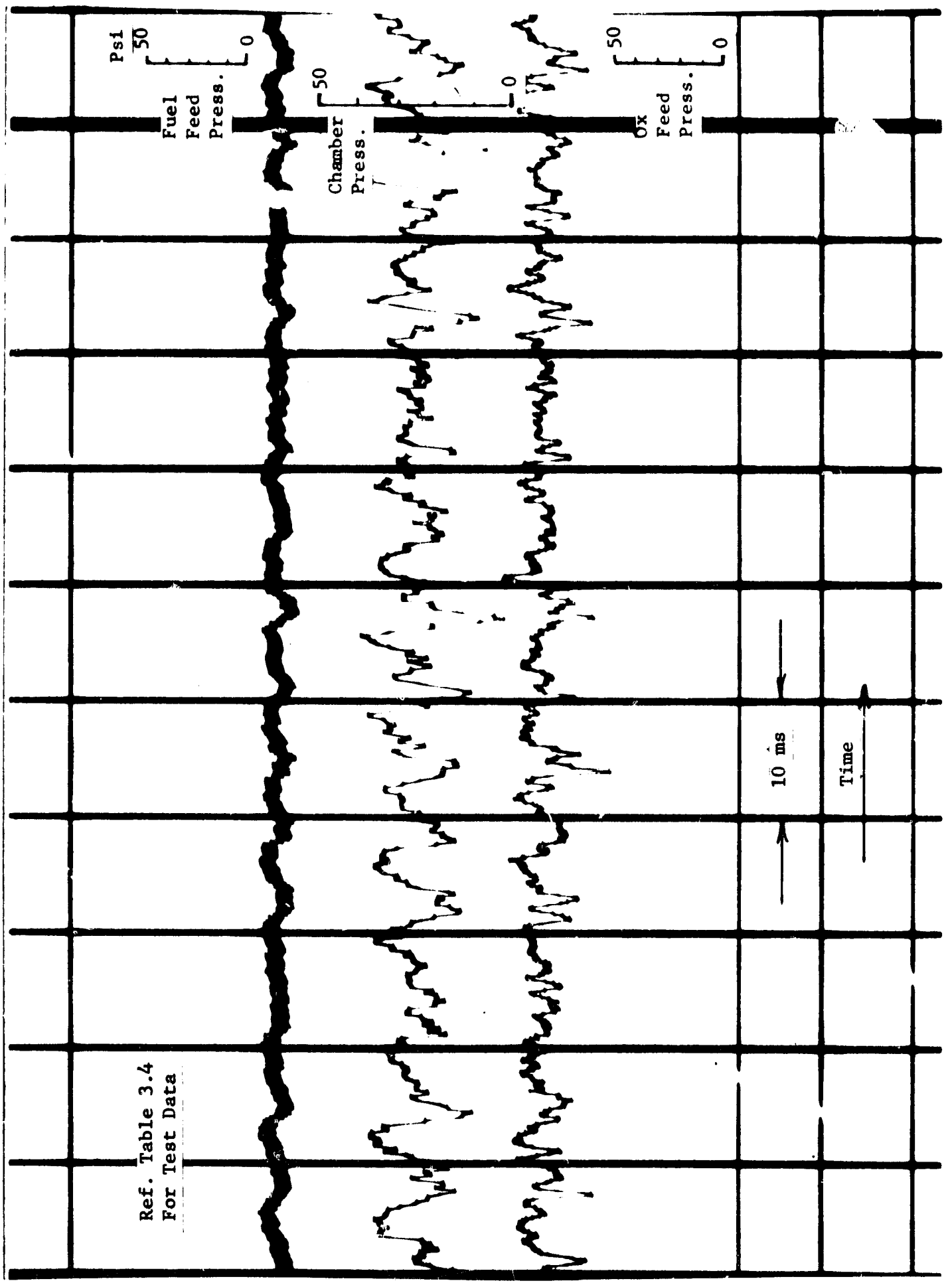

67-0069

Figure 3.22

WLR23 INTEGRAL SPRAY
INJECTOR ES156989
Run No. 23-114

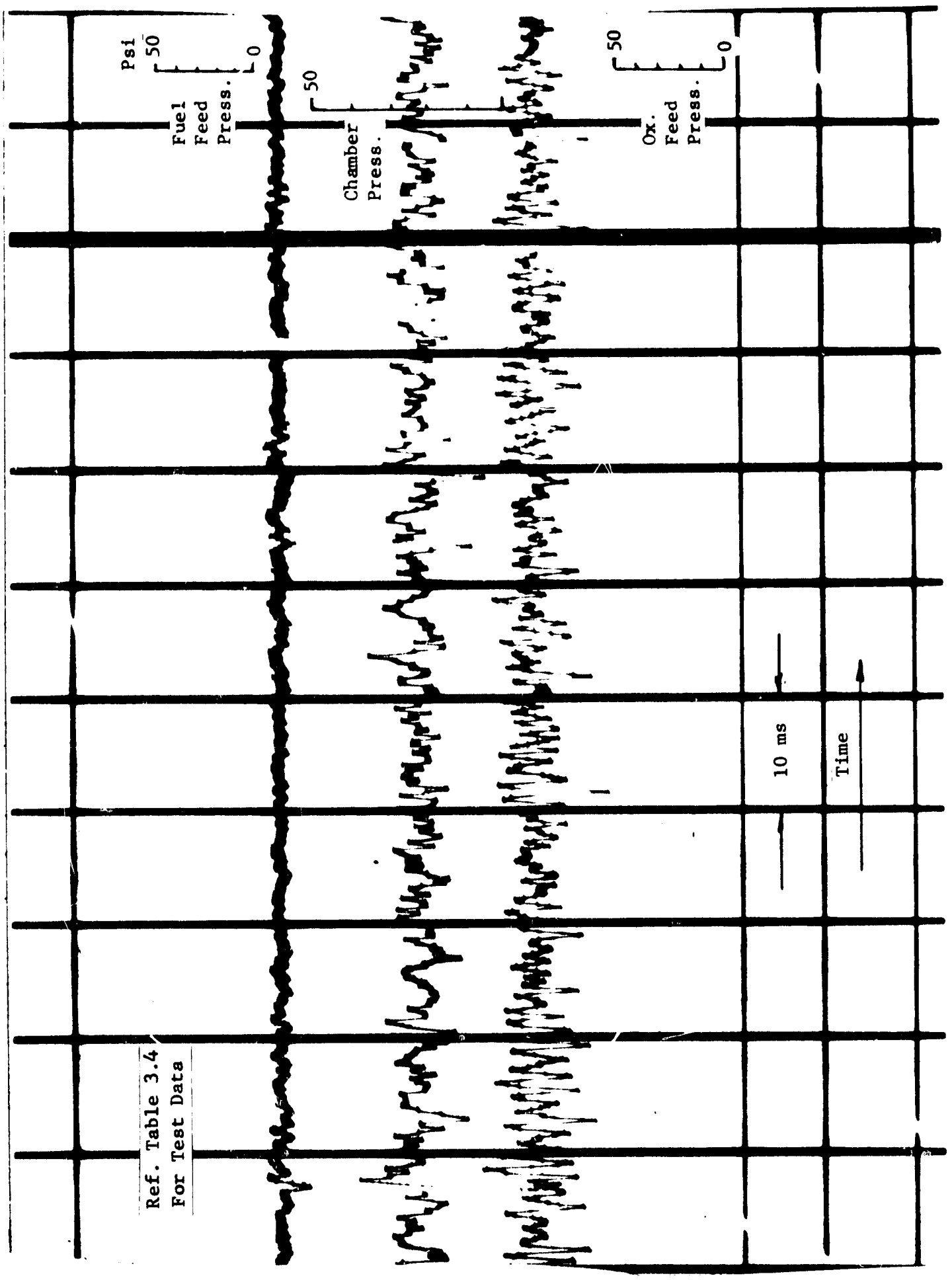

67-0087

Figure 3.23

WLR23 INTEGRAL SPRAY
INJECTOR ES156989
Run No. 23-115

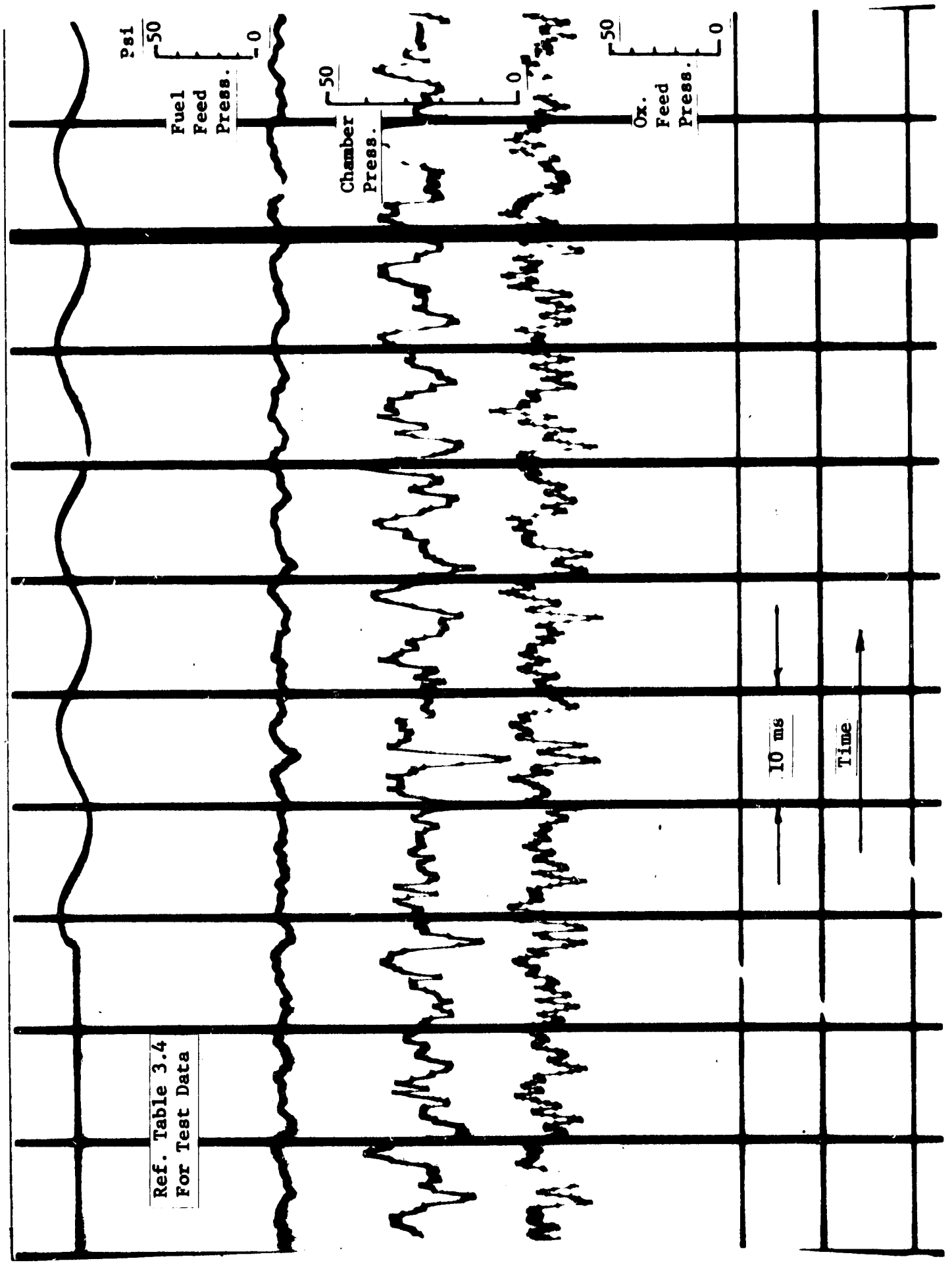

67-0092

Figure 3.24

WLR23 INTEGRAL SPRAY
INJECTOR ES156989
Run No. 23-116

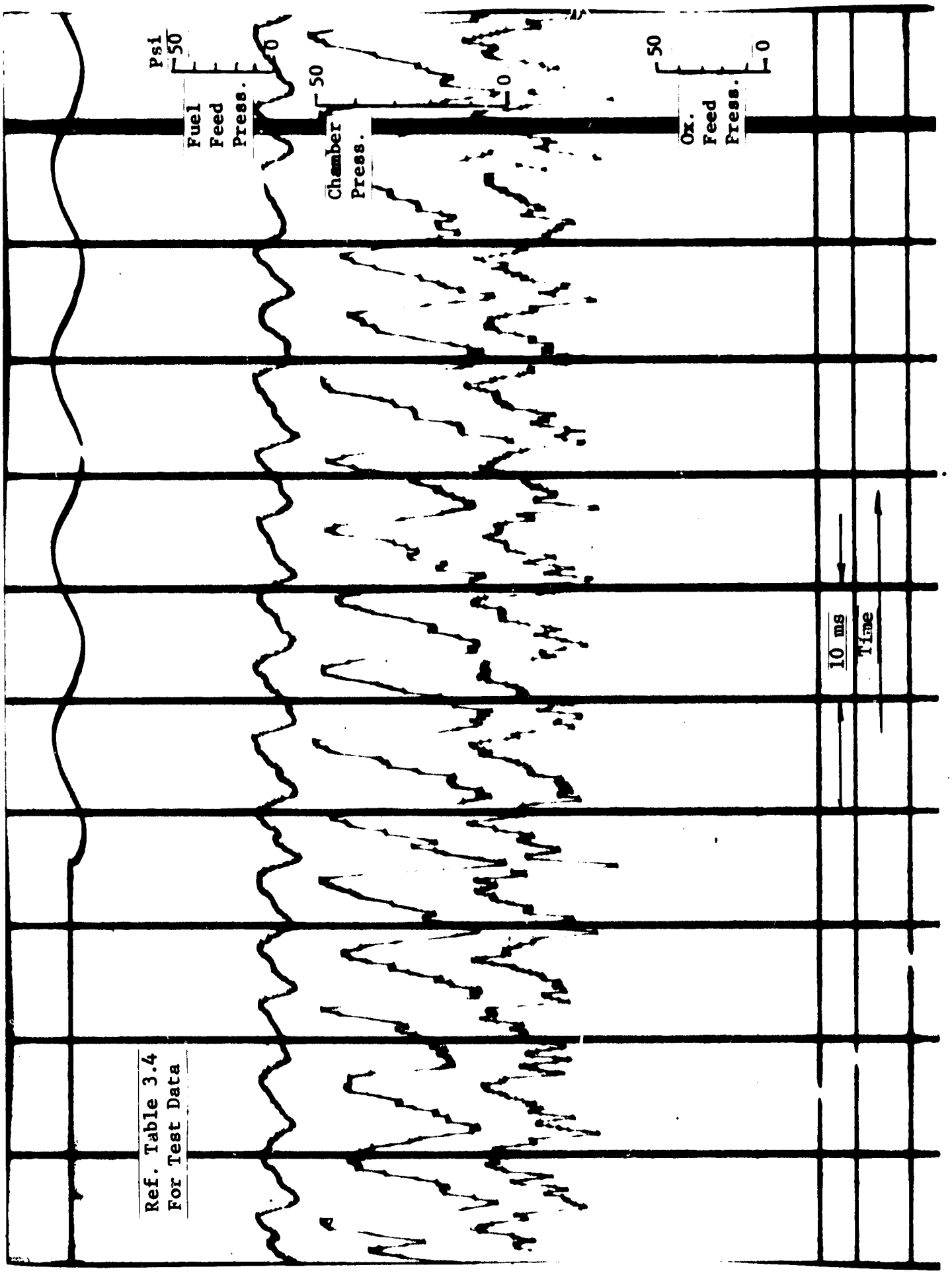

67-0071

Figure 3.25

WLR23 INTEGRAL SPRAY

INJECTOR ES156989

Run No. 23-117

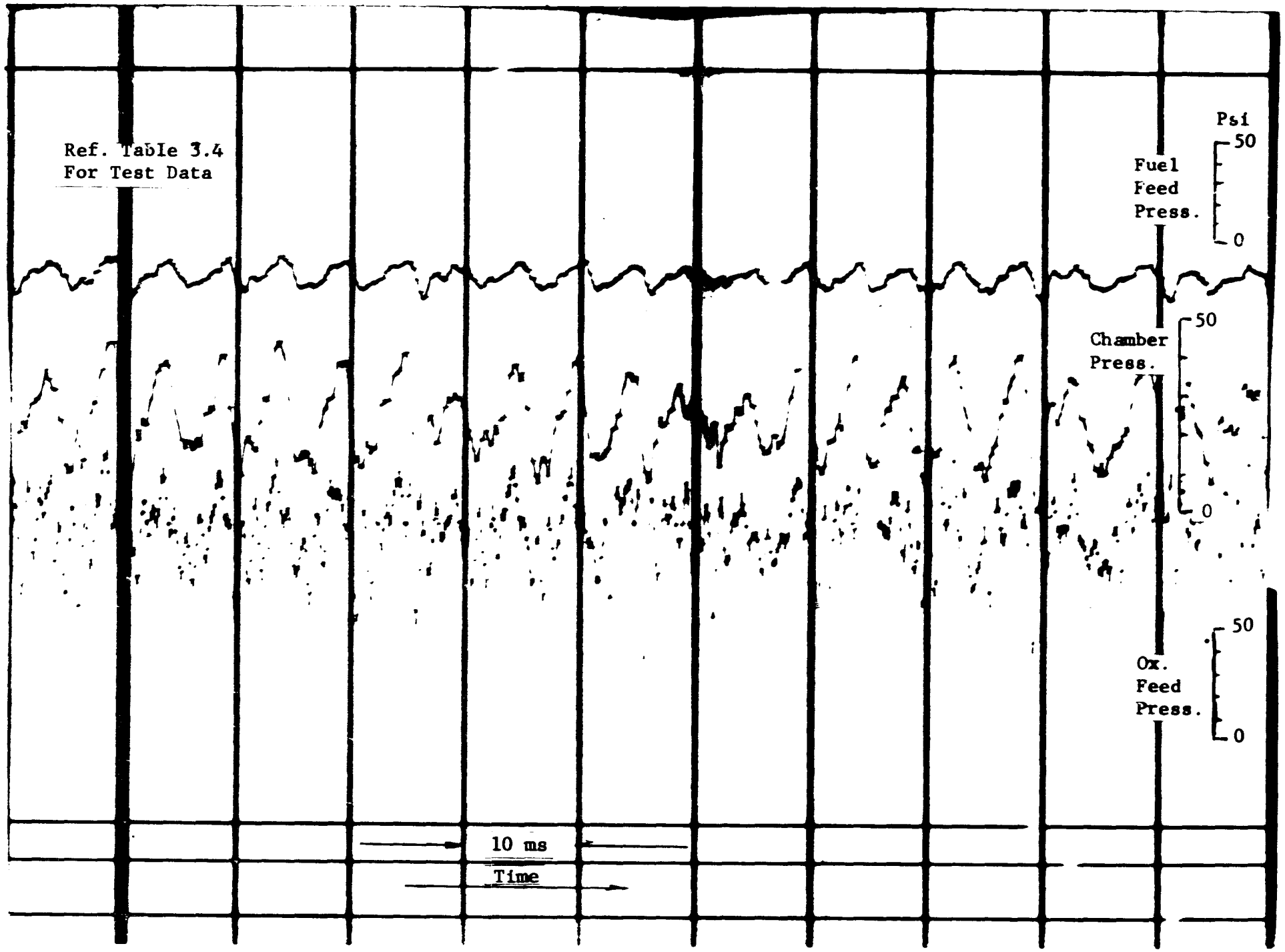

Figure 3.26

WLR23 INTEGRAL SPRAY
INJECTOR ES156989
Run No. 23-118

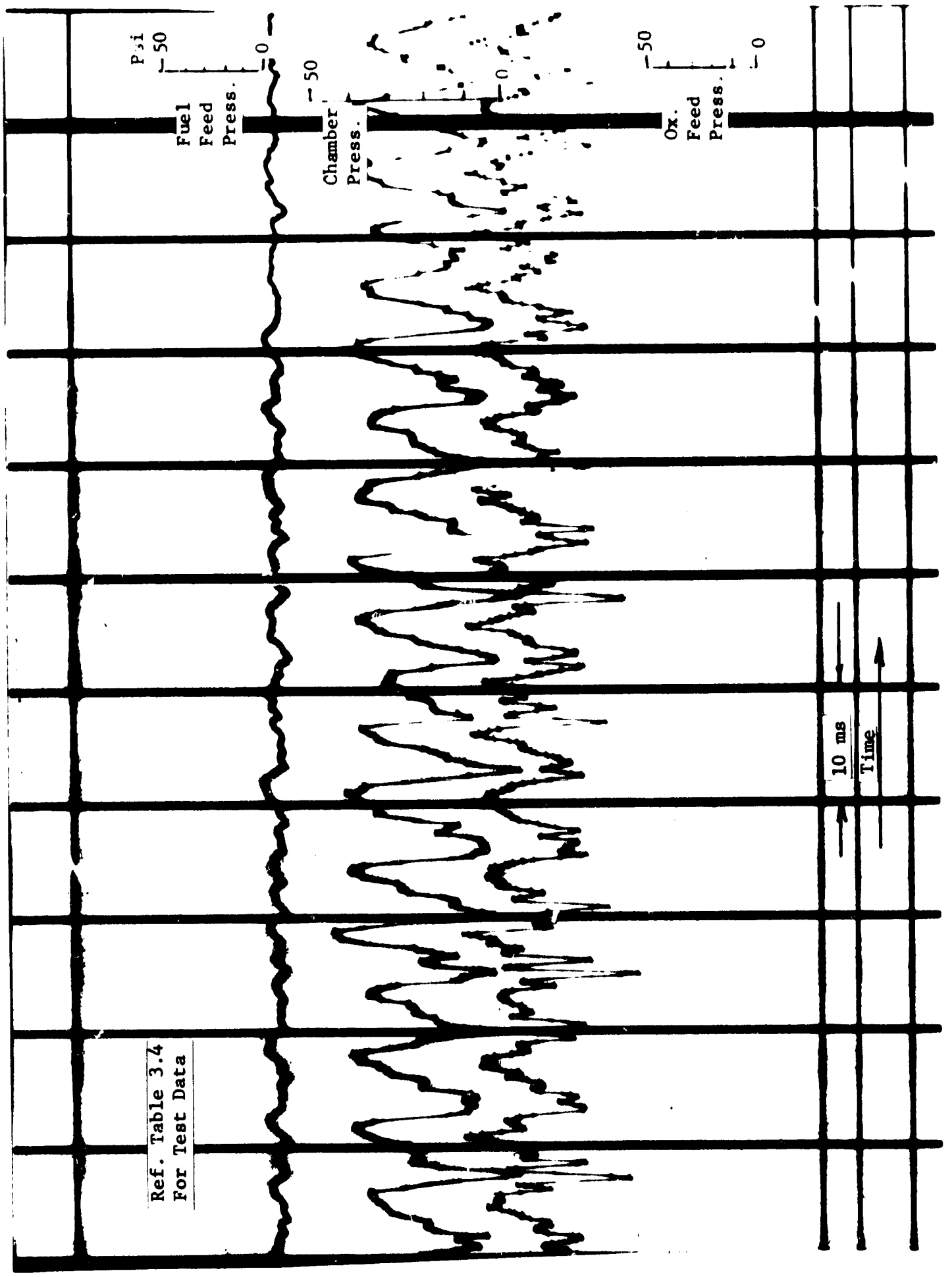

67-0090

Figure 3.27

WLR23 INTEGRAL SPRAY
INJECTOR ES156989
Run No. 23-119

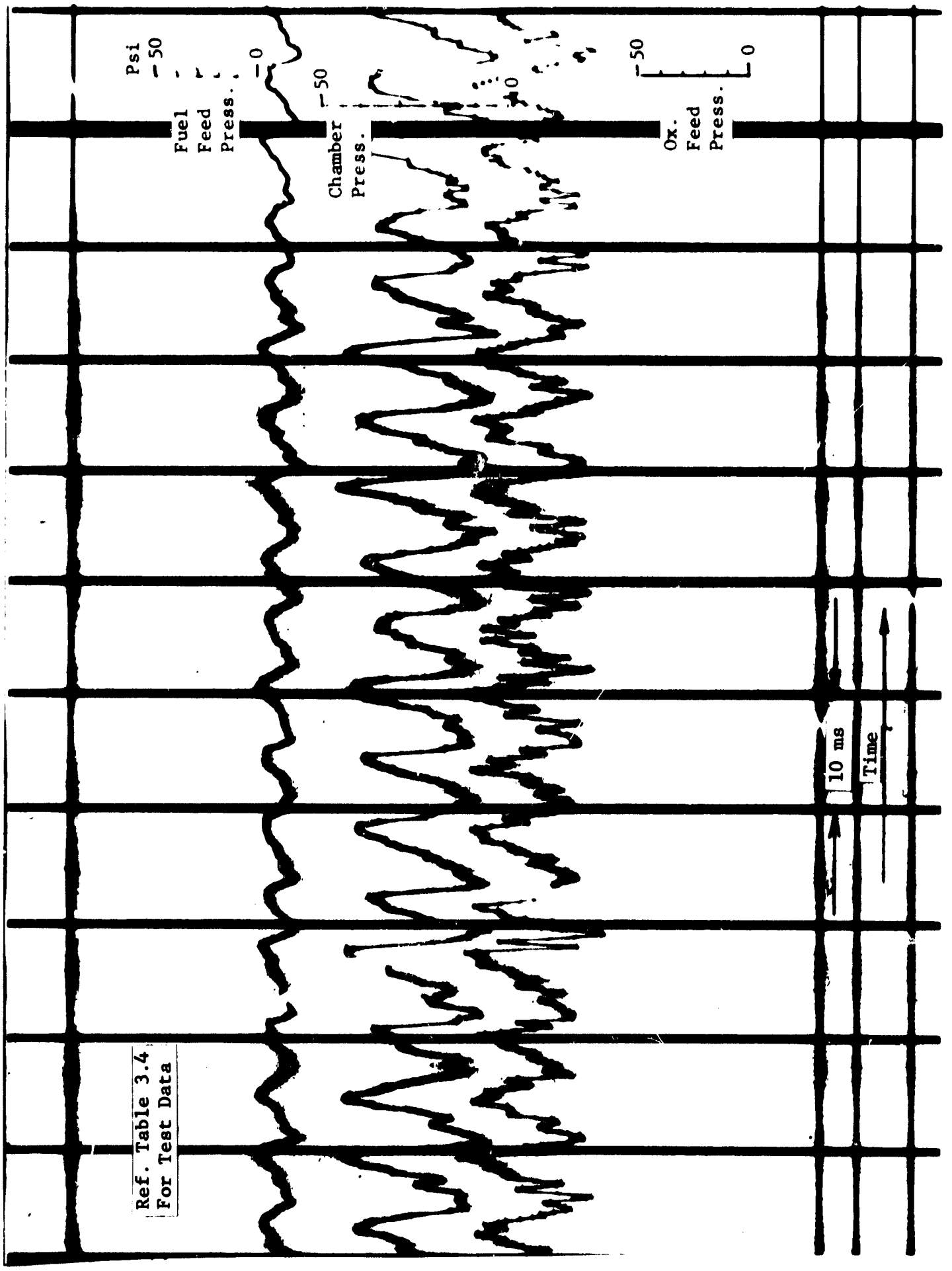

67-0097

Figure 3.28

WLR23 INTEGRAL SPRAY
INJECTOR ES156989
Run No. 23-120

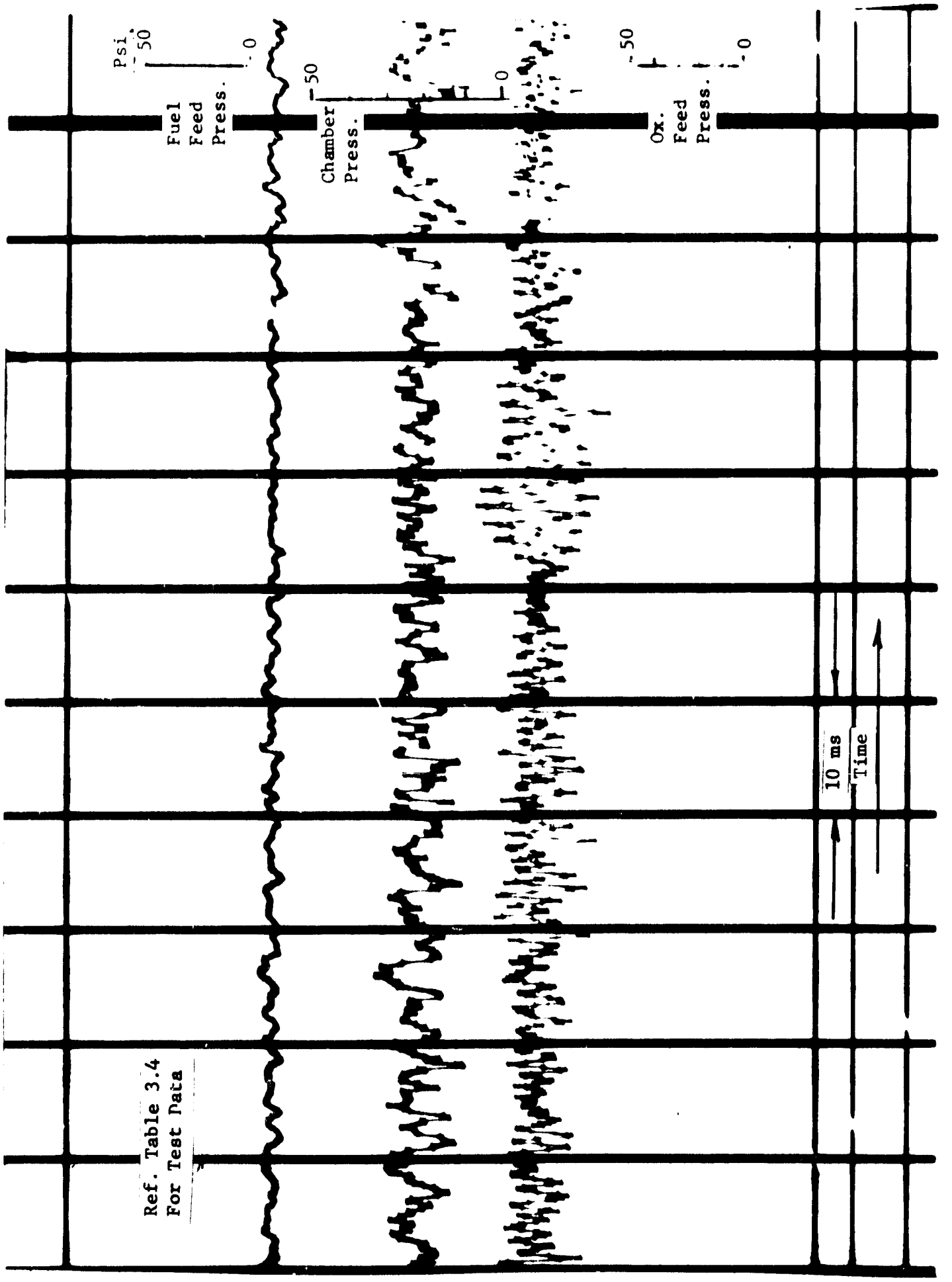

67-0011

Figure 3.29

WLR23 INTEGRAL SPRAY

INJECTOR ES156989

Run No. 23-121

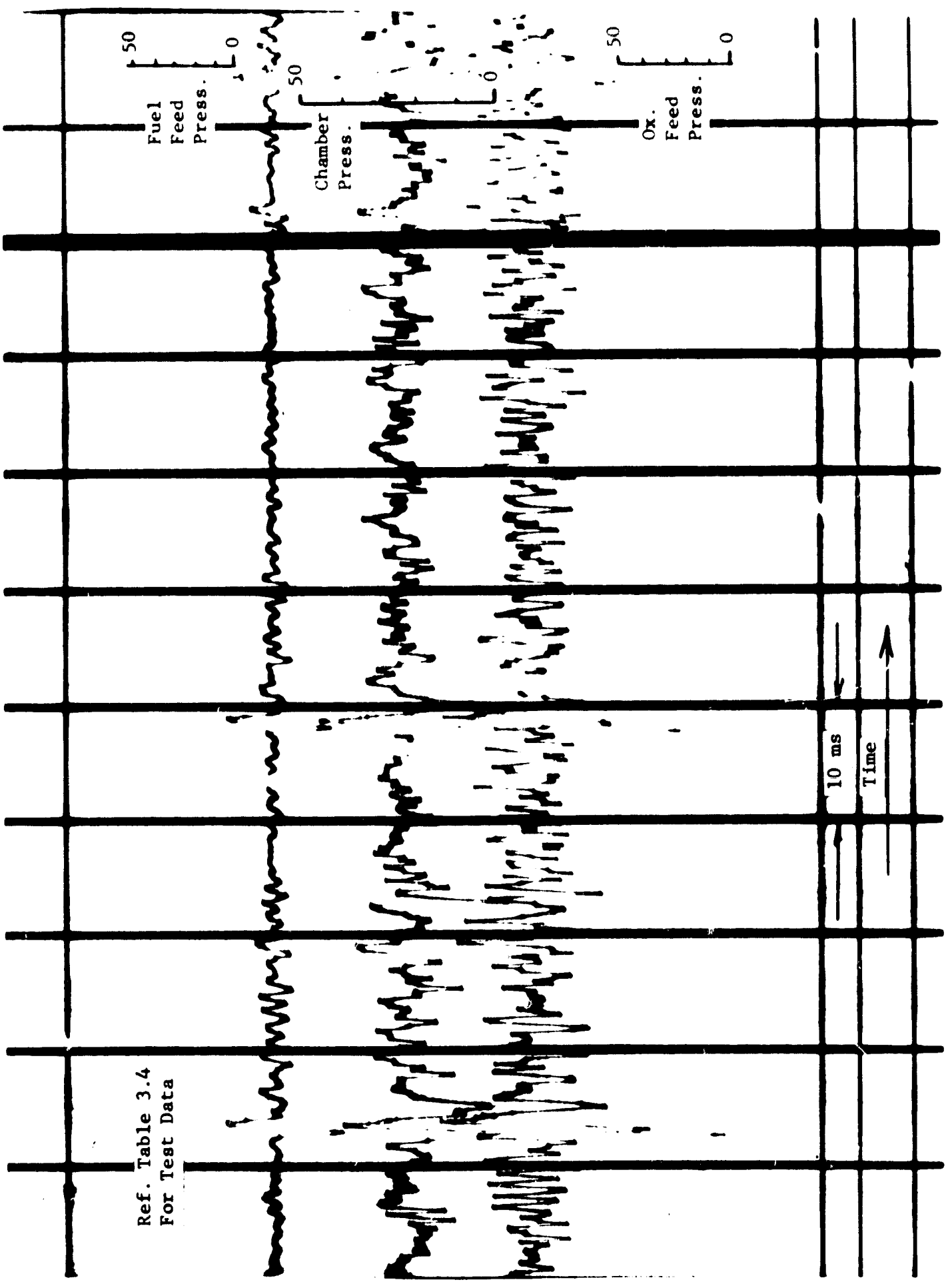

67-0012

Figure 3.30

SUMMARY OF INJECTOR FLOW DATA

	Oxidizer				Fuel			
Inlet Fitting								
Velocity ft/sec	17.5				14.0			
Reynolds No. at 70°F	74,500				18,550			
at 20°F	54,900				9,500			
Manifold								
Flow Fraction	1/2	3/8	1/4	1/8	1/2	3/8	1/4	1/8
Velocity ft/sec	5.75				2.15			
Reynolds No. at 70°F	24,800	22,400	18,800	12,700	4570	3920	3050	2280
at 20°F	18,700	16,900	14,200	9,580	2360	2020	1570	1175
Feed Holes to Orifices								
Axial & Radial Connecting (body)								
Velocity ft/sec	7.0				5.7			
Reynolds No. at 70°F	16,400				4160			
at 20°F	12,100				2140			
Radial Connecting (insert)								
Velocity ft/sec	9.8				7.9			
Reynolds No. at 70°F	19,500				4890			
at 20°F	14,400				2510			
Spray Manifold Feed Hole								
a) Radial								
Velocity ft/sec					10			
Reynolds No. at 70°F					7900			
at 20°F					4060			
b) Axial								
Velocity ft/sec					11.75			
Reynolds No. at 70°F					8570			
at 20°F					4460			

Table 2.1

TABLE 2.2

REDUNDANT SHEAR (SHEAR PER UNIT LENGTH LBS./IN.)

Time (Seconds)	V_1	V_2	V_3	V_4
700	-3473	-605.3	-211.9	41.4
500	-3078	-507.3	-200.1	21.3
200	- 396.5	-168.9	- 60.82	14.1

TABLE 2.3

REDUNDANT MOMENTS (MOMENTS PER UNIT LENGTH IN. LBS./1N.)

Time (Seconds)	M_1	M_2	M_3	M_4
700	104.0	-67.24	50.97	3.95
500	67.21	-60.19	47.93	2.02
200	37.27	-12.52	34.56	1.34

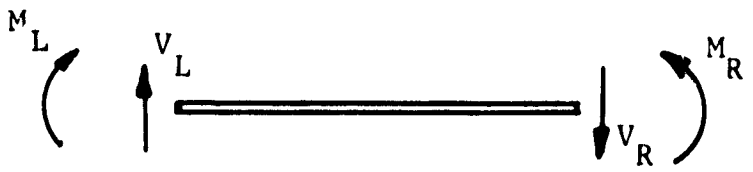

Positive Shears and Moments

HOUSING STRESS SUMMARY

Time (Seconds)	Stress Designation	Flange @ 1	Shell @ 2	Shell @ 3	Shell @ 4	Flange @ 4
700	σ_M		63,830	7,350	4,080	
	σ_H	-11,520	14,590	-5,660	-2,710	-52,000
500	σ_M		54,930	6,350	3,260	
	σ_H	-11,520	13,000	-5,540	-1,390	-26,800
200	σ_M		15,130	4,300	2,970	
	σ_H	-11,520	4,330	-3,350	- 930	-19,800

σ_M = Meridional or Axial Stress

σ_H = Circumferential or Hoop Stress

Positive Stress indicates tension

Table 2.4

SWIRL CUP ORIFICE CALIBRATION

INJECTOR ES156989

MMH ORIFICES			N_2O_4 ORIFICES		
Orifice No.	Orifice Press. Drop psi	Flow lb/sec MMH at 70°F	Orifice No.	Orifice Press. Drop psi	Flow lb/sec N_2O_4 at 70°F
2	60	.01254	1	30	.02371
	70	.01293		40	.02701
	80	.01398		50	.03000
	90	.01493		60	.03261
4	60	.01223	3	30	.02395
	70	.01293		40	.02717
	80	.01358		50	.03011
	90	.01457		60	.03309
6	60	.01244	5	30	.02469
	70	.01309		40	.02782
	80	.01374		50	.03086
	90	.01455		60	.03361
8	60	.01223	7	30	.02450
	70	.01299		40	.02717
	80	.01390		50	.03043
	90	.01455		60	.03323
10	60	.01229	9	30	.02383
	70	.01277		40	.02701
	80	.01321		50	.03015
	90	.01426		60	.03237
12	60	.01182	11	30	.02395
	70	.01257		40	.02733
	80	.01329		50	.03027
	90	.01390		60	.03309
14	60	.01231	13	30	.02383
	70	.01293		40	.02690
	80	.01398		50	.02984
	90	.01455		60	.03290
16	60	.01182	15	30	.02383
	70	.01254		40	.02719
	80	.01344		50	.03027
	90	.01419		60	.03323

Table 3.1

ASSEMBLY CALIBRATION

INJECTOR ES156989

MMH SYSTEM

Pressure Drop psi	Flow lbs/sec MMH at 70°F
40	.0786
50	.0867
60	.0951
70	.1016
80	.1079
90	.1144

N_2O_4 SYSTEM

Pressure Drop psi	Flow lbs/sec N_2O_4 at 70°F
20	.1398
30	.1739
40	.2012
50	.2269

Table 3.2

SPRAY COOLING RING ORIFICE CALIBRATION

INJECTOR ES156989

Pressure Drop psi	Flow lb/sec MMH at 70°F
20.0	.0316
30.0	.0335
40.0	.0376
60.0	.0461
71.6	.0486
80.5	.0522
70.4	.0489
60.5	.0451
50.4	.0414
40.0	.0387
30.0	.0339
20.0	.0308

Table 3.3

FOLDOUT FRAME 1

TEST DATA - WLR23 INTEGRAL SPRA
INJECTOR ES156989

	Run No. 23-	97	98	99	100	101	102	103	104	105
N_2O_4 SYSTEM	Ref. Figure 3.	6	7	8	9	10	11	12	13	14
Tank Pressure	psig	320	279	277	300	235	312	279	320	342
Engine Feed Pressure	psig	182	158	163	172	139	179	159	180	196
Flow	lbs/sec	.225	.2025	.200	.210	.181	.213	.201	.219	.232
MMH SYSTEM										
Tank Pressure	psig	336	298	316	315	343	345	297	336	336
Engine Feed Pressure	psig	213	188	197	200	202	214	188	210	214
Flow	lbs/sec	.152	.138	.1465	.144	.151	.150	.136	.148	.145
INJECTOR MMH SYSTEM										
Fuel Manifold Inlet Pressure	psig	178	157	164.5	166	163	176	155.5	173.5	178
Spray Cooling Manifold Pressure	psig	139	122.8	127.4	131.2	122.4	137.8	124	137.2	141.
Swirl Cup Flow*	lbs/sec	.102	.096	.101	.098	.101	.103	.095	.100	.098
Spray Cooling Flow*	lbs/sec	.0384	.036	.038	.0378	.0405	.039	.0365	.0383	.037
PERFORMANCE PARAMETERS										
Swirl Cup Pressure	psia	120	109.1	108.5	113.7	97.9	116.7	108.7	120.1	125.
Combustion Chamber Pressure	psia	112.7	102.4	102.1	106.9	90.7	110.2	102.5	111.2	116.
Swirl Cup Pressure Ratio - Psc/P_c		1.062	1.053	1.06	1.062	1.078	1.060	1.06	1.078	1.07
Total Propellant Weight Flow	lbs/sec	.376	.341	.3465	.354	.336	.363	.337	.367	.378
Oxidizer/Fuel Ratio (Overall)		1.47	1.47	1.365	1.46	1.17	1.42	1.48	1.48	1.60
Oxidizer/Fuel Ratio (Swirl Cup)		2.20	2.11	1.98	2.14	1.79	2.06	2.11	2.19	2.38
C* Measured	ft/sec	5280	5300	5200	5330	4760	5350	5360	5350	5450
C* Efficiency	%	93.2	93.5	92.5	94.0	86.4	94.4	94.5	94.5	95.6
STABILITY										
Amplitude	psi	10	20	22	16	70	12	15	16	17
Frequency	cps	1100	600	400	500	140	600	600	500	700
Amplitude/P_c	$\pm$ %	4.4	9.8	10.6	7.5	39	10.9	6.7	7.2	7.3
Chugging		-	-	-	-	Yes	-	-	-	-
Incipient Chugging		-	Yes	Yes	Yes	-	Yes	Yes	Yes	Yes
Random Peaking	psi	18	80	80	22	-	25	29	36	56

* Derived from manifold pressure and cold flow calibration

106	107	108	109	110	111	112	113	114	115	116	117	118	119	120	121
15	16	17	18	19	20	21	22	23	24	25	26	27	28	29	30
346	283	298	252	290	307	375	265	304	336	266	344	266	267	253	170
210	164	171	145	173	182	216	149	166	189	143	185	150	150	142	144
.2375	.207	.2145	.1925	.208	.220	.249	.204	.228	.235	.209	.250	.215	.2165	.205	.220
336	282	285	301	280	299	338	219	220	280	253	314	253	260	264	167
218	205	188	218	198	211	239	162	164	202	172	210	178	173	157	150
.140	.109	.0985	.117	.103	.118	.125	.097	.094	.111	.109	.1205	.107	.1108	.131	.124
184	186	173	196	179	190	215	148	152	182	174	210	178	173	157	150
150	-	-	-	-	-	-	-	-	-	-	-	-	-	122	120
.104	.12	.111	.117	.111	.116	.123	.098	.095	.11	.11	.12	.115	.108	.095	.090
.0403	-	-	-	-	-	-	-	-	-	-	-	-	-	.036	.0342
124.3	96.3	100.7	88.7	104.7	108.7	121.3	96.9	104.3	112.5	102.7	120.7	104.7	105.1	107.7	109.7
118.0	88.5	93.1	81.8	96.1	100.7	113.9	90.3	97.4	104.5	94.3	113.0	97.1	97.7	101.4	103.4
1.053	1.087	1.08	1.082	1.09	1.08	1.067	1.071	1.072	1.077	1.088	1.058	1.076	1.075	1.06	1.06
.3775	.316	.3055	.3095	.311	.338	.374	.303	.322	.346	.318	.3705	.322	.3273	.335	.344
1.69	1.90	2.18	1.65	2.02	1.86	1.99	2.1	2.42	2.12	1.92	2.07	2.00	1.96	1.56	1.77
2.28	1.90	2.18	1.65	2.02	1.86	1.99	2.1	2.42	2.12	1.92	2.07	2.00	1.96	2.16	2.44
5510	4940	5380	4660	5350	5230	5350	5220	5300	5300	5200	5380	5300	5230	5320	5280
98.5	87.4	96.0	82.0	95.0	92.0	95.3	93.4	96.0	94.1	91.6	95.4	93.8	92.6	94.0	96.0
15	45	42	50	40	38	40	30	16	20	50	32	42	42	12	20
700	170	140	190	160	160	190	150	1100	180	170	200	160	170	700	700
6.4	25.4	22.5	30.5	20.8	18.9	17.6	16.6	8.2	9.5	26.5	14.2	21.5	21.5	5.9	9.7
-	Yes	Yes	Yes	Yes	Yes	Yes	Yes	-	Yes	Yes	Yes	Yes	Yes	-	-
Yes	-	-	-	-	-	-	-	Yes	-	-	-	-	-	Yes	Yes
21	-	-	-	-	-	-	-	55	--	-	-	-	-	26	100

Table 3.4